Czech Technical University in Prague

Faculty of Electrical Engineering

METHODS FOR ELECTRONIC COMPONENTS RELIABILITY IMPROVEMENT

Doctoral Thesis

August 2014 **Ing. Jan Formánek**

Czech Technical University in Prague
Faculty of Electrical Engineering
Department of Microelectronics

METHODS FOR ELECTRONIC COMPONENTS RELIABILITY IMPROVEMENT

Doctoral Thesis

Ing. Jan Formánek

Prague, August 2014

Ph.D. Programme: Electrical Engineering and Information Technology
Branch of study: Electronics

Supervisor: Doc. Jiří Jakovenko, Ph.D.

Acknowledgements

I would like to thank to my supervisor Doc. Jiří Jakovenko, Ph.D. for the great cooperation on our research topic, for his patience and guidance throughout the entire work. He has provided me with lot of valuable remarks, comment and advices helping my thesis to be successful. He has led my work toward the goal and helped me to overcome many difficulties. I also greatly appreciate helpful advices and discussions of my colleagues from the Department of Microelectronics especially from the CEMIS group.

Table of Content

Abstract

The presented doctoral thesis reports the results of the author scientific and research activities in the field of lifetime evaluation and improvement of the electronic structures, parts, components and whole systems. The thesis touches the knowledge about the new methods of lifetime prediction by using electromechanical structures behaviour models. The modelling is performed by advanced computer technology and available software tools. The methods known in the field of mechanical engineering and material engineering are treated by the author by means of the new knowledge and applied for specific development and optimization of modern electro mechanical structures. The author focuses on effects influencing the product function lifetime and shows principles for structure optimization in order to improve the lifetime and reduce final product cost. For this purposes, the author extends the virtual prototyping methods by optimizing the three-dimensional model of the structure. The new methods application is practically presented on development and optimization of a single product which appears throughout the work. For this purpose, the structure of modern light source based on the semiconductor light-emitting diodes is suitable. The LED sources are characterized by high thermal stresses and the necessity of a wide range optimization of various properties. In recent years the LED lighting is one of the fastest growing areas of electronics and thus it is also a very suitable area for current and future research. The author also deals with the evaluation and optimization of the structure thermal loading, which can cause significant mechanical stress due to the different thermal expansion coefficients of parts connected together. The value of the thermo mechanical loading is accurately examined because it primarily affects the structure damage. This can be carried out by various physically-structural phenomena, which are also presented by the author. Based on information obtained about the product structure thermo mechanical behavior, the author proposes and shows solutions for the lifetime optimization.

The methods and simulation models are verified by measurements. In his dissertation thesis the author presents the measurement methods that either is based on some standard procedures or are unique in their principle. Among the unique method which is also patented by the author can be mentioned the system for highly accelerated lifetime testing of concentric printed circuit boards solder joints. The thermo mechanical lifetime expectation is measured by using a set of specific cyclic external forces. They can cause structure damage similar to the damage which occurs during thermal cycling. However, the time required to the lifetime measurement is much shorter.

Abstrakt

Předložená disertační práce prezentuje výsledky vědeckovýzkumné činnosti autora v oblasti hodnocení a optimalizace funkční životnosti elektronických struktur, součástek, komponent i celých systémů. Práce přináší poznatky o nových metodách odhadu životnosti s využitím modelování chování elektromechanických struktur pomocí moderní výpočetní techniky a dostupných softwarových nástrojů. Metody známé z oblasti strojírenství a materiálového inženýrství jsou autorem rozvíjeny o nové poznatky a aplikovány ve specifické oblasti vývoje a optimalizace moderních elektro mechanických struktur. Autor se podrobně zabývá vlivy ovlivňujícími funkční životnost produktu a uvádí principy optimalizace jeho struktury za účelem zvyšování životnosti a snižování ceny vyvíjeného produktu. Pro tyto účely rozvíjí metody virtuálního prototypování optimalizováním trojrozměrných modelů struktury. Aby mohl být ukázán podrobný proces aplikace nových metod, jsou prakticky prezentovány při jejich využití k vývoji a optimalizaci konkrétního typu produktu. Pro tyto účely vyhověla struktura moderního světelného zdroje na bázi polovodičových svítivých diod, která se vyznačuje velkým tepelným namáháním a nutností optimalizace širokého rozsahu různorodých vlastností. Oblast světelných zdrojů se svítivými diodami je v posledních letech jedním z nejdynamičtěji rozvíjených oborů elektroniky, a proto je zároveň vhodnou oblastí pro současný a budoucí výzkum. Autor se ve své práci podrobně zabývá hodnocením a optimalizací tepelného namáhání struktury, které dále, díky vlivům rozdílné teplotní roztažnosti různých částí struktury, způsobuje značné mechanické namáhání. Jeho rozsah a vliv na životnost konečného produktu jsou podrobně zkoumány s ohledem na mechanickou destrukci struktury. Ta probíhá vlivem různých fyzikálně strukturních jevů, které jsou autorem také uváděny. Na základě získaných informací o teplotně mechanickém chování struktury jsou navrhována řešení vedoucí k optimalizaci životnosti produktu.

Metody a simulační modely chování jsou dále ověřovány příslušnými měřeními. Autor ve své disertační práci uvádí metodiky měření, které buď aplikačně navazují a rozšiřují některé standartní postupy nebo jsou svým principem unikátní. Mezi unikátní autorem patentovanou metodu lze uvést systém testování životnosti pájených spojů koncentrických desek plošných spojů. Jejich teplotně mechanická životnost je měřena za aplikace specifických cyklických externích sil. Ty vyvolávají obdobné poškození struktury, jaké vzniká při cyklickém teplotním namáhání. Čas potřebný k změření životnosti produktu je však mnohonásobně kratší.

List of Shortcuts

AST	Alumina Substrate Technology
BLP	Bottom leaded plastic
CAD	Computer-Aided Design
CAE	Computer-Aided Engineering
CASE	Critical accumulated strain energy
CNM	Centre Nacional de Microelectronica
CSSL	Consumerizing Solid State Lighting
FEM	Finite Element Method
FIT	Failures in Time
FR4	Fire Resistant
FVM	Finite Volume Method
GPIB	General Purpose Interface Bus
IMC	Intermetallic Compound
IMS	Insulated Metal Substrate
IR	Infra-Red
LED	Light Emitting Diode
LFM	Lead Frame Mould
MEMS	Micro Electro Mechanical System
MTTF	Mean Time to Failure
PDE	Partial Differential Equations
SSL	Solid State Lighting
TIM	Thermal Interface Layer

List of Symbols

c_p	Specific heat capacity
E	Young's modulus
H_1	Constant of hyperbolic sine function constitutive model by Schubert at al.
I_F	LED forward current
K	Thermal conductivity
k_B	Boltzman constant
n	Constant of hyperbolic sine function constitutive model by Schubert at al.
P_{TH}	Thermal power dissipated by LED junction
P_{OP}	Optical power (luminous flux)
q	Heat density
Q	Generated internal heat
R	Stress ratio
T	Temperature
T_j	Junction temperature
V	Electric potential
V_F	LED forward voltage drop
α	Constant of hyperbolic sine function constitutive model by Schubert at al.
α_E	Thermal expansion
ε	Equivalent total strain
ε_{el}	Equivalent elastic strain
ε_{pl}	Equivalent plastic strain
ε_{cr}	Equivalent creep strain
ε_{th}	Equivalent thermal strain
σ	Equivalent stress
σ_A	Equivalent alternating stress
σ_M	Equivalent mean stress
σ_{MIN}	Minimum of equivalent stress
σ_{MAX}	Maximum of equivalent stress
λ	Thermal Conductivity
ν	Poisson ratio

1. Motivation and Goals

During the electronic part and component development cannot be taken into account only the current functionality in the period shortly following their manufacture. It is necessary to consider the issue of the possible failure of their functionality after the specified period of the active service. The time period or number of loading cycles since working start-up until the time when the component is unable to perform desired properties is called the lifetime. The end of life can be appointed not only at the moment of complete failure of the electronic components but also at the moment when deterioration of some of their characteristics starts to occur, for example increasing noise generated by the resistor, reduced intensity of light generated by the LED, deterioration of the speaker frequency response, etc. The lifetime is influenced not only by the quality of used materials, complexity of structure and production technology, but also mainly by operating conditions where the electronic system is used. The lifetime is generally highly dependent on the operating temperature humidity presence of corrosive substances radiation etc. In case of consumer electronics manufacturers try to estimate the lifetime of its products and appropriately adjust it with the view to optimizing production costs. The lifetime of electronic system is usually estimated only on the basis of the used separate electronic part lifetime and on the basis of statistic results of measurements on the small number of final products. The measurement of lifetime is generally very expensive and time consuming.

Modern and little-recognized way to evaluate the behaviour of designed product is the simulation of the adequate computer model and its decomposition into the finite number of elements. This method known from the mechanical engineering is beginning to be used in design of the electronic components. After appropriate modifications of methods for designing and simulations of mechanical components thermo mechanical behaviour they can be used for the development of electro-mechanical components. Proposed methods could enable the precise evaluation of component behaviour from the thermo-mechanical point of view including determining its short-time and long-time durability.

Newly created methods aim to shorten the time required for the new product development and its lifetime validation. These methods enable faster and cheaper placing to the market as well as the possibility of the effective and quick development of products with improved properties, longer life and lower cost.

Presented research area is becoming very actual and a lot of work still has to be done. From those reasons, I am setting out following goals:

- Develop new methods for the precious modelling and validation of thermal distribution and the heat transfer optimization for the thermal reliability improvement
- Develop methods for the precious thermo mechanical reliability modelling and evaluation
- Extend the methods for the product virtual prototyping from thermal, mechanical and reliability point of view
- Extend the methods for a lifetime characterization

2. State of the Art

Design and product development has been historically based mainly on the experience of developers and designers and their judgment in design of initial concepts. Then all the other development efforts have been fixed and tended to produce physical prototypes. Thanks to them it was possible to identify the performance and functionality of the designed products. Very often, the concept did not satisfy initial expectations and the first prototypes exposed to many weaknesses due to it was necessary to remodel the design several times. Today mechanical engineering commonly use methods of virtual prototyping. In practice it means the widest possible usage of the CAD (computer-aided-design) and CAE (computer-aided engineering) programs for verifying and testing the design before producing the first prototype. Mechanical engineers generate computer models of the initial concept which are then virtually assembled in the CAD system. Thermo-mechanical and fatigue behaviour of single parts or assemblies are then simulated using specialized software tools. It allows the iterative improvement of product design until they meet the predefined criteria of functionality. This will reduce costs, optimize production respecting desired quality and reduce time of placing the product on the market.

In the field of mechanical engineering, the concept of virtual prototyping is spread in the large technology discipline. It deals with the design of model parts, numerical analysis (strength, dynamic, kinematic, fatigue) and manufacturing simulations. The aim of this conception is to create the product model that gives the designers, technologists but also dealers and the company managements the vision of the future product, its functionality, its physical properties and behaviour in operating conditions and eventually about manufacturability. With the development of computer technology possibilities in the field of numerical mathematics designers have new possibilities solving very complex tasks. The most common used methods include the finite element method (FEM) and the finite volume method (FVM).

Designers of electronic components are using the principle of virtual prototyping very rarely. Mechanical aspects of the design are mostly being left at the standardized procedures and time consuming functional verification for example accelerated temperature loading lifetime tests [B106].

Several important research groups deal with problems of use of these simulation methodologies to study the thermo-mechanical behaviour of electronic components and systems. Common applications can be found in the research of packages and structures of electronic components in case of their soldering with the lead-free solder and thermal cycling [B1], [B2], [B3], [B4], [B5], [B6], [B7], etc. In these works the linear thermo-mechanical simulation of highly simplified structures is commonly used. Critical parts of structures are localized by simulations however their precise evaluations are still based on the thermal cycling tests. Complex nonlinear simulations that would allow creating the more general model of the behaviour of electronic structure are not applied in this field. In the case of

including more aspects of nonlinear behaviour, including the application of nonlinear approximate models of materials we were able to propose the behaviour model of the electronic structure which would be able to simulate precisely the performance of real structures. This behaviour can be simulated in the relatively large range of operating conditions, for example in the large temperature range, under various external pressures, mechanical loading, in different environments etc.

The common specialized FEM simulation tools can be found for the development of MEMS structures. Due to the low ductility of semiconductor materials, linear simulations are sufficient in the case of simulation in the small temperature range [B8], [B9], [B10], [A5]. When we try to apply the developed structures in the wider temperature range, the accuracy of simulations is significantly limited by considerable temperature dependence of the mechanical behaviour of materials. Therefore it is suitable even in this area to move away from the established linear simulations and apply the developed methodology known from mechanical engineering.

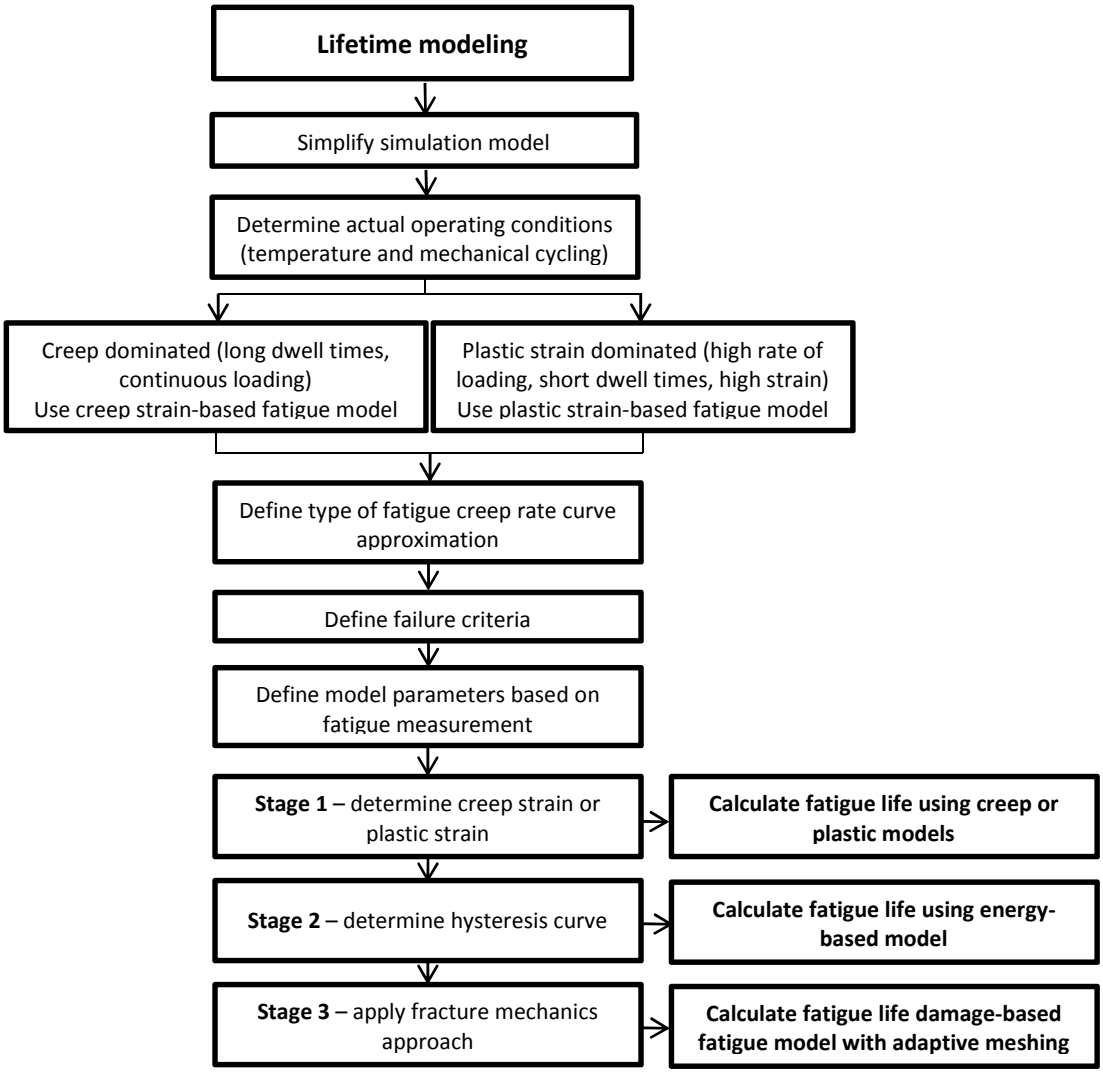

Figure 2.1 - Lifetime modelling methodology

Development of non-linear mechanical simulations can provide the ability of lifetime estimation of the electronic structure. From the field of mechanical engineering we know several levels of approaches to estimate the lifetime (Figure 2.1). Unfortunately even in this field the full implementation of the proposed theory has not been reached. Complex fatigue simulations and crack propagation simulations are performed only on the simple model cases [B11], [B12]. When we fully apply these simulations in our field, it would mean the significant contribution to the knowledge of the failure of electronic devices and the ability to easily modify the structure to enhance the lifetime or reduce the production cost.

The simulations can´t truly reflect the reality without precious measurements. The problematic and time consuming lifetime measurements lead me to search for methods that would be faster and cheaper. The samples of the real product or the product components are usually heated and subsequently cooled in the thermal chamber which usually the specific heating system allows the relatively fast cycling of the temperature. Testing samples are cooled or heated mainly by the radiation and the air convection. The heat capacity of the samples and the thermal chamber rapidly slow down the testing process. Depending on the sample size, cycling range and the type of the chamber, one thermal cycle takes several tens of minutes or units of hours [B13], [B14]. In the case of high power electronics, where predicted number of lifetime cycles are in the range of thousands, the testing in standard thermal chamber commonly takes several months. So the result can't be flexibly used during the development. The testing is also high energy consuming. The principles studied by authors M. Bevan, M. Wuttig [B15] and testing methods published in [B16], [B17], [B18] inspired me to the idea of designing the new methodology for accelerated lifetime tests, which aims to replace the time consuming thermal cycling tests. The methodology describes the set of specific simulations and measuring apparatus for the specific thermo mechanical loading which should approximate the distribution of the mechanical stress normally generated by the thermal expansion of the different materials used in the structure. The principle of the apparatus is to achieve the similar formation and propagation of cracks in critical parts of the structure normally caused by temperature cycling but with using the constant temperature and mechanical cycling. This principle has not been used for the lifetime testing, according to my knowledge. Some specific thermo mechanical lifetime testing was studied by the research team of J.H.L Pang, Kar Hwee Ang, X.Q. Shi and Z.P. Wang [B19]. Their work focuses only on the specific cases of the BGA solder joints testing. But the full replacement of the thermal cycling tests in the thermal chamber has not been developed, validated and published yet. Especially there is not the one which is able to estimate the lifetime of the real product. The new proposed life time methodology, evaluation process, design of measurement apparatus and validation on the realistic product testing will be presented in the following chapters. These will be demonstrated on newly developed electronic LED lamps. The technology of the solid state lightning (SSL) is state of the art in the lightning technologies and many effort on its development is being spend. Also the choosing of one product enables me to show the whole design flow.

3. Solid State Lighting Technologies

Proposed methodologies and developed evaluation methods will be demonstrated on the high power SSL lamp design. This chapter focuses on the short cross-section of the modern LED lamp design as the replacement of classic incandescent bulb. The chapter shortly describes the state of the art in the lighting, LED lamps design and LED technologies.

3.1. Current Light Sources

The developments in lightning technologies recorded significant technological benefits in the last few decades. Due to the innovations in material engineering of halogen lamps introduced efficiency of fluorescent lamps has increased significantly and thanks to the development of electronic components it can be integrated as the replacement for incandescent lamps. The development of the optoelectronic devices in the past few years enables foundation of the concept of lightning sources, where the luminous flux is generated in one or more semiconductor light-emitting diodes (LEDs).

In the last few years the usage of SSL (solid state lighting) lamps has been increasing almost exponentially because of the rapid development in LED design. The Figure 3.1 shows historical and predicted efficacy in Lumens per Watt of most common light sources.

The solid-state lighting has the potential to revolutionize the future lighting industry. We can predict that the LED replacement lamp market will speed up the progresses.

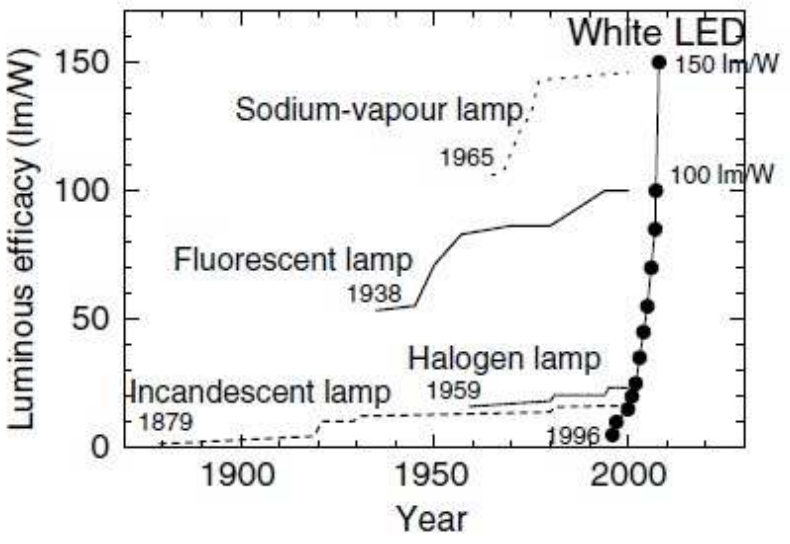

Figure 3.1 - Efficacy of Light sources [B20]

The advantages of modern solid-state LED lamps:

- SSL produces a light with reduced heat generation or other parasitic energy dissipation
- More than ten times longer lifetime in comparison with incandescent light technology
- Better quality of light output (LEDs produce minimum ultraviolet and infrared radiation)
- High Shock resistance - light is emitted by solid-state electroluminescence
- Smaller volume of light bulb
- No emitting ultraviolet radiation
- Fully dimmable (depends on driver design)
- Green technology (no environmentally harmful materials as mercury, lead, etc.)
- SSL lamps colour can be easily changed from cool blue to warm yellow

Table 3.1 compares 800 lumen SSL lamps to adequate incandescent and fluorescent lamps. SSL lamps cost considerably more than incandescent lamp, but if we compare the lifetime and operating costs, difference in purchase price will be vanished. Also after the market penetration the future SSL purchase price are expected to be significantly reduced.

Table 3.1 - Current light sources

Lamp type	SSL lamp	Fluorescent	Incandescent
Input Power (W)	60	13 - 15	6 - 8
Life time (hours)	~ 50 000	~ 8 000	~ 1200
Retail price	10 - 40 €	5 - 10 €	< 1 €
Equivalent operating cost per year	3,29 €	7,67 €	32,86 €
Infra-red emission	~ 0 %	~ 37 %	~ 73 %
Environment impact	Low	Toxic mercury	Low
RoHS Compilant	Yes	No (contains 1to 5mg of mercury)	Yes
Sensitivity to high and low temperatures	No	Yes	Some
On/off cycling sensitivity	No	Reduce lifetime significantly	No

3.1. LED Technologies for SSL

This work does not deal with basics of LED technology. Reader can find the information in the literature[1]. We should mention some important facts related to SSL and LED reliability.

White light output for general illumination can be generated by the two different approaches. The first approach assumes that the white light is created by the set of LEDs emitting light at different wavelengths. The white light is generated by mixing of discrete wavelength with using appropriate optics. The colour-mixing technology does not contain phosphor. The biggest problem of this technology is the absence of efficient green light LEDs that significantly limits achievable efficacy.

The second approach assumes that the white light is generated by converting of the blue light[2] (generally around 450 - 460 nm) which is emitted directly from the LED die. The blue light is than down-converted to the longer wavelengths by phosphor. Phosphor can be placed on the diode chip or on separate component which light passes. Today the most efficient yellow phosphor is still the YAG phosphor, with less than 10 % stoke shift loss. Losses attributable to internal optical losses due to re-absorption in the LED chip and in the LED packaging itself account typically for another 10 % to 30 % of efficiency loss.

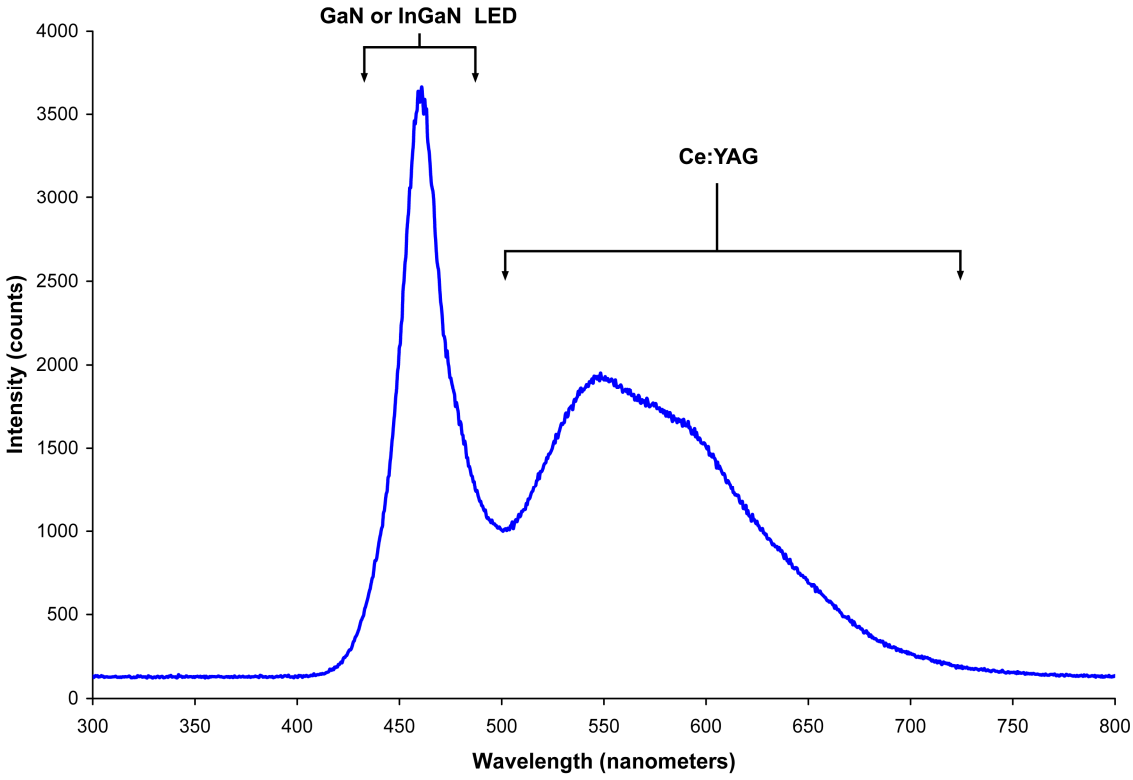

Figure 3.2 - Spectrum of a "white" LED showing blue light directly emitted by the GaN LED and the stokes shifted yellowish light emitted by the Ce:YAG phosphor [B22]

[1] For example in [B21], [B22], [B23], [B24], etc.
[2] The blue light is mostly generated by GaN LED chip which is today most effective in the sense of the ratio of luminous flux to the input electrical power.

Currently, in the area of phosphor LED development, much effort is being spent on optimizing these devices to the higher light output and higher operation temperatures. For instance, the efficiency can be raised by adapting the better package design or by using the more suitable type of phosphor. The conformal coating process is frequently used to address the issue of varying phosphor thickness. The phosphor-based white LEDs encapsulate GaN blue LEDs inside phosphor coated epoxy. The common yellow phosphor material is cerium-doped yttrium aluminium garnet (Ce^{3+}:YAG) [B25].

The white LEDs can also be made by coating near-ultraviolet (NUV) LEDs with the mixture of high-efficiency europium-based phosphors that emit red and blue, plus copper and aluminium-doped zinc sulfide (ZnS:Cu, Al) that emits green. This is the method analogous to the way fluorescent lamps work. This method is less efficient than the blue LEDs with YAG:Ce phosphor, as the stoke shift is larger, so more energy is converted to heat, but yields light with better spectral characteristics, which render colour better. Due to the higher luminous flux generated by ultraviolet LEDs than of the blue ones, both methods can offer comparable brightness. A concern is that UV light may leak from the malfunctioning light source and cause harm to human eyes or skin [B21].

Today's SSL mainly uses the second principle. Blue power LED with phosphor is located on the high heat conductive component because big portion of the heat is generated in high power LEDs. Good thermal management is perhaps the most important aspect of successful SLL lamp system design. If the heat is not removed, the LEDs run at high temperatures, which not only lower their efficiency, but also make the LED less reliable.

3.2. Retrofit LED Lamp Design

For a quick introduction on consumer markets, manufacturers had to develop retrofit LED lamps as the instant upgrade from incandescent, compact fluorescent and halogen lamps. The retrofit LED lamps had to fit not only in the modern lighting fixtures but also in old chandeliers.

The most important SSL retrofit lamp requirements are:

- Lamp shape - customers want the "traditional" light bulb shape to replace old incandescent light bulbs
- Natural light colours
- Distributed light angle
- Dimming possibilities

The Figure 3.3 shows the cross-section of retrofit shape SSL lamp with the most important parts. For FEM simulation the precise 3-D model of the 8 W LED Lamp has been designed. The model represents the retrofit LED lamp including six LEDs mounted on PCB board. On each of the LEDs the silicone lens are placed in order to get the wide angle light beam. The LED package contains ceramic body with one thermal and two electrical copper

pads. The polycarbonate dome containing phosphors has been installed for light conversion. The high power LEDs are usually based on the GaN solid state semiconductors and emit light in the narrow blue range of the visible spectrum. The blue light must be converted by luminophores into the white light (same as incandescent lamp). The dome also changes light distribution angle. The model contains also the electronic driver board, the thermal cone and housing (heat sink). Other details as E27 cap, shell, potting material, reflective cover, driver support and TIM between LED board and thermal cone are also included in the model [A18].

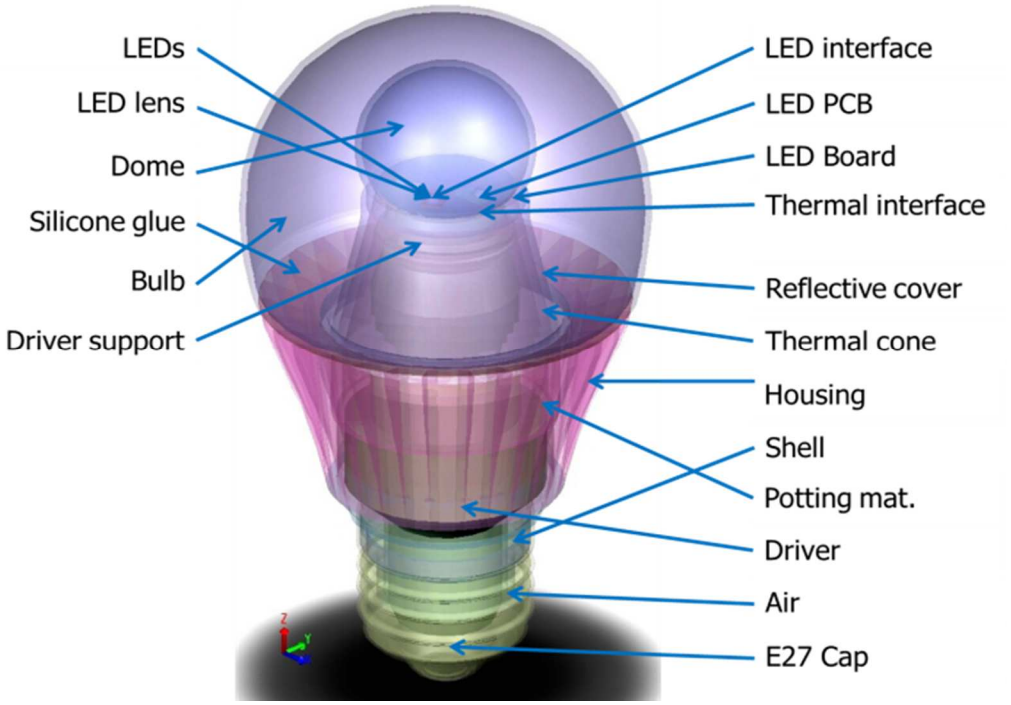

Figure 3.3 - Master LED Glow 8 W lamp parts

4. Reliability, Lifetime and Failure Mechanisms

The reliability can be defined as the ability of the system or the component to perform its required functions under stated conditions for the specified period of time. The reliability experts often describe the reliability of the population of electronic products using the graphical representation known as the Bathtub Curve as illustrated in the Figure 4.1. The bathtub curve describes the particular form of the hazard function and it can be divided into three periods. The first one is the initial period of infant mortality where the defective/weak products fail. This is followed by the normal life of the product with the low and relatively constant failure rate. Following this is the final period of the product lifetime where wear-out mechanisms of the product kick in and the failure rates increase. It is important to understand that the Bathtub Curve does not depict the failure rate of the single item but describes the relative failure rate of the entire population of products over time. Some of the units will fail during the infant mortality period; others will last till the wear-out period while a few of the units will fail during the normal life.

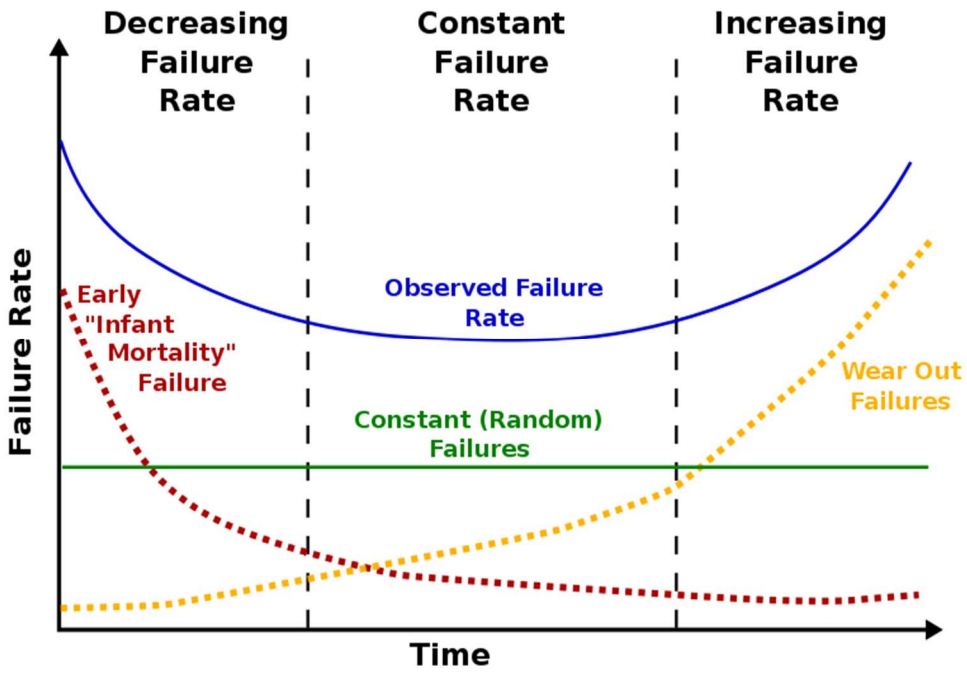

Figure 4.1 - Reliability Bathtub curve [B28]

The reliability deals with random failures in the population of products and is expressed in terms of rates such as Failures in Time (FIT) or Mean Time to Failure (MTTF). The MTTF is the theoretical accumulation of random statistical failures of all components in the product expressing the “constant failure rate” over the lifetime. On the other hand the lifetime refers to the length of time or number of cycles that the single product may be expected to function properly before the known wear-out mechanism renders the product unfit for use. The

lifetime is typically expressed in hours and normally indicates the duration of time with the minimum survival rate of 90 % (obtained from the MTTF calculations). For instance, the lifetime of 10 000 hours implies that under normal conditions in the typical installation (population), 90 % of the products installed would be expected to last 10 000 hours before failure [B27], [B28]. The lifetime can be also expressed in number of cycles of defined loading, which is typical for the product use. This approach will be used for the expression of the lifetime of designed SSL lamp, which is worn out due to temperature cycling during switching on and off.

For the good protecting against the system failure, we have to determine the mechanism that can cause it. Four main classes of failure mechanisms are outlined. The following list was taken from [B29].

The Mechanical Failure Mechanisms. The main mechanisms are fatigue and fracture of various parts of the system which can be a result of thermal cycling together with the different thermal expansion coefficients of parts connected together. Vibration and shock also frequently accelerates the mechanical failure. Wear and friction are often increased by presence of sand and dust.

- Temperature – Thermal cycling can cause fatigue and fracture by inducing stresses in different components structure. For example, the different thermal expansion coefficients of electronic component package and PCB can cause the fracture of the solder joints which are connecting them together. The probability of damage depends on the magnitude of thermal cycling and on the prolongation time between cycles
- Shock and Vibration - Shocks and vibrations can also cause many mechanical failures. For example the flexing of leads and interconnects as well as the damaging of components such as bearings is common. We can find some ways to reduce the loading such as dampers which can absorb shocks and isolate components.
- Sand and Dust – Sand and dust can be dangerous for a moving parts and optical surfaces which can become dirty or scraped.

The Electrical Failure Mechanisms. External currents conducted into the electronic structure such as those caused by electrostatic discharge (ESD) or atmospheric lightning can also cause the components destruction especially of the integrated circuits. ESD can be caused by large the large potential formed by rubbing together of two different materials.

The Corrosion Failure Mechanisms. Corrosion can also cause major damage or accelerate the mechanical failure. It is caused by the chemical process of metal parts which is interacting with the environment. This process can also destroy electronic component or degrade component parameters. Conditions accelerating the corrosion failure mechanism include relative humidity, high temperatures and the presence of chemical compounds or dirt [B30]. The presence of moisture is also very important in the process of corrosion. Corrosion failure mechanism can occur in many ways, the details can be found in Pecht's publication [B30], but the brief list is shown below.

- Surface Oxidation
- Galvanic Corrosion
- Pitting Corrosion
- Crevice Corrosion
- Corrosion due to Microorganisms
- Defects in Passivation

The Radiation Failure Mechanisms. The external radiation is another effect which can cause failure. We know many different types of radiation effects which can cause both mechanical and electrical degradation. Mechanical defects can be also caused by the material properties deterioration due to the radiation absorption. For example the radiation can deteriorate the mechanical, optical, thermal and electrical properties of metals. Electrical failures can physically occur during the operation. The absorbing and accumulation of the alpha particles causes the additional interference. The data communication can fail which result in the system failure [B30].

5. Methods for Precise Simulation Model Design

The work deals with lifetime improvement done by virtual prototyping of newly designed products. Some aspects of product thermo mechanical behaviour can be hardly studied analytically. Than the method of finite element modelling can provide valuable results. But this cannot be done without having of the simulation models which precisely describes the real geometry, material parameters, external environmental conditions, etc. Unlike of already published works ([B1], [B7], [B11], [B83], etc.) my reaches immerse more deeply into methods known from mechanical engineering. Building the precise simulation model of electronic structure and its behaviour requires making the accurate geometry model, specify the set of material parameters and correct boundary conditions.

5.1. Finite Element Modelling

The theories of elasticity, plasticity, creep and other analytical theories can be used to solve many engineering problems. But practical engineering problems cannot be solved analytically due to the complexity of the structure's geometry and extensive boundary conditions.

The finite element method came from the need to solve complex problems in structural mechanics and aerospace engineering construction. Its development can be traced to the work of A. Hrennikoff (1941) and R. Courant (1942). Although these approaches used by the pioneers are fundamentally different and have one common characteristic: mesh discrete areas into separate sub-sets. Hrennikoff's work divides the area by a grid also Courant separates it into the finite number of triangular sub-regions for solution of elliptic partial differential equations of the second degree which were developed from the task devoted to torsion of the cylinder. Courant's evolutionary approach was applied to large solids with previously obtained solutions of differential equations derived by Lord Rayleigh, Ritz and Galerkin. The development of the finite element method began in the early 50-ies of the 20th century to solve problems of structural mechanics. The driving force of development came in 60ties from the research centre in Berkeley, focused on civil engineering. The method was elaborated together with the precise mathematical apparatus in 1973 in the publication by Strang and Fix called Analysis of The Finite Element Method which has been generalized into the separate field of applied mathematics for numerical solution of physical systems across the diverse range of engineering disciplines such as electro-magnetic fluid dynamics.

From the mathematical point of view the finite element method is used to find the approximated solution of partial differential equations (PDE) and integral equations such as heat conduction equation. The procedure is based either on the complete elimination of the differential equation (stationary task) or to convert the PDE into the equivalent ordinary differential equation, which is then solved by standard techniques such as finite differences etc. Solving partial differential equations is the essential step in formation of the new

equation. That approximates the original solution of the equation that is numerically stable in the sense that errors in input data and supporting calculations do not accumulate to such absurd results. There are many possible techniques, all with certain advantages and disadvantages. The finite element method is the reasonable choice for solving partial differential equations on complex areas. I my case, ANSYS workbench simulation software was used [B26], [B103].

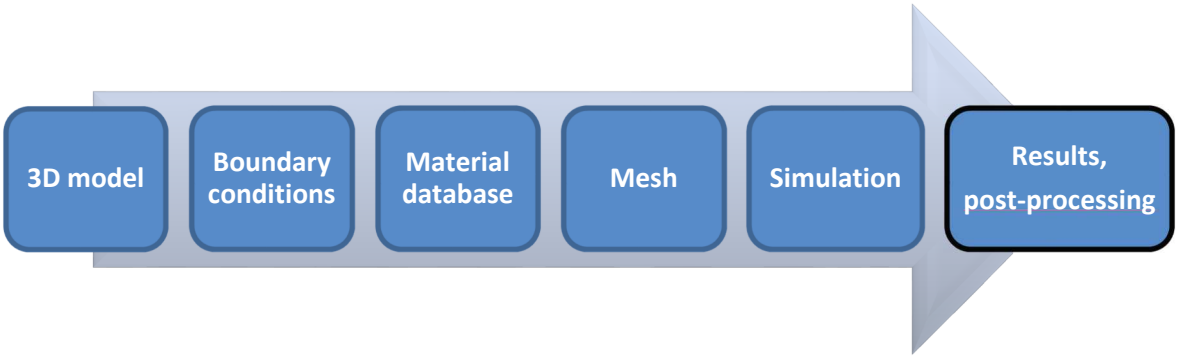

Figure 5.1 - FEM simulation procedure

5.2. Precise Geometry Model Design

In my case the LED lamp model is composed from many different parts made from the different materials. The complete three-dimensional model of retrofit 8 W LED Lamp has been designed for the FEM simulation with all necessary details (Figure 5.2). The model represents the retrofit LED lamp including six high-power blue LEDs mounted on the PCB board. The model contains also the electronic driver board the thermal cone and housing (heat sink). Other details as E27 cap, shell potting material reflective cover mounted on thermal cone driver support and thermal interface layer between LED board and thermal cone etc. are also included in the model (Figure 5.2).

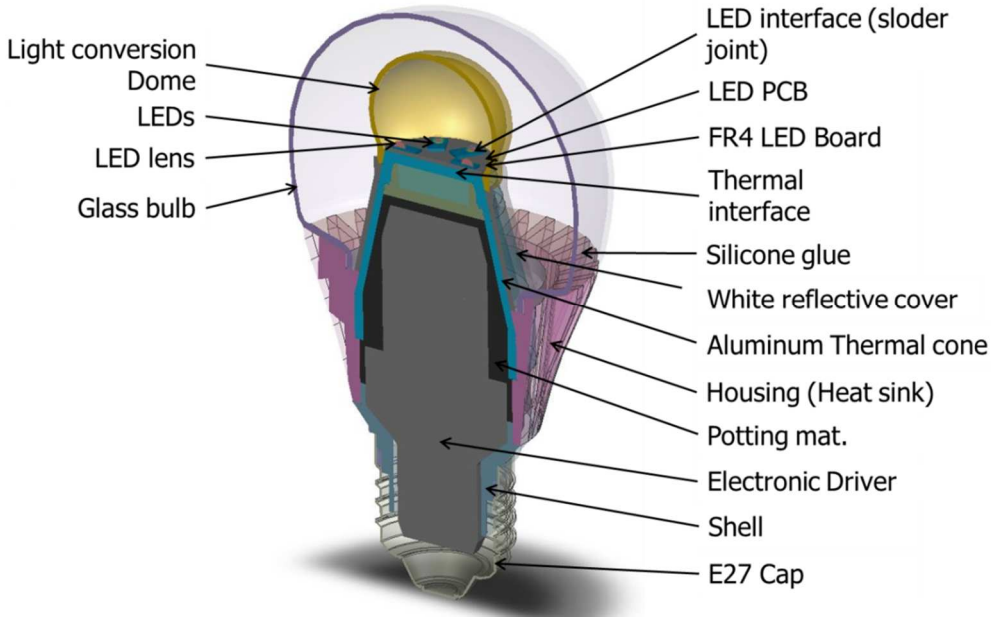

Figure 5.2 - SSL Lamp 3-D model includes sixteen different compact parts. Air inside light bulb and inside light conversion dome was included to the model

One important aspect of the three-dimensional finite element simulation is the precision of the mesh generation which affects the accuracy of the final simulation results. The LED lamp FEM model mesh is designed suitably fine in order to have acceptable accuracy. Because of the non-orthogonal parts in the model tetrahedron elements are used to merge and extrude all layers in order to produce the continuous mesh. To reduce the number of nodes and therefore the computing time the element distribution is adapted to the shape of the bodies; in the specific places the number of elements is increased to capture the small features in the model. The designed model contains approximately 490 000 nodes [A3].

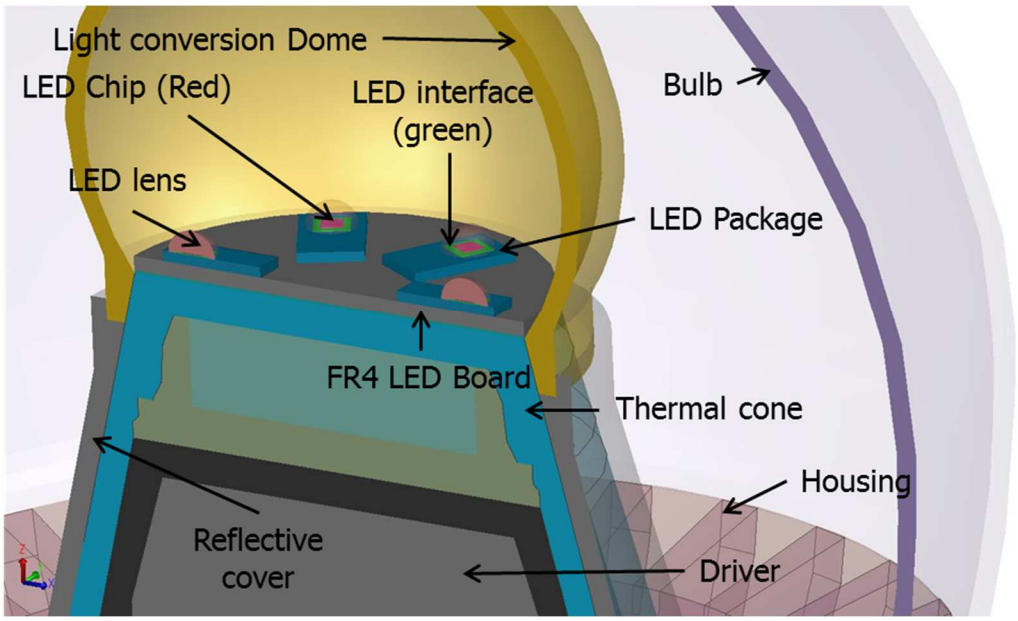

Figure 5.3 - Detailed view on LED board placed on aluminium alloy thermal cone. The board includes six LED with Al_2O_3 package and LED chip

The geometric model is still the ideal model as the designer wishes it. The model so far does not include the effects of imperfections caused by the manufacturing process, imperfections of the parts geometry or failures built in during manufacture, storage or transport. In order to achieve the truly accurate simulation model, we have to firstly get the idea of the quality of product manufacturing, storage and transportation.

Some of the phenomena can expected relatively well in advance and the geometry of the simulation model can be customized. For example:

- Anisotropy of layer etching used on printed circuit boards and chips
- Inequalities of fabricated mechanical components surfaces
- Inaccuracy of some of dimensions given by production process
- Etc.

However, we can find more defects in the structures that cannot be expected in the whole group of manufactured products. According to degree of influence on the

functionality and the lifetime of the products it is necessary to individually decide which defects will be removed during the selection after production, which must be considered in the design and evaluation of products and which can be neglected. We further consider only the events that should be included in the design of the simulation model because it has significantly occur in the population of evaluated products and also affect the lifetime of the products. We can mention for example:

- Reducing the contact surfaces between structure parts
- Reducing the strength of layer contacts, for example due to the poor wettability of the surfaces
- Bubbles and impurities in the solder layers, in the moulding materials or in another fabricated parts
- Cracks formed during the fabrication process
- Etc.

Every effect is often detectable only by the deep investigation of the individual components details, these must be subjected to more extensive testing methods known from metallurgy, fabrication technology, mechanical engineering etc. Due to the time consumed on such exploration, as well as complexity of designed simulation model it is possible to consider only the most significant failures.

In the model case of the SSL lamp development several failure phenomena were examined, but I will show for example only the most significant. During the development I found that the lifetime of the real product is greatly influenced by the quality of the solder joint between the LED package and the printed circuit board. Examining in more details with using X-rays have been found frequently occurring large bubbles in the layer of lead free solder, which came from the wrong manufacturing process (Figure 5.4).

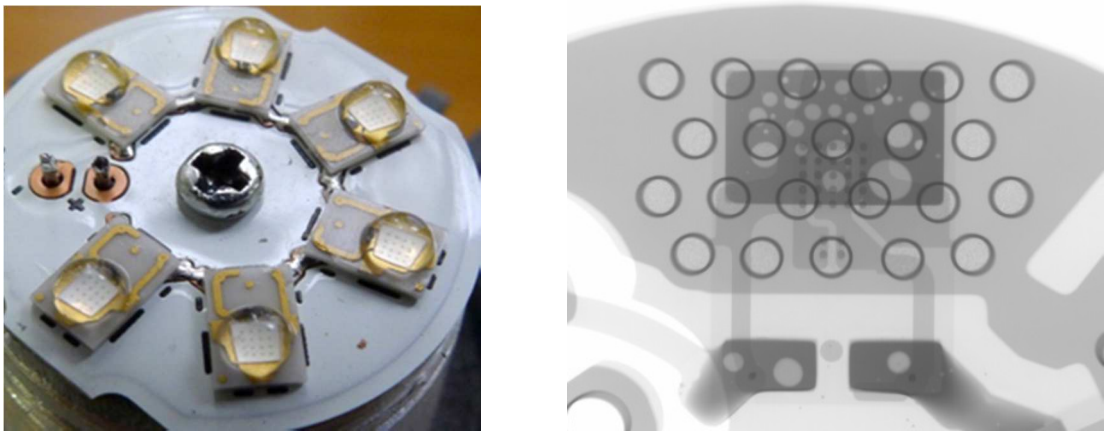

Figure 5.4 - SSL Lamp LED board: a) FR4 LED board for 400 lumen SSL lamp; b) X-ray image

During the research, some of simulation models (Figure 5.5) were further adjusted so the distribution of the bubbles in the solder layer was proportional to the most common real distribution and has been done examination of their impacts on lifetime of the whole product. The bubbles cause the problem mostly during the low cycle thermo mechanical

lifetime evaluation because they behave as a crack seeds and at the same time they reduce the solder joints strength. Figure 5.6 and Figure 5.7 show that due to the bubbles in the solder layer more extensive damage of the structure can be seen and formation of higher equivalent built-in stress just after fabrication process of investigated LED board is detected. This board has been further loaded with temperature cycles in the range of 0 - 90 °C and indicated bigger creep strain rate (Figure 5.8). Due to above mentioned we can expect the earlier damage formation in investigated structure and thus reducing of the whole product lifetime. The level of detail examination of the product has the direct relationship with the quality of the subsequent lifetime estimation.

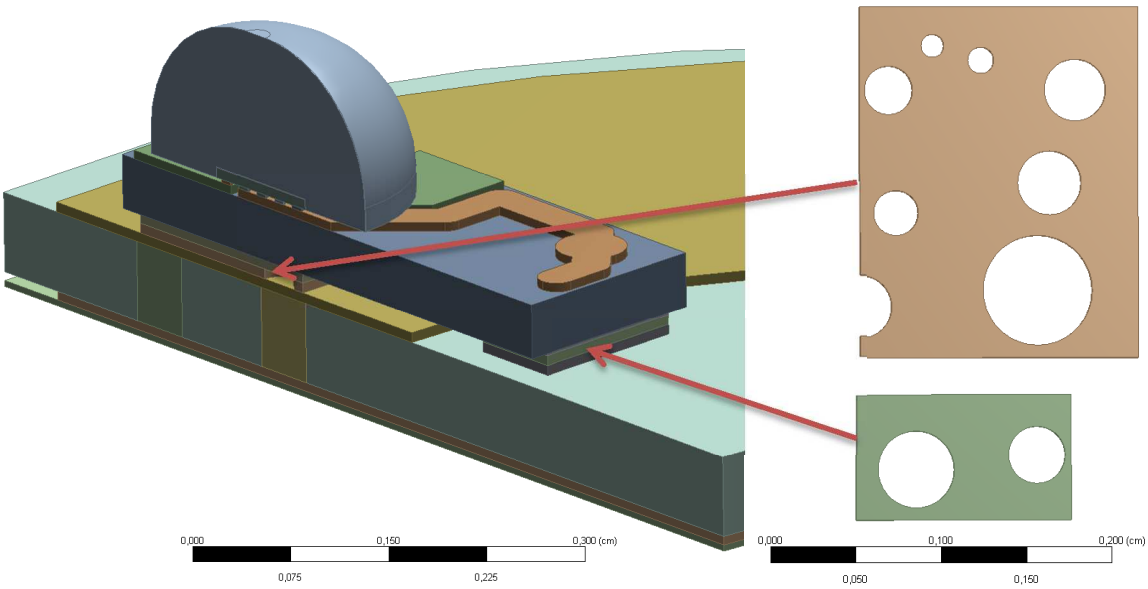

Figure 5.5 - SSL Lamp master LED board model including bubbles in solder layer

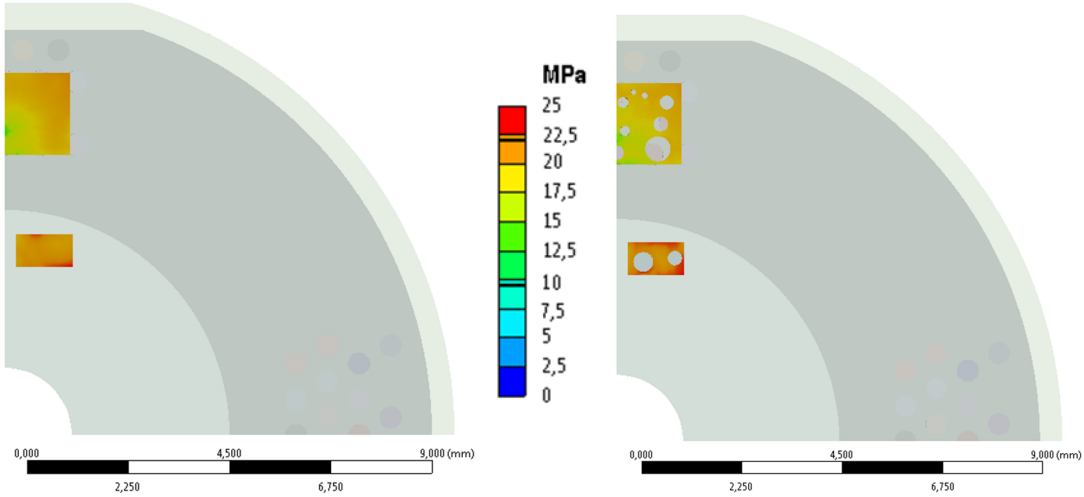

Figure 5.6 - Built-in stress at room temperature (20 °C) just after fabrication process a) Ideal model of FR4 LED board; b) Realistic model of FR4 LED board

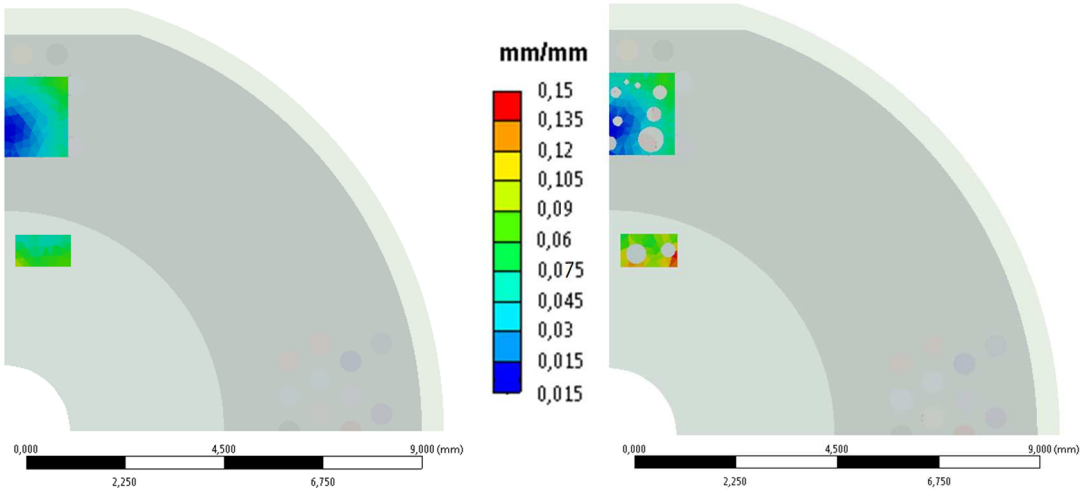

Figure 5.7 - Creep strain at room temperature (20 °C) just after fabrication process a) Ideal model of FR4 LED board; b) Realistic model of FR4 LED board

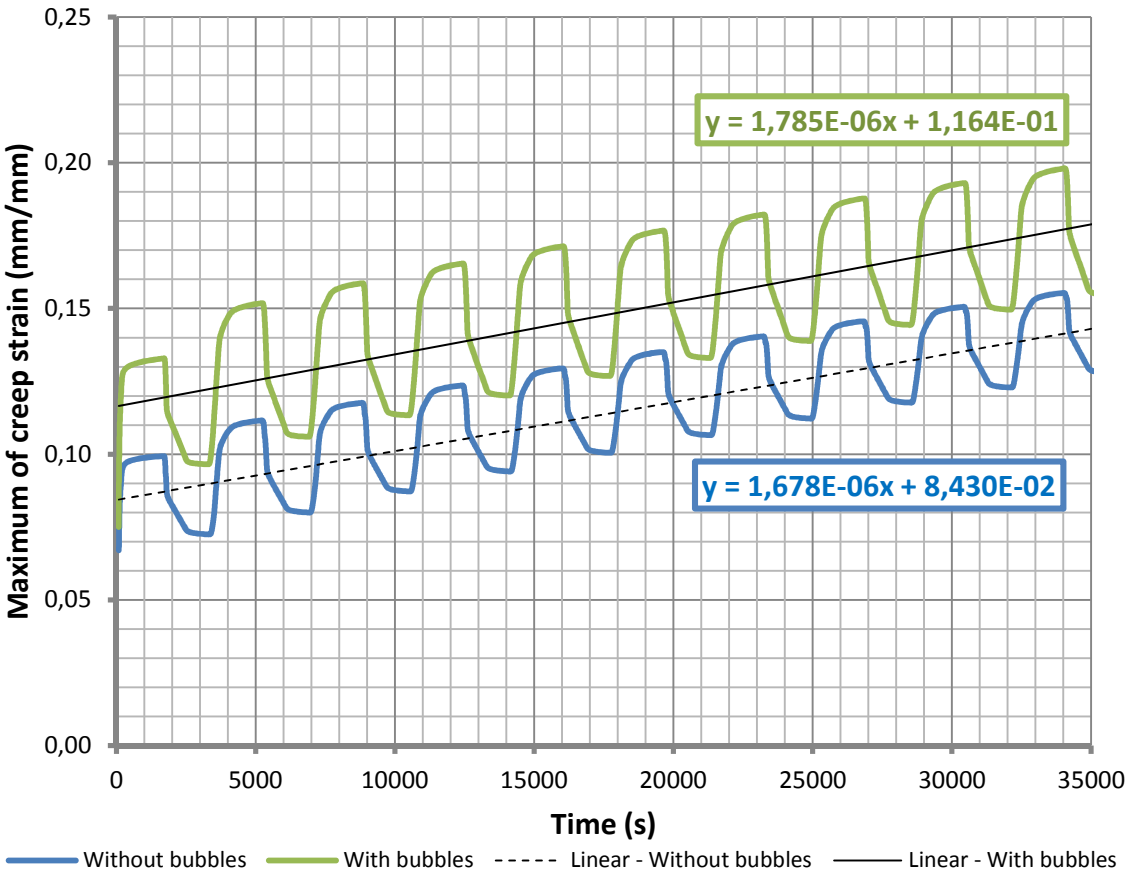

Figure 5.8 - Creep strain rate comparison between models without bubbles and with bubbles

5.3. Material Parameters Database which Includes Nonlinear Behaviour

The validity of simulation results are limited not only by the precision of the 3D model and its mesh, but also by the accuracy of the material properties data. In the SSL lamp simulation model (Figure 5.2) sixteen different materials are used. Thermal and mechanical coefficients for each of these materials were taken from different sources [B31 to B62]. Moreover, in some cases the material properties are not defined consistently for all sources. Different sources refer to not the same values for given material properties because of different measuring conditions and material quality.

Table 5.1 - Thermal and mechanical material properties used for SSL lamp simulation

Material	Thermal parameters		Mechanical parameters				References
	Thermal Conductivity	Specific heat	Thermal expansion	Young's modulus	Poisson ratio	Mechanical behavior	
	λ (W/mK)	Cp (J/kgK)	α_E (e-6/K)	E (GPa)	ν (-)		
GaN	130	490	5.6	200	0.35	Elastic	[B31, B58]
Silicon	130	700	2.46 @ 20°C	170	0.27	Elastic	[B1, B37, B38]
Aluminium alloy	144 @ 0 °C	880	23.4	70	0.33	Plastic	[B38, B48]
Copper	400	385	17	110	0.35	Plastic, creep	[B38, B40]
Brass Ni	122	380	20	100	0.33	Plastic	[B38, B48]
Glass	1.1	840	8	70	0.25	Elastic	[B56, B57, B38]
Polycarbonat	0.2	2000	50	5	0.33	Elastic	[B33, B60, B56]
Silicone	0.22	1460	220	1	0.49	Elastic	[B33, B32, B56]
Via filler	80	385	17	1.1	0.35	Plastic	[B51, B61, B48]
PBT	0.27	1700	25	9	0.3	Elastic	[B56, B57, B48]
Polyamide6	4	1130	40	15	0.4	Elastic	[B56, B57, B48]
FR4	0.25	1085	23.4	70	0.33	Plastic	[B58, B59]
LED board	40	1085	23.4	70	0.33	Elastic	Estimated
Chip bonding mat.	64	385	22	25 @ 0 °C	0.36	Plastic	Estimated
Solder SAC305	64	385	22	250 @ 0 °C	0.36	Plastic, creep	[B61, B62, B56]
Leadframe filler	0.26	1460	30.6	5 @ 23 °C	0.49	Plastic	[B35, B36, B37]
Ceramic	21	880	55 @ 25 °C	370 @ 22 °C	0.22	Elastic	[B49, B50]

For achieving the more accurate results it is necessary to make precise measurements of parameters of specific samples of each material. It should be taken into account that some of the values are dependent on the technology of manufacturing process, especially on the temperature profile and the quality of production characterized by achieving the good homogeneity of the structure.

The thermal and mechanical material properties used for the model of the LED lamp are summarized in the Table 5.1. The mechanical parameters shown in the table is expected to be necessary in simulations of thermo-mechanical behaviour. For common simulations in small-scale loading is usually considered only the elastic behavior of the material and suffice the parameters specified in Table 5.1. Because of the high temperature and mechanical stress and due to the efforts to achieve high precision, I added simulation of nonlinear material behavior.

The nonlinear plastic behaviour of materials is specified by setting temperature dependence stress-strain curves. Some important basic characteristic can be also set as temperature dependent. The temperature dependent stress-strain curves have to be specified for metal parts exposed to high thermal stresses. For example the quasilinear approximations of the stress-strain curves for copper are shown on Figure 7.2 [B40]; curves for lead-free solder are shown on Figure 5.10 [B62].

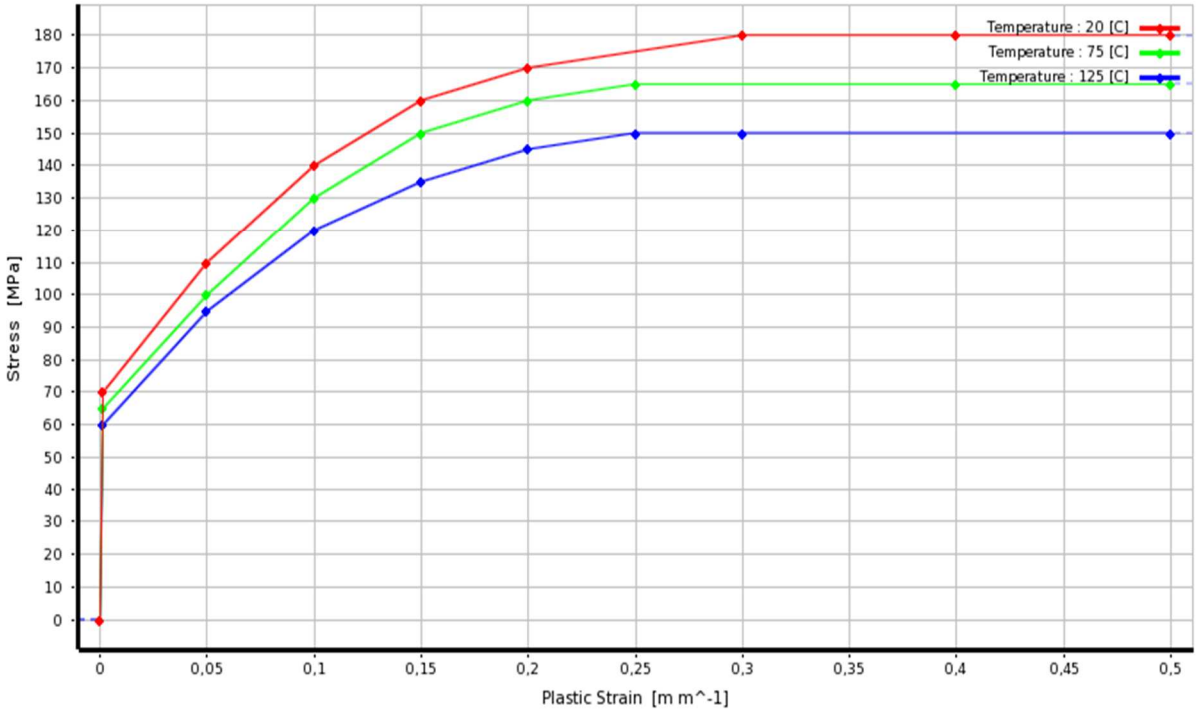

Figure 5.9 - The temperature dependent stress-strain curves for copper – quasilinear approximation for simulator [B40]

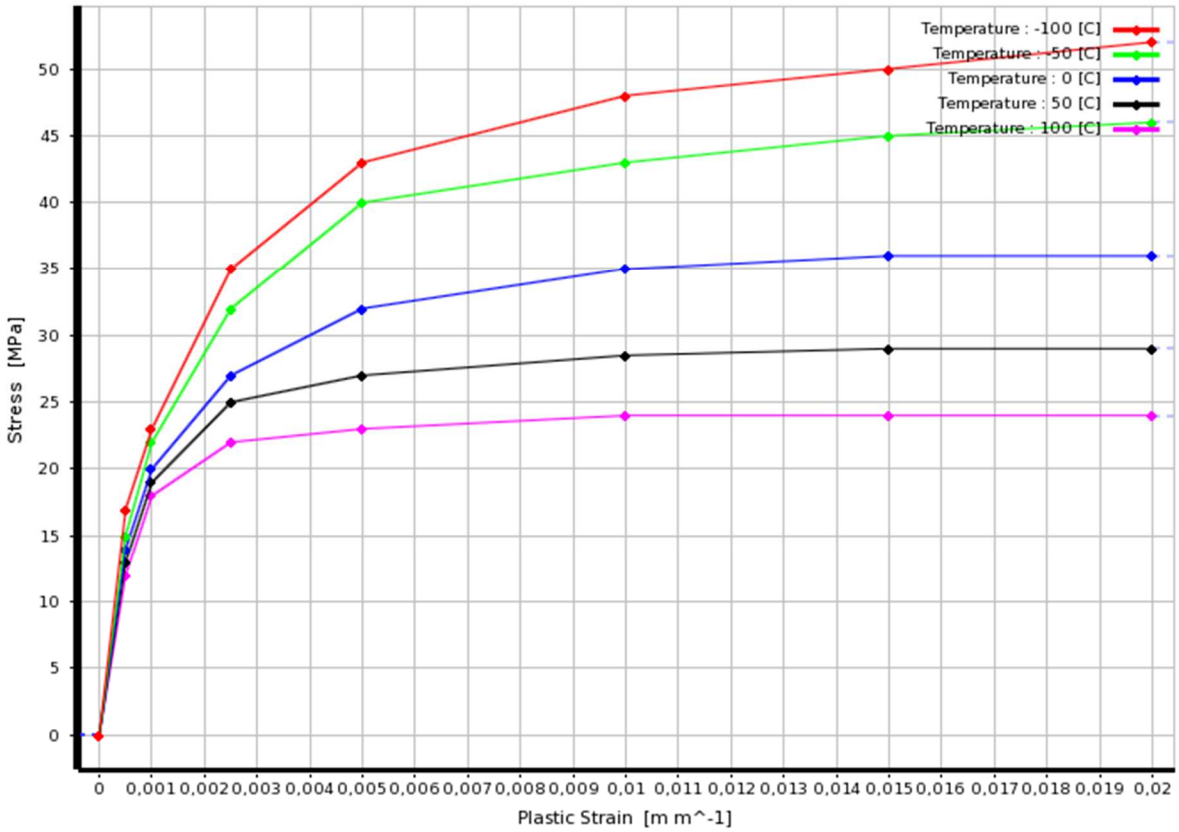

Figure 5.10 - The temperature dependent stress-strain curves for SAC305 SnAgCu solder - quasilinear approximation for simulator [B62]

This allows reaching the high precision of the simulations opposed to usually published work. Differences between linear and nonlinear simulations will be shown in the chapter 7.2.

6. Thermal Management Evaluation and Improvement

The very important part of the SSL LED Lamp design for the lifetime improvement is to keep the LED junction temperature as low as possible. The problem of cooling is commonly solved by methods of calculations of adequate thermal circuits. By using this method we can calculate thermal resistance of sets of components or equivalent temperatures at the interfaces [B63]. These calculations are very approximate especially for complex shape parts. My work aims to make the methodology for exact simulations of thermal distribution by using FEM tools and validate it by the set of measurements. My method allows knowing the exact location of the cooling problem and quickly improves the design.

From the reliability point of view the most thermally stressed is LED junction. The junction temperature depends on the heat generated by loses during light emitting and on the quality of thermal dissipation. In SSL lamp the heat is dissipated from the LED die through the LED package, solder pads, LED board, TIM layers and heat sink to the ambient. Typical thermal resistance network of packaged LED is shown in Figure 6.1. LUXEON LEDs are used in the SSL lamp under development.

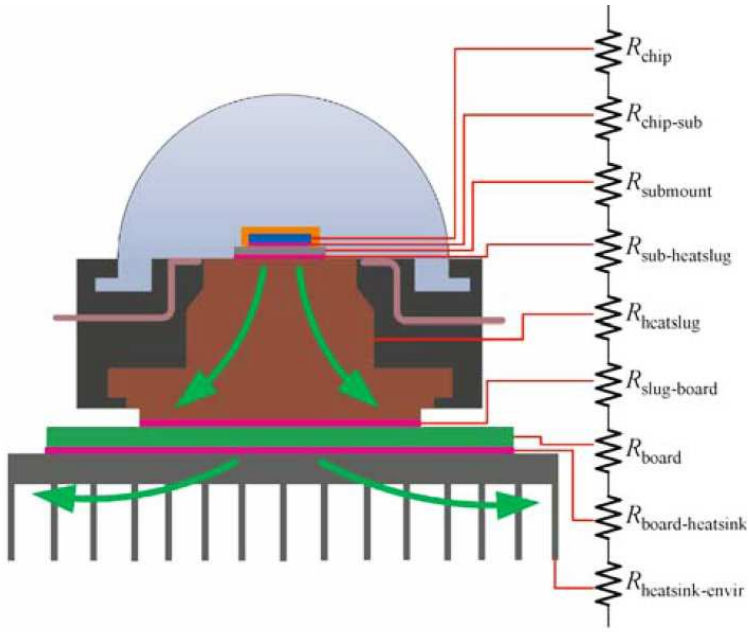

Figure 6.1 - Thermal resistance network of Luxeon LED [B25]

The LED chip used in LUXEON LEDs is encapsulated in the low thermally conductive transparent resin. The chip is connected by flip-chip technology to the LED package which conducts almost all generated heat from LED junction to thermal and electrical pads placed on the bottom of LED package. LED packages are typically soldered on the LED board which is mostly attached by the TIM (thermal interface layer) to heat sink where the heat is distributed to ambient. In case of designed retrofit SSL lamp aluminium thermal cone is placed between the TIM and heat sing (Fig. 5.2).

The lifetime of LEDs is highly dependent on operating temperature. High working temperatures results in accelerated lumen depreciation of LED chips and thus shortened its useful life. The graph shown on Figure 6.2 illustrates the typical curve of junction temperature (T_j) vs. Lifetime. It shows that by maintaining T_j at 25 °C designer can expect to have the lifetime of 300k hours (>30 years) continuous usage before the LED output intensity will degrade by 30 %. However with a T_j of 50 °C the LED will degrade 30 % intensity in 50 000 hours (~5 years). Generally, every 10-15 °C increase in working temperature reduces lifetime to half. The research is aggressively improving the durability of LEDs at higher operating temperatures. Many produced LEDs have 30 % lumen intensity degradation after more than 50 000 hours with drive currents more than 1000 mA and T_j around 120 °C. High working temperatures affects not only lifetime but also the short-time performance such as colour shift and actual light output reduction. This implies the need to preciously design thermal management of SSL laps, quality of cooling directly affects lifetime of designed product.

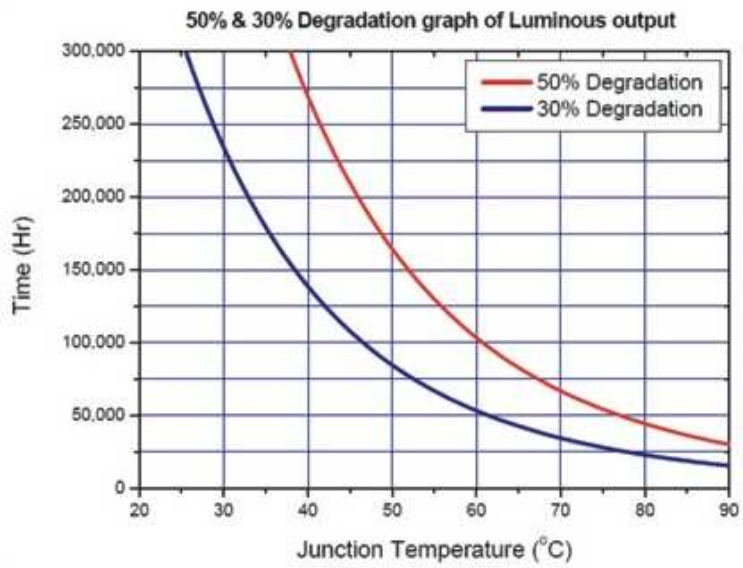

Figure 6.2 - Useful lifetime of high brightness white LEDs at different operating temperatures [B64]

6.1. Simulation of Thermal Distribution in Existing SSL Lamp

The thermal distribution of simulated model can be obtained by finite element simulation (in this case ANSYS tool is used). FEM software compute heat generation, heat transfer and temperature distributions by using heat equations. For simple case of isotropic homogenous material, the heat equation [B109] can be written as:

$$\rho . C_p . \frac{dT}{dt} = \nabla(K \nabla T) \quad (1)$$

Where ρ is the density (kg/m^3), C_p is the specific heat capacity (J/(Kg.K)), K is the thermal conductivity (W/(m.K)) and T is the temperature (K). In our case equation have to be extended because some parts are generating heat in volume by Joule's heat or by nonradiative electron transitions between energy levels.

$$\rho . C_p . \frac{dT}{dt} = \nabla(K \nabla T) + q + \sigma . |\nabla V|^2 \quad (2)$$

Where q is the heat density (W/m^3), σ is the electrical conductivity (Ω·m), V is the electric potential (V). Material with internal heat generation in real case have to reach steady state (temperature reaches finite value) so parameter q also includes heat which is transferred out of structure. It can be done by done by direct advection, conduction, convection or by radiation.

In case of SSL lamp modelling, convection plays dominant role, because air can freely move around the lamp and also in the Led lamp. Moving air transfers heat out of the structure, heat density can be computed from Newton's cooling law [B109] as:

$$\frac{dQ}{dt} = h . A . (T(t) - T_{env}) = h . A . \Delta T(t) \quad (3)$$

$$q = h . \Delta T(t) \quad (4)$$

Where q is the heat density (W/m^3), Q is the thermal energy (J), h is the heat transfer coefficient (W/m^2 K), A is the surface area of the heat being transferred (m^2), T is the temperature of the object's surface and T_{env} is the temperature of the environment (suitably far from the surface). The heat transfer coefficient depends on physical properties of the body and the situation in which convection occurs. It has to be found experimentally for each analysed system.

The second significant phenomenon which transfers heat from SSL lamp structure is the Radiation. This occurs on faces which are heated near to 400 K or more and it can be calculated from Stefan-Boltzmann radiation law [B109] as:

$$\frac{dQ}{dt} = e . \sigma . A . T^4 \quad (5)$$

$$q = e . \sigma . T^4 \quad (6)$$

Where e is the emissivity of the surface (-), T is the temperature of surface (K) and σ is the Stefan-Boltzmann constant (5.670373×10^{-8} W.m^{-2}.K^{-4}).

The equations allow calculation of the thermal behavior only in elementary bodies or in very simple structures. As already mentioned, due to the complexity of the structure it is necessary to perform calculations at discrete points (FEM), where for each node and connection line will be prepared the set of thermal equations. Determination of the number of points in the structure and its distribution is the compromise between accuracy and duration of simulation. By examining of this dependence I came to the distribution shown in Figure 6.3, which contains 115 758 nodes distributed in proportion to the complexity of the structure parts, the given loading and the required calculation precision of temperature

equations. The thermal properties of each material parts of the structure are set according to Table 5.1.

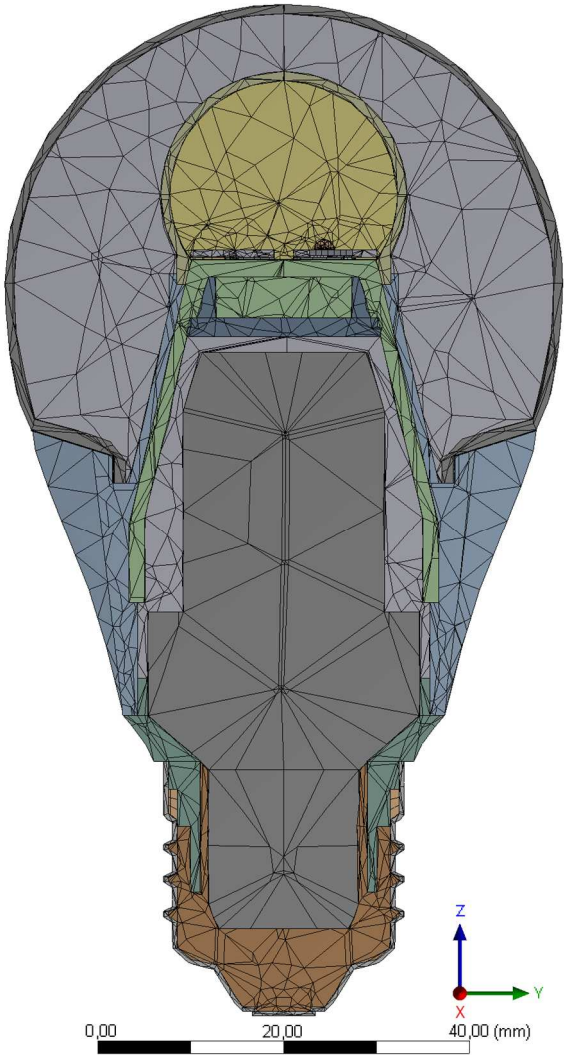

Figure 6.3 - Mesh distribution in SSL lamp model

For solving the equation we need to set boundary conditions and parameters such as:

- Heat generation caused by Joule heating in all electrical parts
- Heat generation produced by loses in light conversion dome and in light bulb
- Heat convection on the outside parts that are in contact with the air
- Radiation (determined for all model faces that are in contact with the air

In our case the heat generation in SSL lamp takes place in LED driver 1.2 W (was measured by CNM Barcelona [B65]), in six LEDs 4 W (calculated from datasheet) and in polycarbonate light conversion dome 1.5 W (evaluated by optical measurement by CEA Grenoble)[3].

[3] Some of the optical and thermal measurements were done by our project partners. The issues of SSL lamp design were solved under an ENIAC Joint Undertaking CSSL project (Grant Agreement No. 120219).

The thermal convection coefficient for outer surface of glass bulb was set to 2.5 W/m^{2}K; 1.5 W/m^{2}K for heat sink; 20 W/m^{2}K for metal cap. Values were adjusted according to material study and measurement. The radiation affect to ambient (temperature of 22 ^{o}C in simple case) was also taken into account for all inner and outer parts of the lamp which are exposed to the air. It is very important to define emissivity coefficients for all materials of used lamp components.

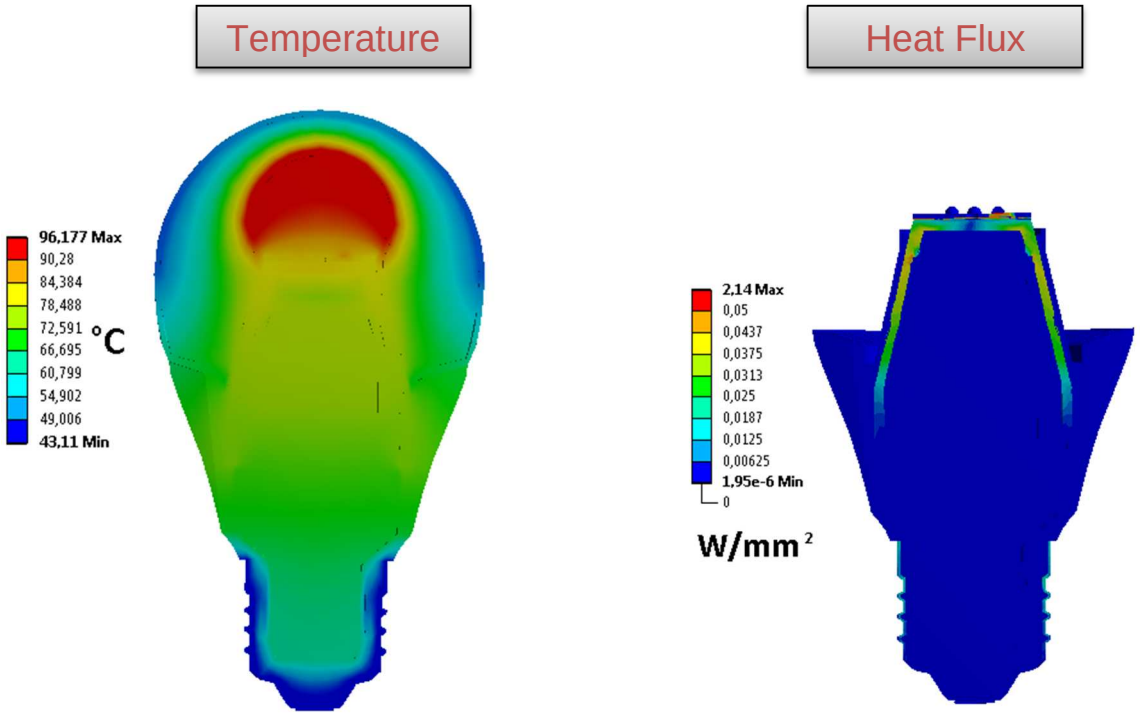

Figure 6.4 - Results of thermal simulation of 3D model of SSL LED lamp.

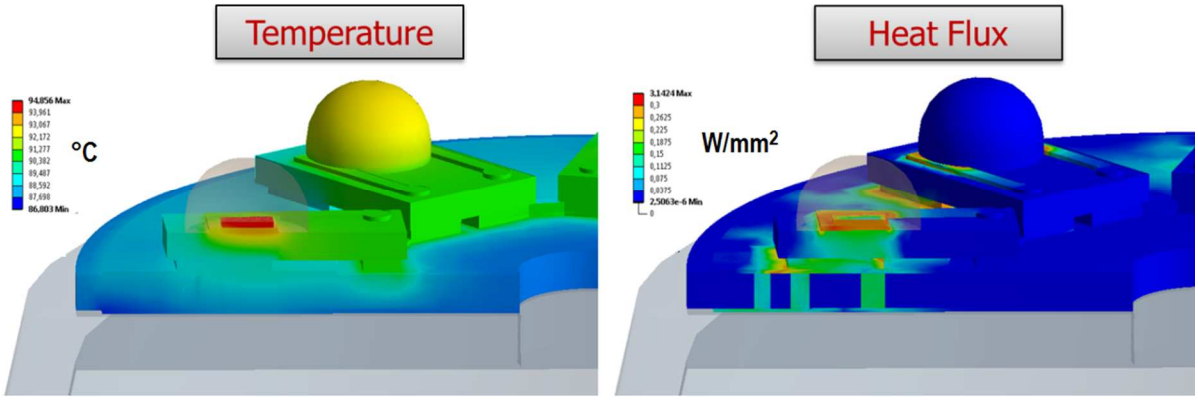

Figure 6.5 - Detailed 3D model of LED board with results of thermal simulation. Die temperature is 95.2 °C

Figure 6.4 and Figure 6.5 show results of precious thermal simulation of complex detailed model of SSL lamp[4]. Determined thermal distribution and heat flux can be used for thermal management improving. This allows reliability enhancement.

[4] The work was published at international conferences [A17] and [A18]

6.2. Thermal Validation and Measurement

The complex thermal simulations cannot be done without the set of measurements that prove the results of consequent accuracy of input data. Measurements were performed by two ways so that the results could be compared.

The first measurement (directly by sensors) requires preparing measurement test set-up which allows obtaining temperatures in defined places on the surface of the measured product. Measuring methodology and set-up allows getting comparable results from more samples of the same product or more prototypes from multiple phases of development. The SSL lamp was placed in the reflection-less thermal chamber (Figure 6.7a).

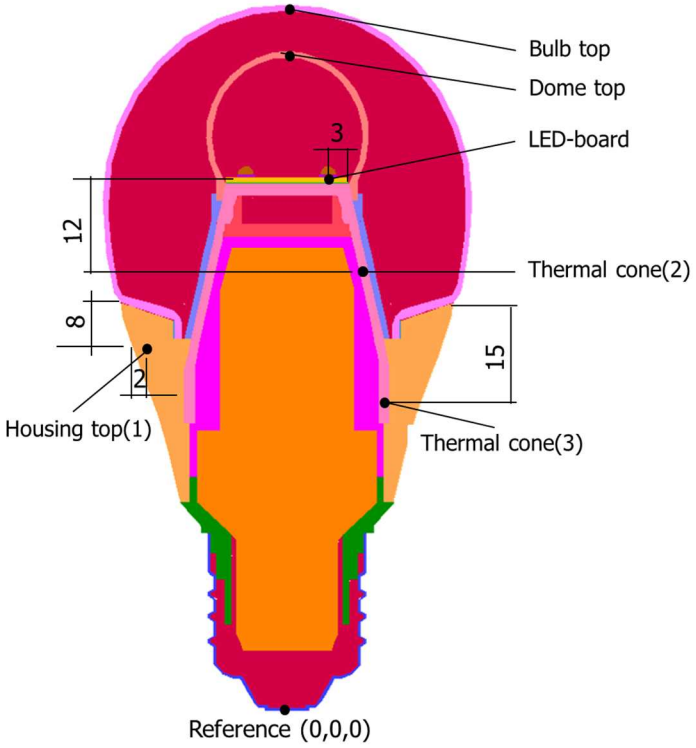

Coordinates to be used in simulation model

	X [mm]	Y [mm]	Z [mm]
Bulb top	0.0	0.0	108.0
T_junction	-3.5	6.1	82.7
LED Board	0.0	8.0	82.0
Thermal cone(1)	-3.5	6.1	81.8
Thermal cone(2)	-6.5	11.2	65.0
Thermal cone(3)	-7.9	13.6	47.5
Housing top(1)	-10.0	20.0	54.8
Housing top(2)	-9.1	17.1	54.8
Shell	-6.5	11.3	29.1
Ambient	0.0	52.0	92.0

Figure 6.6 - Measuring points locations

The thermal measurement was performed in the room with the air temperature control (23 ^{o}C). The temperature was measured as the function of time at several SSL lamp monitor points inside and outside of the lamp using SMD PT1000 micro-scale temperature sensors (Figure 6.6, Figure 6.7b). The temperature sensors are placed on the LED board thermal cone heat sink top of the dome and top of the lamp. The ambient air temperature in the temperature chamber was measured as well.

The Figure 6.8 shows the results of the direct temperature transient measurement with temperature sensors. The steep temperature growth is observed at the beginning of the test within 2 hours the temperature reaches the steady-state condition. The figure also shows the results of the steady-state ANSYS simulation at the time of 6 200 seconds where the temperature transient has already reached the steady state. The calculated and measured temperatures agree with the good tolerance.

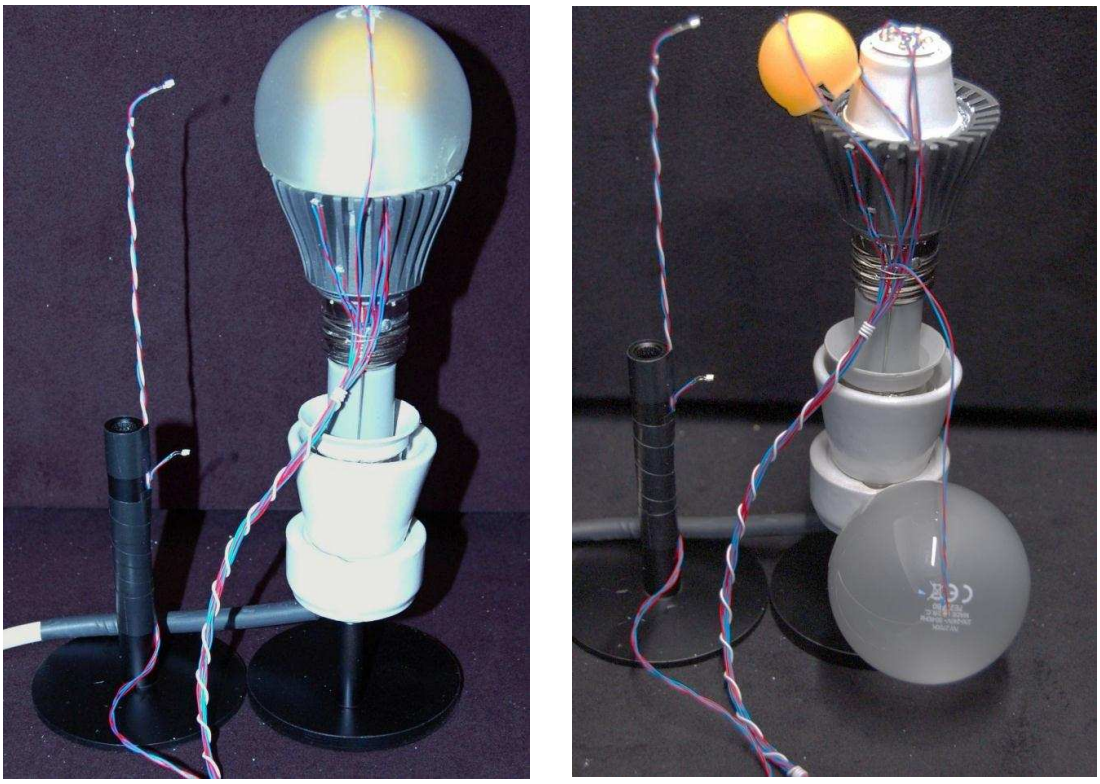

Figure 6.7 - Measurement setup in reflection-less thermal chamber. a) Assembled SSL lamp. Wires leads to temperature sensors placed inside and outside of the lamp. Temperature sensors measuring ambient temperature are also clearly seen (left). b) Dismounted SSL lamp

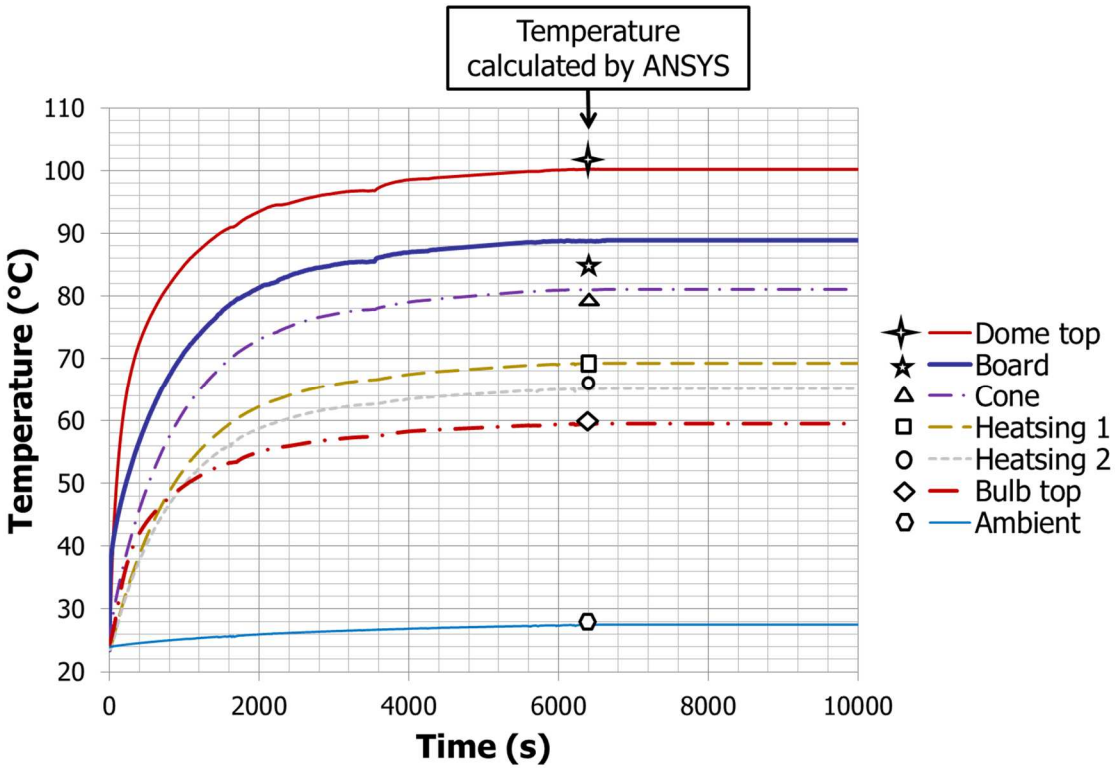

Figure 6.8 - Measured (line) and calculated (symbol) temperatures of the SSL lamp

The difference between simulated and measured temperatures of the dome (108.3 °C ANSYS simulation, 100.2 °C measurement) is caused by not modelling the air flow inside the dome and inside the bulb. The air flow can in reality cool down the surface of the dome. The simulation of the air flow can be also done by FEM tools [B26], [B66] and [B77].

The simulations of such complex components without homogeneous temperature distribution require the high computing power. Therefore they are currently made only in the large research centres. Results of shown thermal simulations and measurements are also used for solving the CSSL project[5]. Therefore, the simulation of the air flow around and inside of the SSL lamp were implemented in collaboration with the TNO Eindhoven research center (Figure 6.9). The performed simulation faithfully models reality.

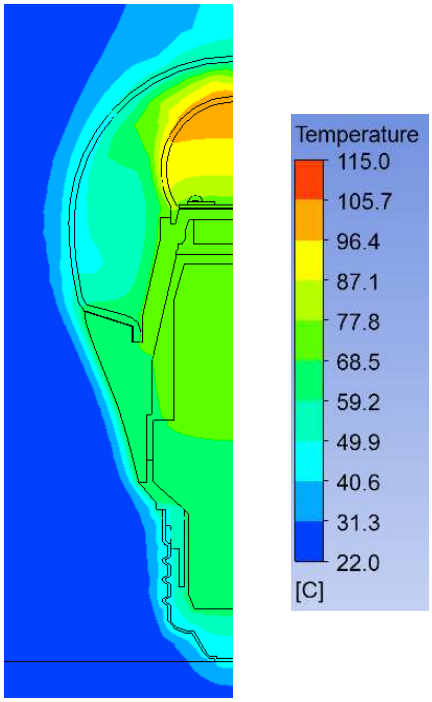

Figure 6.9 - FLUENT fluid flow simulation done by TNO Eindhoven partner

The second measurement method uses the IR (infra-red) camera imaging to obtain temperature distribution of the SSL lamp. In this measurement method the emissivity coefficients must be known for all materials. In this case, there are two approaches how the problem with unknown emissivity can be solved.

- The emissivity of all components can be measured by simple methodology where reference object with known emissivity is heated up to defined temperature together with measured component. The emissivity on IR camera is set to that of reference body and IR image is taken. Then the emissivity can be calculated from the Stefan-Boltzmann Law.
- A black strip with defined emissivity can be made on each part (Figure 6.10). The temperature is than sampled and measured on the black strip, which has the same emissivity for all materials.

[5] Consumerizing Solid State Lighting Project (CSSL) supported by the ENIAC Joint Undertaking (Grant Agreement no. 120219).

All the IR measurements have to be done in reflectionless environment; measured values are not influenced by the reflected radiation. The reflectionless characterization chamber[6] for thermal imaging equipped with the adjustable enforced cooling was made for specified application [8]. The inner surface of the chamber is designed for absorbing radiation in the IR spectrum. The air velocity and thus the interior temperature can be controlled by the built-in regulator on the basis of measuring the temperature in the chamber using PT1000 temperature sensors placed at defined positions. The designed chamber is the low-cost solution to the problem, but provides results comparable with expensive professional equipment.

Figure 6.10 - SSL lamp components with black strip used for IR measurement

The Figure 6.11 shows temperature distribution of the SSL lamp sampled by the IR camera. The temperature distribution inside the SSL lamp was obtained instantly after the glass bulb and the light conversion dome was dismounted to keep the temperature that is not affected by air cooling.

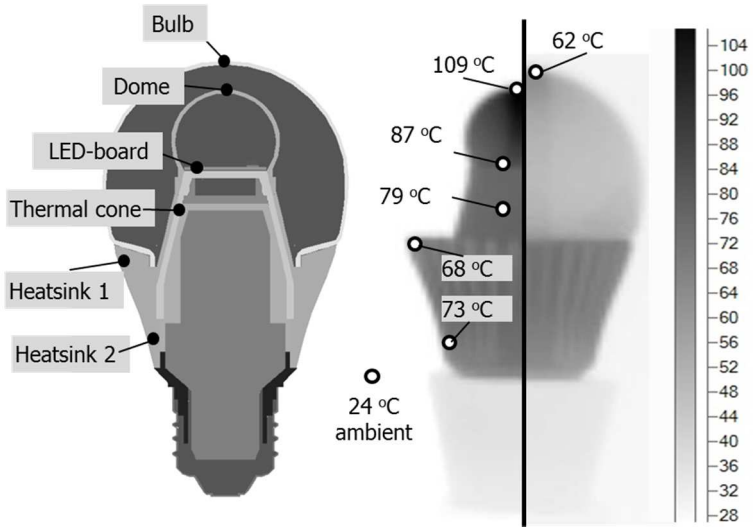

Figure 6.11 - Temperature distribution obtained by IR camera. a) Thermal sensors location used for temperature measurement and comparative temperature samples from simulations. b) Thermal distribution under glass bulb and distribution on the surface

[6] The reflectionless characterization chamber was developed especially for the LED lamp thermal imaging and it is registered as the functional model [A22]

Table 6.1 shows the comparison between simulated and measured temperatures[7] in the same points which is defined on Figure 6.6. The simulation of equivalent model of LED lamp was done not only in ANSYS software but also in COVENTOR. This is intended for MEMS design and for behaviour simulations in small scale therefore it does not support all equations for nonlinear thermo mechanical behaviour. Simulations in ANSYS better reflect the real behaviour of designed SSL lamp.

Table 6.1 - Simulated and measured temperatures comparison

	Temperature (°C)			
	Simulation		Measurement	
	ANSYS	COVENTOR	Temp. sensors	Thermocamera
Bulb top	59.6	55.1	59.5	62.0
Dome top	108.3	105.1	100.2	109.0
Board	85.6	84.3	88.9	87.0
Cone	80.6	79.8	81.1	79.0
Heatsink 1	67.1	68.8	65.2	68.0
Heatsink 2	70.8	72.1	69.3	73.0
Ambient	23.0	23.0	24.2	24.0

6.3. Methods for Lifetime Improvement – Lowering of LED Temperature

Reliability and lifetime of LED chip can be done by decreasing of LED junction temperature by improving of heat conduction and dissipation. This can be done in various ways.

The first way is to use an alternative highly temperature conductive materials that can improve heat conduction to ambient. To predict the influence of new materials, material parametric analyses were carried out to explore future thermal management improvements.

Figure 6.12a shows the influence of thermal conductivity of the housing (heat sink) on LED chip characteristic temperature (figure shows also temperature change of other main parts). If we use aluminium for housing instead of polyamide 6 the LED chip temperature drops about 6 °C. However the aluminium is more expensive material and also the fabrication of aluminium housing is more expensive. The effect of the temperature drop can be reached also by another technique, for example by better housing design. This part of work was also done by our project partner TNO Eindhoven. They were looking for influence between the junction temperatures and thermal housing design. They studied parameters such as cone material, housing material, number and shape of the cooling ribs etc. (Figure 6.13).

[7] The work was published in impacted journal Radioengineering in April 2012 [A3]

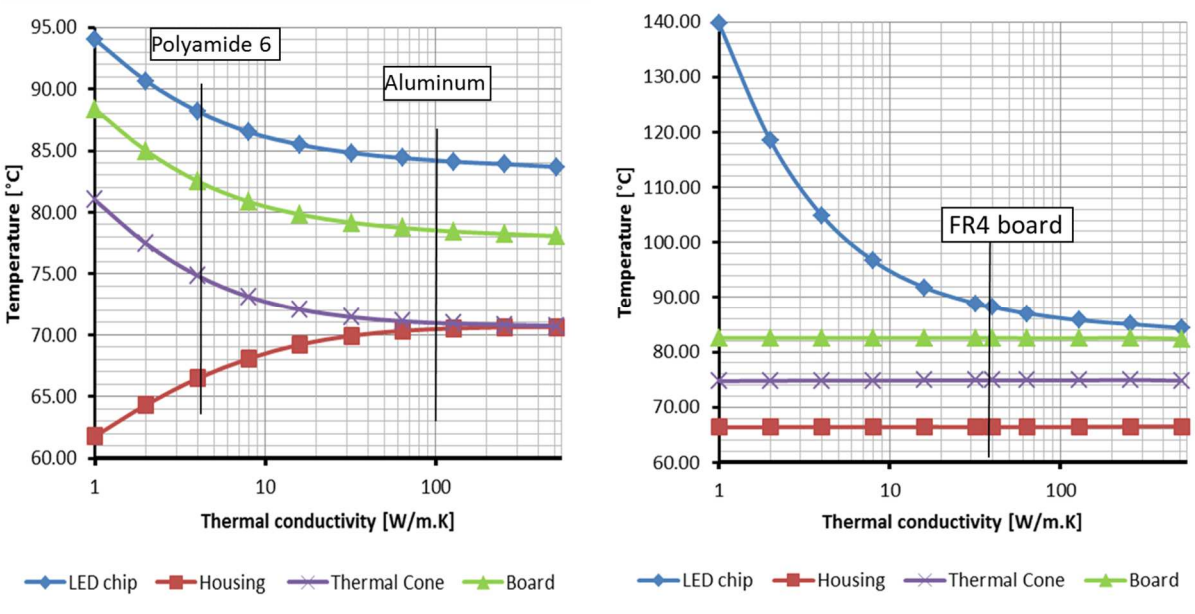

Figure 6.12 - Thermal conductivity parametric study that was swept in range 1 to 500 W/mK. a) Housing (heat sink) temperature difference; b) LED board where value for current FR4 board is marked.

The second way how to reach lower junction temperature is thermal optimization of the LED board. Figure 6.5 shows high value of heat flux in volume of LED board. Design of this part and used materials have significant impact on quality of heat transfer from LEDs to housing. LED board also provides additional functions such as current conduction to the LEDs, mounting, insulation etc. We can say that LED board is critical part from thermal and mechanical point of view.

Figure 6.13 - Examples of thermal cone and housing designs done by TNO Eindhoven

Figure 6.12b shows the influence of LED board basic material thermal conductivity[8]. We can make the point on results of simulation of current board design. Measured value of thermal conductivity of the FR4 LED board with thermal vias is 40 W/m.K. The improvement of LED board thermal resistance can be hardly done by material change or design improvement. We have to use another technology of LED board design.

[8] The work was published at international conferences [A17] and [A18]

For better insight in the thermal behaviour we have to define some main thermal parameters of LED board. Firstly, we can make detailed thermal resistance equivalent model of LED board with mounted LEDs. Figure 6.14 shows thermal model representing connection between components for heat generation and components for heat conduction.

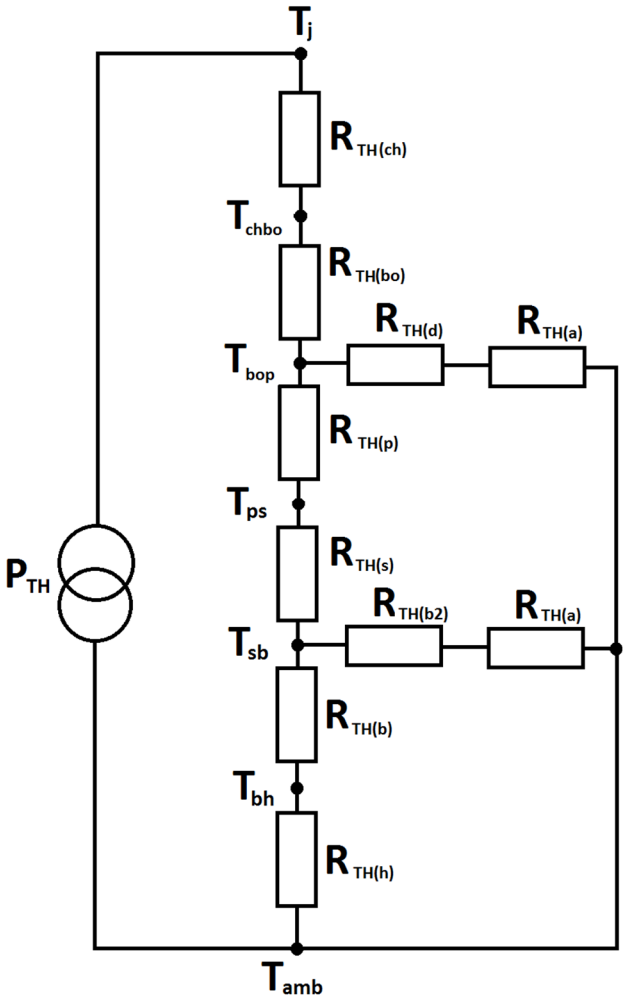

P_{TH} is the power dissipated by the device
T_J is the junction temperature in LED diode
T_{chbo} is surface temperature where the LED chip is attached to the chip bonding material
T_{bop} is surface temperature where the LED chip bonding material is attached to the LED package
T_{ps} is surface temperature where the LED package is attached to the solder pads
T_{sb} is surface temperature where the solder pads is attached to the LED board
T_{bh} is surface temperature where the LED board is attached to the heat sink and other components of Light bulb
T_{amb} is the ambient temperature
$R_{TH(ch)}$ is the thermal resist. of the LED chip
$R_{TH(bo)}$ is the thermal resistance of the LED chip bonding material
$R_{TH(d)}$ is the thermal resistance of the transparent LED lens
$R_{TH(p)}$ is the thermal resist. of the LED package
$R_{TH(s)}$ is the thermal resist. of solder pads
$R_{TH(b)}$, $R_{TH(b2)}$ is the thermal resistances of LED board
$R_{TH(h)}$ is the thermal resistance of heat sink and other components of Light bulb
$R_{TH(a)}$ is the thermal resistance of air

Figure 6.14 - Equivalent thermal model of LED board

During the creation and evaluation of new designs we are forced to find effective way how to compare it. We should choose only the most important parameters which we can evaluate and also influence by better design at the same time.

It can be:

- T_J - the junction temperature in LED chip – because of the high thermal conductivity of GaN, measured temperature in volume of LED chip is homogenous with the good tolerance
- T_S - mean value of surface temperature where the solder pads is attached to the LED board
- T_B - surface temperature where the LED board is attached to the heat sink and other components of Light bulb, this temperature is measured just under thermal pad of LED package which is also the place of highest heat flux

Then we can calculate:

- $R_{TH(p)}$ - the thermal resistance of the LED package between LED junction and thermal pad with solder
- $R_{TH(b)}$ - the thermal resistance of bottom of LED board evaluated in the place under LED thermal pad

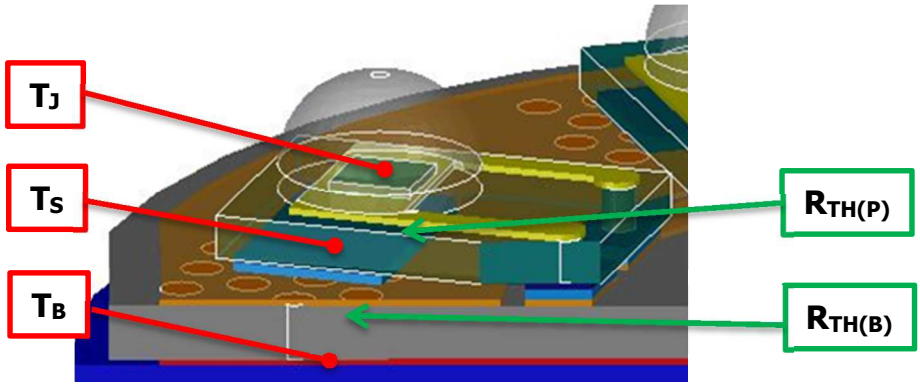

Figure 6.15 - Most important thermal parameters of LED board

Thermal resistances can be evaluated from simple definition:

$$R_{TH(P)} = \frac{T_J - T_S}{P_{TH}} \quad (7)$$

$$R_{TH(B)} = \frac{T_S - T_B}{P_{TH}} \quad (8)$$

Where P_{TH} is thermal power dissipated by LED junction (W). This mainly depends on LED chip design and input electrical power. Electrical power is transformed into optical power (luminous flux) P_{OP} and thermal power P_{TH}.

$$P_{EL} = P_{TH} + P_{OP} \quad (9)$$

$$P_{EL} = I_F . V_F \quad (10)$$

Where I_F is the LED forward current (A) and V_F is the forward voltage drop (V). Dependence between P_{TH} and I_F respectively P_{OP} on I_F was measured for LEDs used in CSSL project by project partner CNM Barcelona. Result of measurement is an approximative equation which shows dependence of luminous flux (P_{OP}) on forward current at 25 °C:

$$P_{OP} = 0.105 + 1.1286 \times I_F \quad (11)$$

For simple comparison of new LED board design we assume same LED chip which can be used with standard LED package or with newly designed LF package. In our case where LUXEON rebel LEDs was used P_{TH} is set 0.561 W per LED chip according to measurement.

6.4. Method for Lifetime Improvement – LED Board Prototyping

The lifetime improvement can be simply done by making the new designs of LED boards. For this study, six different LED boards were designed and calculated with respect their thermal and mechanical behaviour. They are designed as possible replacement in designed 806 lumen retrofit SLL lamp.

The board itself is proposed in the following technologies:

- **FR4** (Fire Resistant) – well known low cost material composed of woven fiberglass cloth with an epoxy resin which is plated with Cu layers on both sides. In this case, 650 μm thick board with 80 μm Cu layers was used. The top Cu layer makes electrical connection between the LEDs. Higher thermal conductivity of FR4 the board was achieved by thermal vias (500 μm in diameter) placed under and around the thermal pads the of LED packages
- **IMS** (Insulated Metal Substrate) - consists of a metal baseplate covered by a thin layer of insulation layer and a metallic interconnection layer of copper. In our case, IMS500 was used where the main substrate is made from 500 μm thick aluminium plate. Interconnection layer (35 μm thick) is insulated by 50 μm of epoxy-based layer
- **AST** (Alumina Substrate Technology) – sintered ceramic substrate (96% Al_2O_3 alumina 1000 μm in this case) with printed silver conductive layer (14 μm thick). Shape of substrate is made by stamping of green sheet before sintering process in tunnel furnaces
- **LFM** (Lead Frame Mould) – newly developed type of board which is using injection moulding technology known from integrated circuit package fabrication process. Parts of board which have to conduct electrical current or heat flux are cut from 200 μm thick copper plate and moulded in lead frame by high thermal conductive plastic

Six diodes are soldered on each of the designed boards. For the simple comparison, standardly sold Luxeon REBEL LEDs (LXML-PR01-0500) are used. LED chip used in Luxeon LEDs is encapsulated in the poor thermally conductive transparent resin. Chip is connected by flip-chip technology to the ceramic LED package which conducts almost all generated heat from LED junction to thermal and electrical pads placed on the bottom of LED (Figure 6.16).

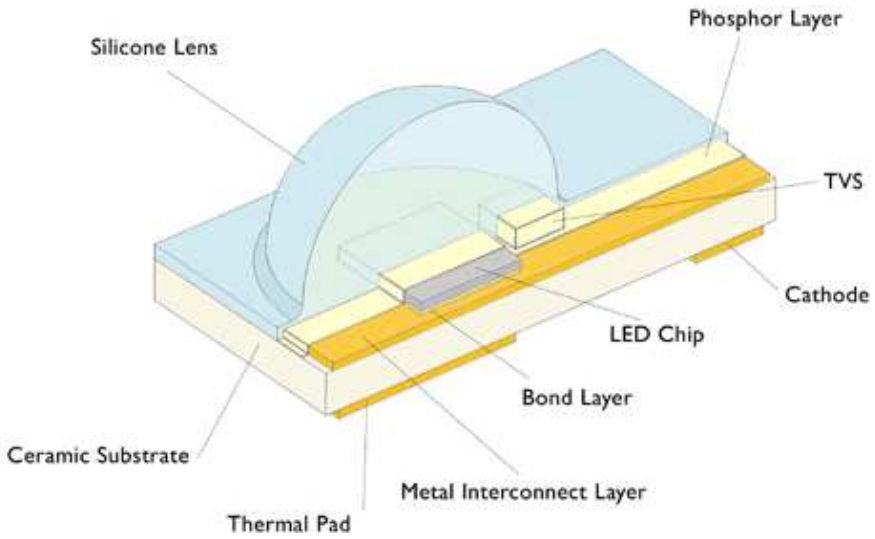

Figure 6.16 - Luxeon REBEL LED package [B44]

The same LED chip and the same bonding technology are used in new concept of LED package. This concept was developed to improve the heat transfer through package by using lead frame moulding technology. Main high conductive core is cut from 200 µm thick copper plate and moulded in lead frame by high thermal conductive plastic. LED chip is connected by flip chip bonding technology on copper core and consequently sealed in silicone (Figure 6.17). Bottom surface is covered by a solder mask.

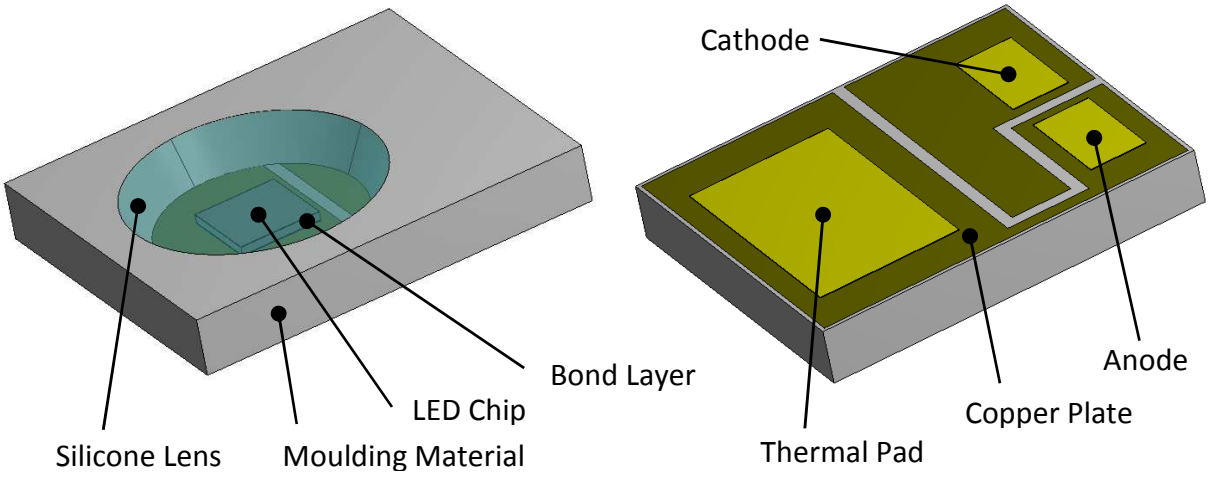

Figure 6.17 - New concept of LFM LED package (left - top view, right – bottom view)

LEDs are soldered on boards by standard lead-free solder SAC305. This alloy contains 96.5 % tin, 3 % silver, and 0.5 % copper. It falls under the JEIDA recommendation for lead-free soldering. It was chosen due to its cost, excellent fatigue resistance, excellent solder joint reliability and the best wetting in Sn/Ag/Cu Alloy category.

We can design many LED boards with using shown technologies. In this study there will be shown only these most interesting combinations (Figure 6.18).

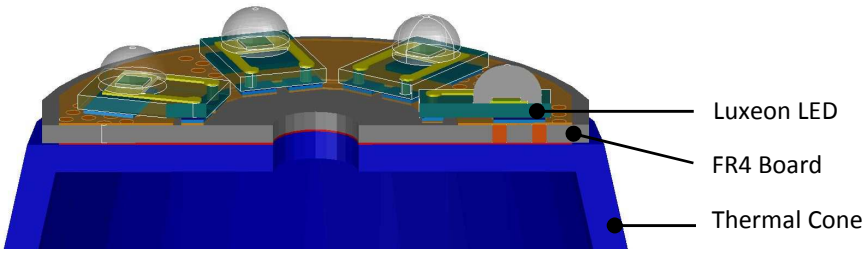

Figure 6.18a - Design A - FR4 board of existing design of retrofit LED lamp (reference model)

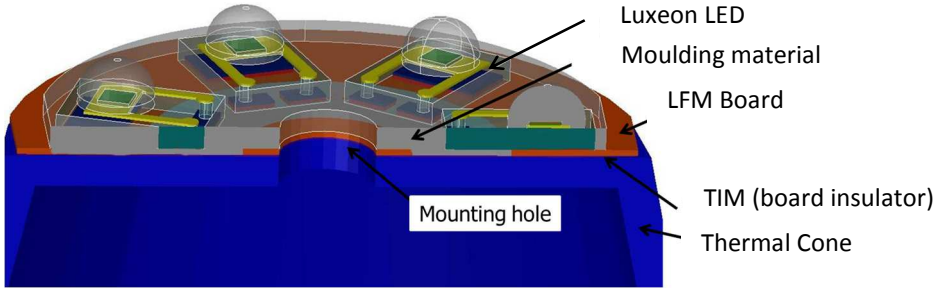

Figure 6.18b - Design B - Insulated LFM LED board concept with Luxeon Rebel LEDs

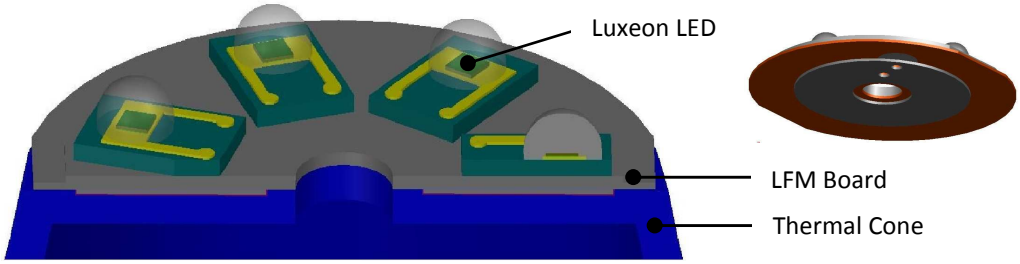

Figure 6.18c - Design C - LFM LED board concept with Luxeon Rebel LEDs

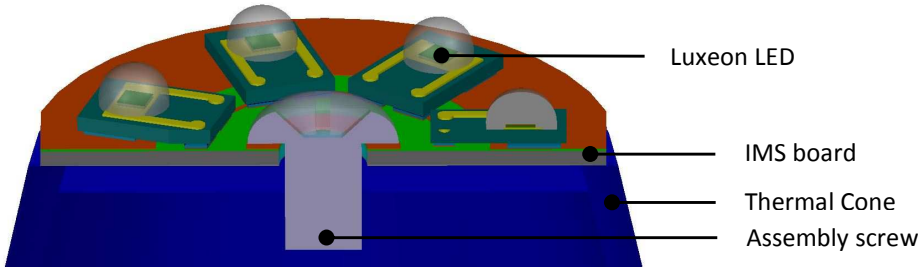

Figure 6.18d - Design D - IMS board with Luxeon Rebel LEDs

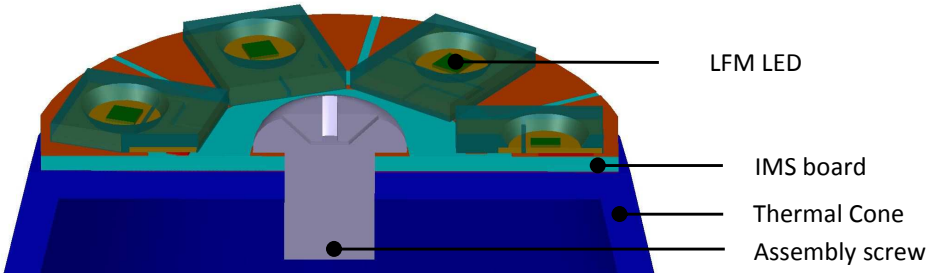

Figure 6.18e - Design E - IMS board with the new LFM package design LEDs

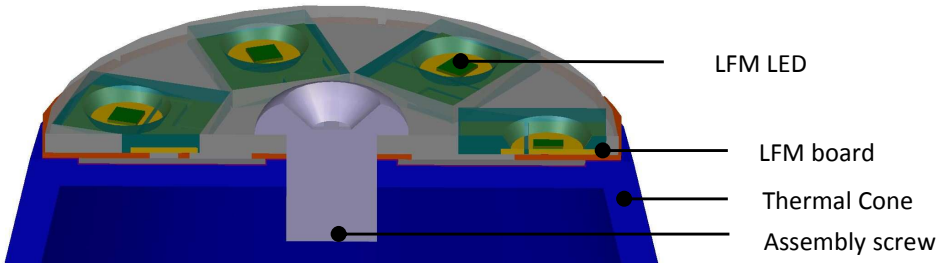

Figure 6.18f - Design F - Insulated LFM LED board concept with the new LFM package design LEDs

As Figure 6.18 shows, models are simulated with thermal cone and assembly screw which are parts of LED lamp structure. It provides the realistic thermal distribution and mechanical connection. As the reference point for simulation there was chosen the bottom edge of the thermal cone which temperature is kept at 80 °C. The new boards were designed as possible replacement of the reference LED board. Their potential is evaluated by comparing thermal and mechanical properties. In this chapter we focus only on the thermal results of simulations. The quality of the LED boards designs are rated by comparing of temperatures in identical points and by equivalent thermal resistances measured between specific places identical for all boards.

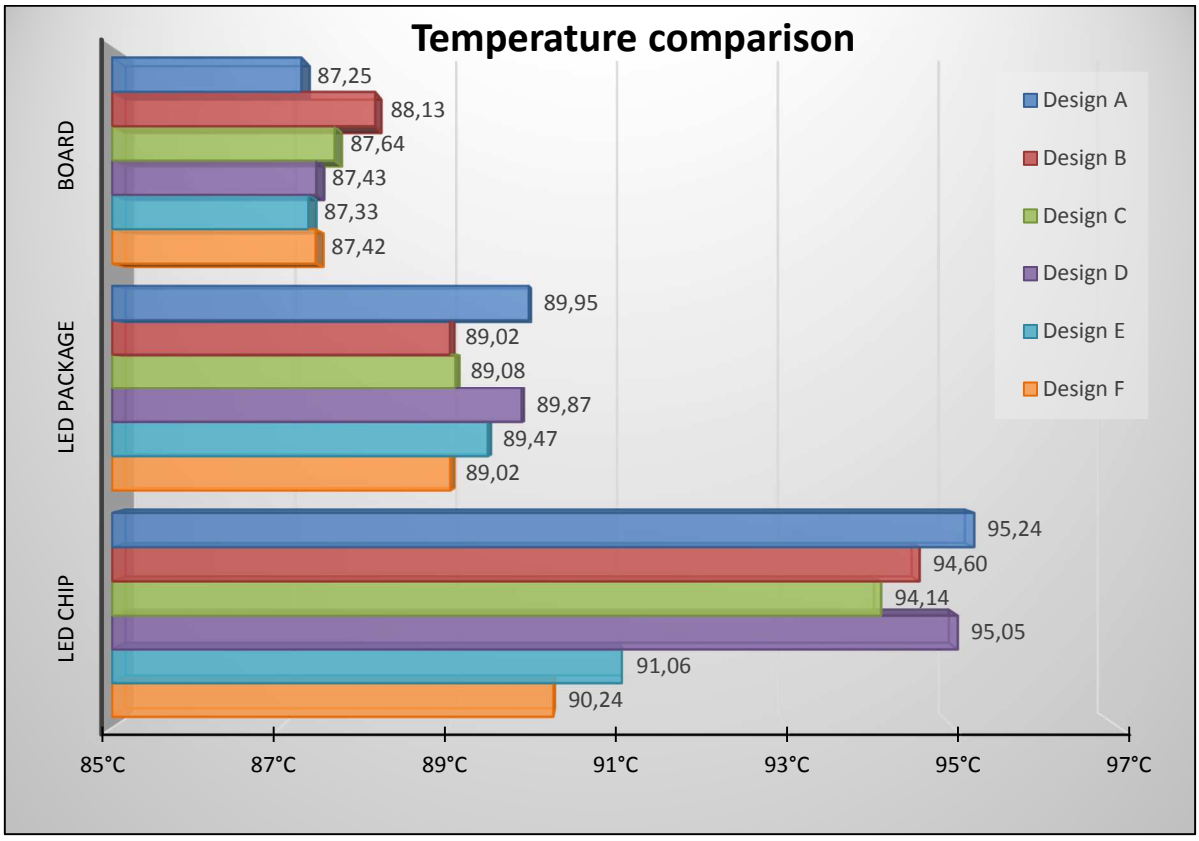

Figure 6.19 - Comparison between LED boards characteristic temperatures

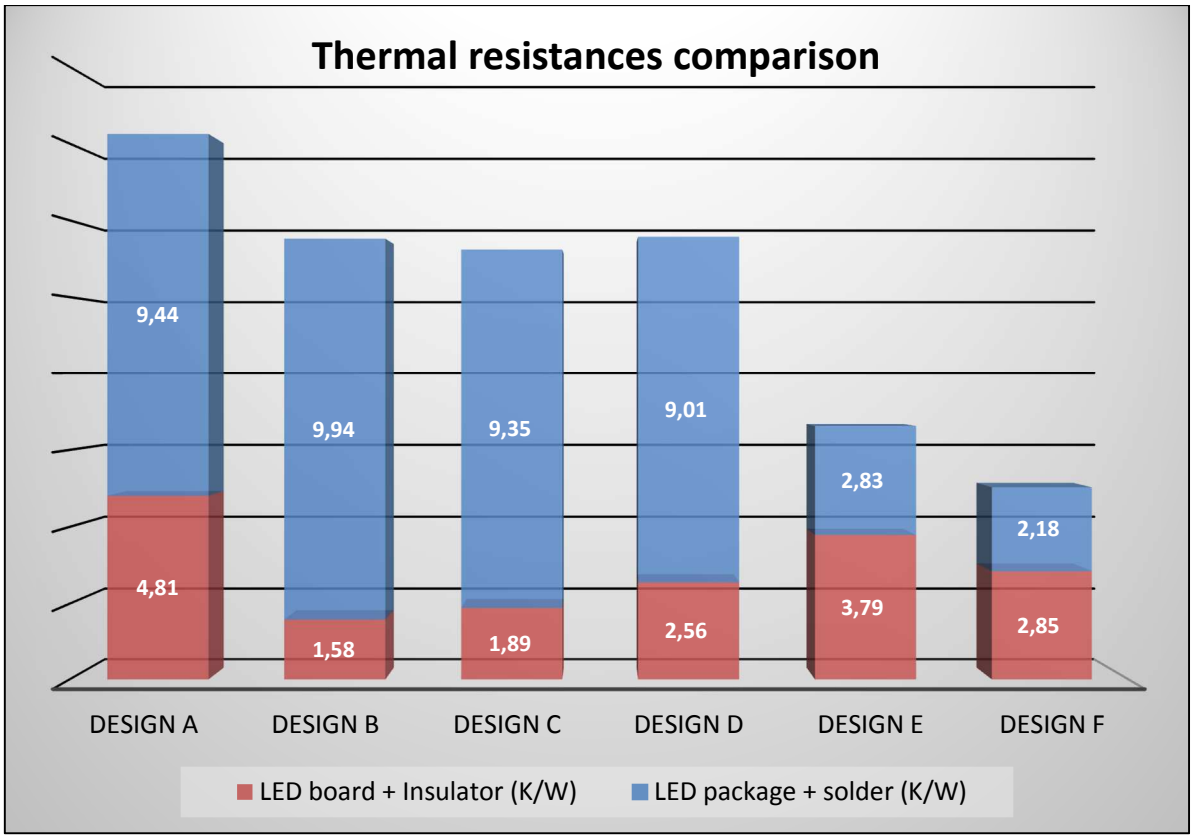

Figure 6.20 - Comparison between LED boards characteristic thermal resistances

Figure 6.19 shows the temperature comparison, among other parts, for the LED chip where the lowest temperature was found for Design F (Insulated LFM LED board concept with the new LFM package design LEDs). There, the LED chip temperature is almost five degrees lower than the temperature at Design A (Reference model - FR4 board of existing design of retrofit LED lamp). More details can be seen from comparison of thermal resistance values (Figure 6.20) which are computed separately for each LED package including soldering layer and for each LED board. I see the big difference between the reference LED board with thermal resistances between 9.01 K/W and 9.94 K/W (Design A-D), and the new LFM LED package design where computed thermal resistance dropped to values between 2.18 K/W and 2.83 K/W. The lowest LED board thermal resistance is calculated for insulated LFM board (1.58 K/W) which is more than three times lower that in case of reference model (4.81 K/W) [9].

[9] The work was published in impacted journal Microelectronics Reliability 2013 [A2] and at the international conference IEEE Eurosime 2012 [A10]

7. Thermo-Mechanical Issues

During solving the issue of the lifetime of electronic components it is necessary to determine the thermo-mechanical behaviour in the whole range of operating conditions. The measurements can provide only the view on deformation of external shape of the object but not the information about distribution of mechanical stress in volume. The methods for simulation of thermo-mechanical behaviour enables us the insight into the interior of the product and better understand its behaviour. It enables us to establish distribution of mechanical stress, strain deformation and thus identify the problem in the design. These simulations are usually used for establishing the behaviour of electronic components their packaging and soldering. In the literature non-linear simulations of components and evaluation of their life are beginning to appear more aspects of modelling of nonlinear behaviour of complex electronic products are not too much published. In the next chapter I would like to present my work progress in the development of the simulation methodology known from mechanical engineering and supplementing it by wider aspects of nonlinear behaviour.

7.1. Thermally Induced Stress and Strain

The thermal expansion of material is well known phenomenon. As we know, any changes in temperature of material result in volume change. The decrease or increase in temperature results in the contraction or expansion of the structure. If the body is not free to expand (for example body contains nonuniform distribution of temperature or when the temperature change is applied on the body which is composed from parts with different temperature coefficient) mechanical stress is induced in structure. Such stresses caused by the temperature change are known as thermal stresses.

Thermally induced strain [B109]:

$$\varepsilon_{th} = \alpha . L . (T_F - T_I) = \alpha . L . \Delta T \tag{12}$$

Where α is the coefficient of thermal expansion (m/m°C), L is the length (m), T_F and T_I are the final and initial temperatures (°C)

For the simple case of homogeneous fully elastic rod mounted between unyielding supports, the thermal stress can be computed by comparing strain caused by thermal stress and by equivalent axial stress [B109]:

$$\varepsilon_{el} = \frac{P.L}{A.E} = \frac{\sigma.L}{E} \tag{13}$$

$$\varepsilon_{tot} = 0 = \varepsilon_{el} + \varepsilon_{th} \tag{14}$$

$$-\alpha . L . \Delta T = \frac{\sigma_t . L}{E} \tag{15}$$

$$\sigma_t = -E . \alpha . \Delta T \tag{16}$$

Where σ_t is the thermally induced stress (Pa), *E* is the modulus of elasticity of the rod (Pa), *P* is the force (N), *A* is the area of the rod cross-sectional (m.m), ε_{tot} is the total strain (m/m), ε_{el} is the elastic strain (m/m).

When we talk about the nonlinear behaviour of structure, for example in metal part whose loading exceeds yielding point[10], nonlinear relationship between stress and strain have to be defined. Then we expand the equation by plastic strain part ε_{pl}.

$$\varepsilon_{tot} = \varepsilon_{el} + \varepsilon_{pl} + \varepsilon_{cr} + \varepsilon_{th} \tag{17}$$

Equation 17 contains also creep strain part ε_{cr} which means structural changes represented as slow permanent deformation under the mechanical or thermal stresses. The simple rod with negligible cross-section is only the ideal example. The real structure has usually complex geometry, anisotropic materials and structure is loaded by several sources. In continuum, parameters can be generally defined as vectors or matrixes.

$$\varepsilon_{ij} = \begin{pmatrix} \varepsilon_{xx} & \varepsilon_{xy} & \varepsilon_{xz} \\ \varepsilon_{yx} & \varepsilon_{yy} & \varepsilon_{yz} \\ \varepsilon_{zx} & \varepsilon_{zy} & \varepsilon_{zz} \end{pmatrix} \quad \sigma_{ij} = \begin{pmatrix} \sigma_{xx} & \sigma_{xy} & \sigma_{xz} \\ \sigma_{yx} & \sigma_{yy} & \sigma_{yz} \\ \sigma_{zx} & \sigma_{zy} & \sigma_{zz} \end{pmatrix} \tag{18}$$

Parameters σ_{xx}, σ_{yy}, σ_{zz} are normal components of resultant stress so that we call it normal stresses. Parameters σ_{xy}, σ_{xz}, σ_{yx}, σ_{yz}, σ_{zx}, σ_{zy} are tangential components of resultant stress so we call it shear stresses and we write them as τ_{xy}, τ_{xz}, τ_{yx}, τ_{yz}, τ_{zx}, τ_{zy}. Matrixes can be simplified because both are symmetric.

$$\begin{aligned} \varepsilon_{xy} &= \varepsilon_{yx} \quad \varepsilon_{xz} = \varepsilon_{zx} \quad \varepsilon_{yz} = \varepsilon_{zy} \\ \tau_{xy} &= \tau_{yx} \quad \tau_{xz} = \tau_{zx} \quad \tau_{yz} = \tau_{zy} \end{aligned} \tag{19}$$

In general approach, elastic strain can be calculated from Hooke's law[11] as:

$$\boldsymbol{\sigma} = \mathbf{E}.\boldsymbol{\varepsilon} \tag{20}$$

Where **σ** is the normal stress tensor, **E** is the Young's modulus matrix and **ε** is the strain tensor.

Using the principle of superposition, the generalized Hooke's law for three dimensional state in the homogeneous and isotropic material can be:

$$\begin{aligned} \varepsilon_{xx} &= \frac{1}{E}\left[\sigma_{xx} - \gamma(\sigma_{yy} + \sigma_{zz})\right] \\ \varepsilon_{yy} &= \frac{1}{E}\left[\sigma_{yy} - \gamma(\sigma_{xx} + \sigma_{zz})\right] \\ \varepsilon_{zz} &= \frac{1}{E}\left[\sigma_{zz} - \gamma(\sigma_{xx} + \sigma_{yy})\right] \end{aligned} \tag{21}$$

Where *E* is Young's modulus and γ is Poisson's ratio.

[10] A **yield strength** or **yield point** of the material is defined in engineering and materials science as the stress at which the material begins to deform plastically. Prior to the yield point the material will deform elastically and will return to its original shape when the applied stress is removed. Once the yield point is passed, some fraction of the deformation will be permanent and non-reversible.

[11] **Hooke's law** is the mathematical statement of the linear relation between stress and strain and usually implies both small strains and small deformations.

For the orthotropic materials we can define Hooke's law in matrix form as:

$$\begin{bmatrix} \varepsilon_{xx} \\ \varepsilon_{yy} \\ \varepsilon_{zz} \\ 2\varepsilon_{yz} \\ 2\varepsilon_{zx} \\ 2\varepsilon_{xy} \end{bmatrix} = \begin{bmatrix} \frac{1}{E_x} & -\frac{\nu_{yx}}{E_y} & -\frac{\nu_{yx}}{E_y} & 0 & 0 & 0 \\ -\frac{\nu_{xy}}{E_x} & \frac{1}{E_y} & -\frac{\nu_{zy}}{E_y} & 0 & 0 & 0 \\ -\frac{\nu_{xy}}{E_x} & -\frac{\nu_{yz}}{E_y} & \frac{1}{E_z} & 0 & 0 & 0 \\ 0 & 0 & 0 & \frac{1}{G_{yz}} & 0 & 0 \\ 0 & 0 & 0 & 0 & \frac{1}{G_{zx}} & 0 \\ 0 & 0 & 0 & 0 & 0 & \frac{1}{G_{xy}} \end{bmatrix} \cdot \begin{bmatrix} \sigma_{xx} \\ \sigma_{yy} \\ \sigma_{zz} \\ \sigma_{yz} \\ \sigma_{zx} \\ \sigma_{xy} \end{bmatrix} \quad (22)$$

When applied loading exceeds yield criteria, material starts to deform plastically. We can use some the well-known criteria, such as criteria of maximum principal strain, maximum shear stress, total strain energy but the simplest criteria which can give us the approximate evaluation is the maximum principal stress. This occurs when stress reaches Yield stress value. This value mostly comes from statistical analysis of experimental y measured values. Yield stress depends on material composition, temperature, direction of loading, dislocations embedded by hardening, etc. The relation between plastic part of strain ε_{pl} and stress is mostly obtained from stress-strain curves which also have to be measured for each material. This curves also depends on temperature, speed of loading, direction of loading, hardening, etc. The simple example of stress-strain curves of copper is shown on Figure 7.2. Materials exposed long temperature which is near to the melting point especially ductile materials are susceptible to creep behaviour. The creep strain occurs already before loading exceeds Yield stress, it can be the majority strain when stress loading is around Yield stress value. Creep, I will discuss in the further chapter.

7.2. Method for Realistic Thermo-mechanical Modelling of Objects Exposed to High Stresses

This chapter deals with calculations of mechanical stresses which are produced by different thermal expansion coefficients of the used materials. Thermally induced stress plays main role in the LED board reliability. The detailed model of the reference LED board was prepared. The LED board model was designed with all LED package details, mounting pads, TIM, metallic leads and thermal vias placed under each LED package (Figure 7.1).

In the beginning of development of SSL lamps I have made linear thermo-mechanical simulations as it is usual in published articles. With these simulations there were found critical parts of the structure. Very high residual stresses can be found at -40 °C, which is considered as the lowest store temperature. The reason for that is defined by high zero stress temperature[12] according to soldering and moulding fabrication process. The highest

[12] Object **temperature** at which shows the zero built-in mechanical stress. This is usually the temperature at which parts of the structure are inseparably connected together.

thermal stresses are located in the solder the LED board and LED package copper layers. The simulated value reaches up to 190 MPa. The linear elastic approach does not describe the real behaviour because it does not take into account the material ultimate yields stresses and material plastic behaviour. For example the value of the yield stress for copper is about 70 MPa at room temperature.

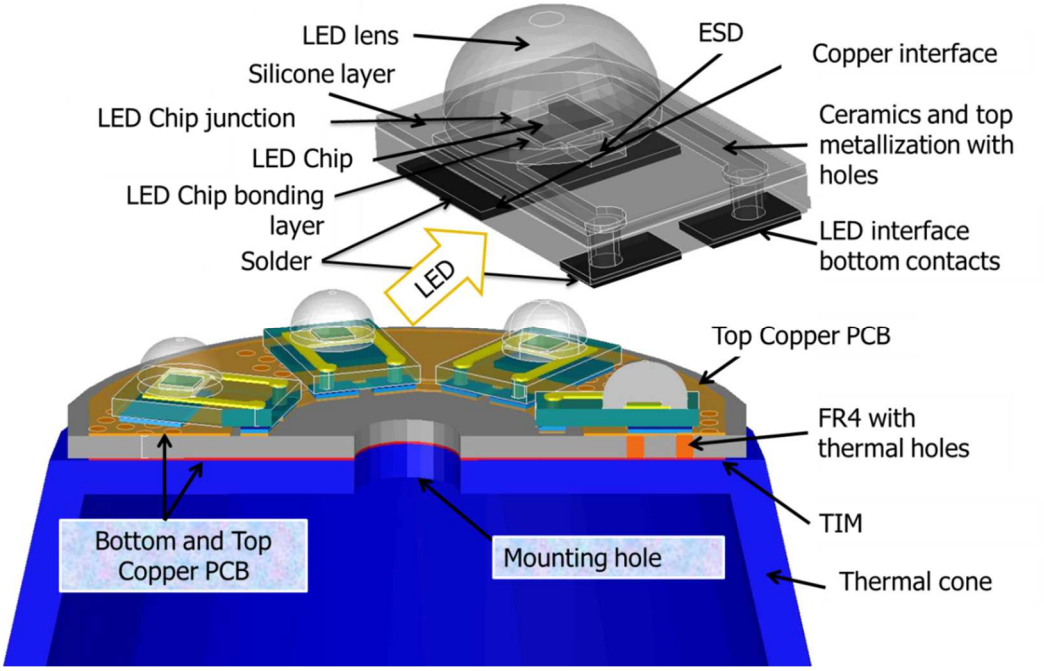

Figure 7.1 - Detailed model of LED board

Improving of accuracy of modelling can be achieved by adding temperature dependence elastic-plastic material properties. It is usually defined by stress-strain curves. The temperature dependent stress-strain curves have to be specified for metal parts exposed to the high thermal stresses. For example, curves for copper are shown on Figure 7.2 [B40].

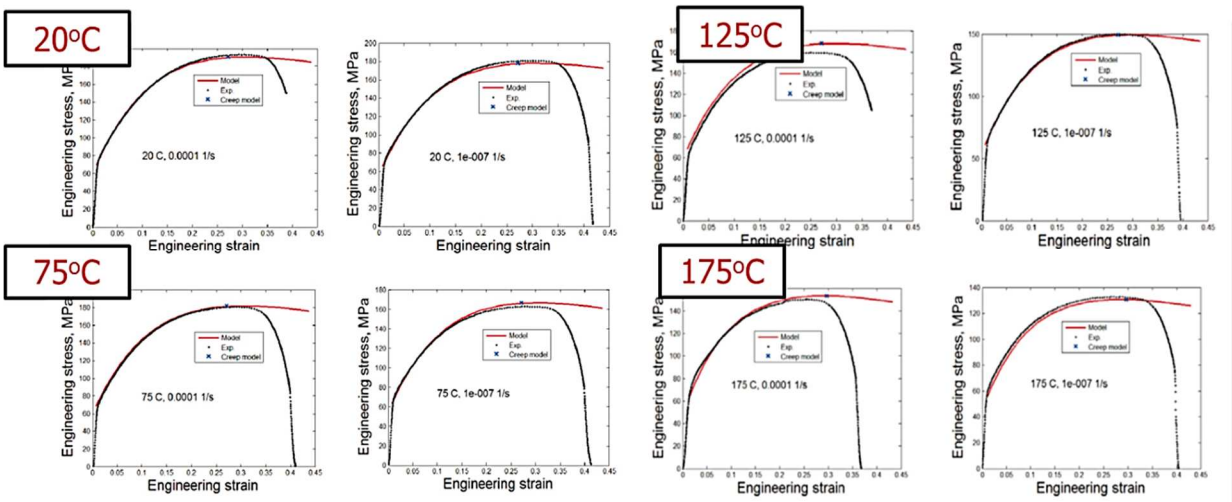

Figure 7.2 - The temperature dependent stress-strain curves for copper [B40]

Figure 7.3 shows the comparison between the simple linear and precious non-linear analysis. Both models of reference LED board were exposed to homogenous temperature -40 °C and stress distributions were studied in volumes modelled LED boards. Mechanical boundary conditions mechanically fix the inner face node of the central hole. This boundary condition reflects the fact that the LED board is fixed to the thermal cone by the central screw. All the other model nodes can freely move in all directions.

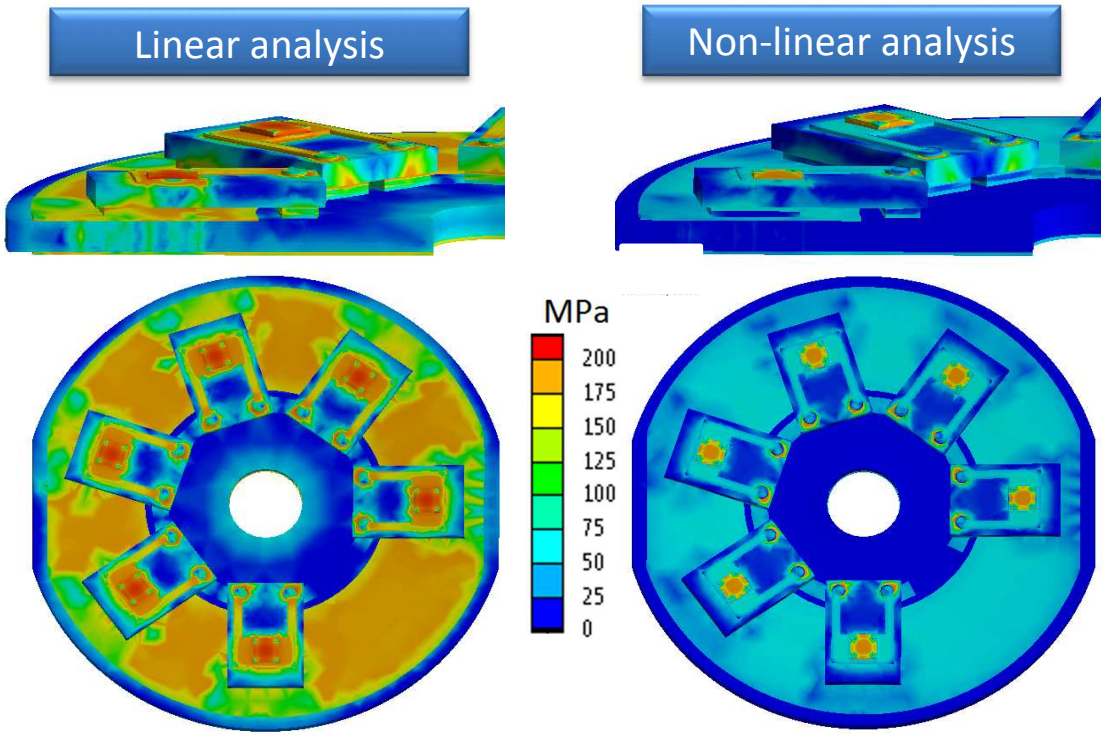

Figure 7.3 - Comparison between linear and non-linear thermo-mechanical analysis

The Figure 7.4 shows strain distribution in extreme temperatures; we can see the importance of plastic component of strain. The plastic strain in critical parts is about one order higher that the elastic strain. Due to performed precious non-linear simulation stresses and strains decreased to real values. The precious nonlinear thermo-mechanical simulations are very interesting research topics for understanding of thermo-mechanical behaviour of the structures.

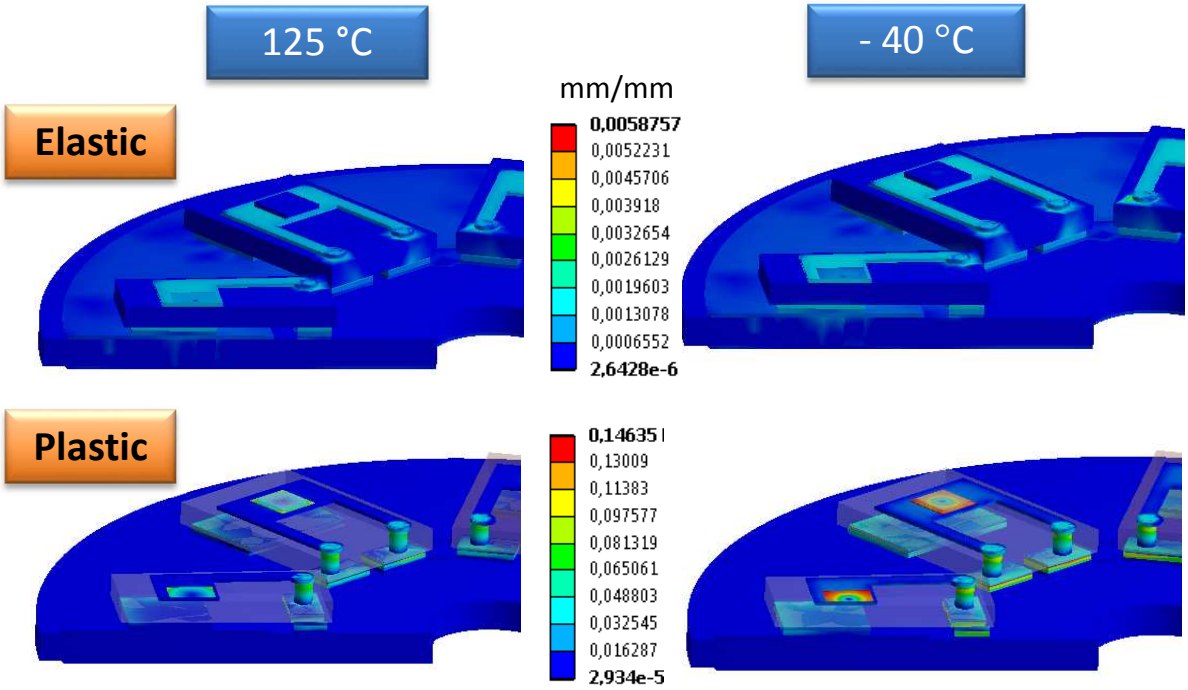

Figure 7.4 - Strain distribution at different temperatures - elastic in top row, plastic in bottom row

7.3. Mechanical Evaluation of New LED Board Prototypes

The LED board prototyping was done not only for achieving the lower LED junction temperature but also for the better mechanical durability and lifetime. This chapter shows the calculated stresses and strains caused by thermal loading of the reference FR4 LED board in comparison with the new LED board designs. Details about LED board prototyping are listed in the chapter 6.4 where the Figure 6.18 shows their structure.

The thermal boundary conditions are set differently for two cases. The first represents LED boards in real operational temperature distribution. For that case the heat flux at the bottom face of the LED boards has been derived from the thermal analysis of the LED lamp model. Convection (5 W/m2K to air) and radiation has been prescribed on the top surface of the board and LEDs. The total heat power dissipation of 4 W has been considered for six LED chips. The second case represents LED board stored in limit temperature -40 °C where uniform temperature distribution has been applied on all parts of the LED model. Zero stress temperature has been defined for all materials according to assumed moulding and soldering fabrication processes. Figure 7.5 shows distribution of thermally induced stress in LED boards. Distributions are evaluated for operating temperature and for lowest storing temperature in reference board and in all newly developed designs. Figures also show the deformation of boards which is 5 times magnified for easier recognition.

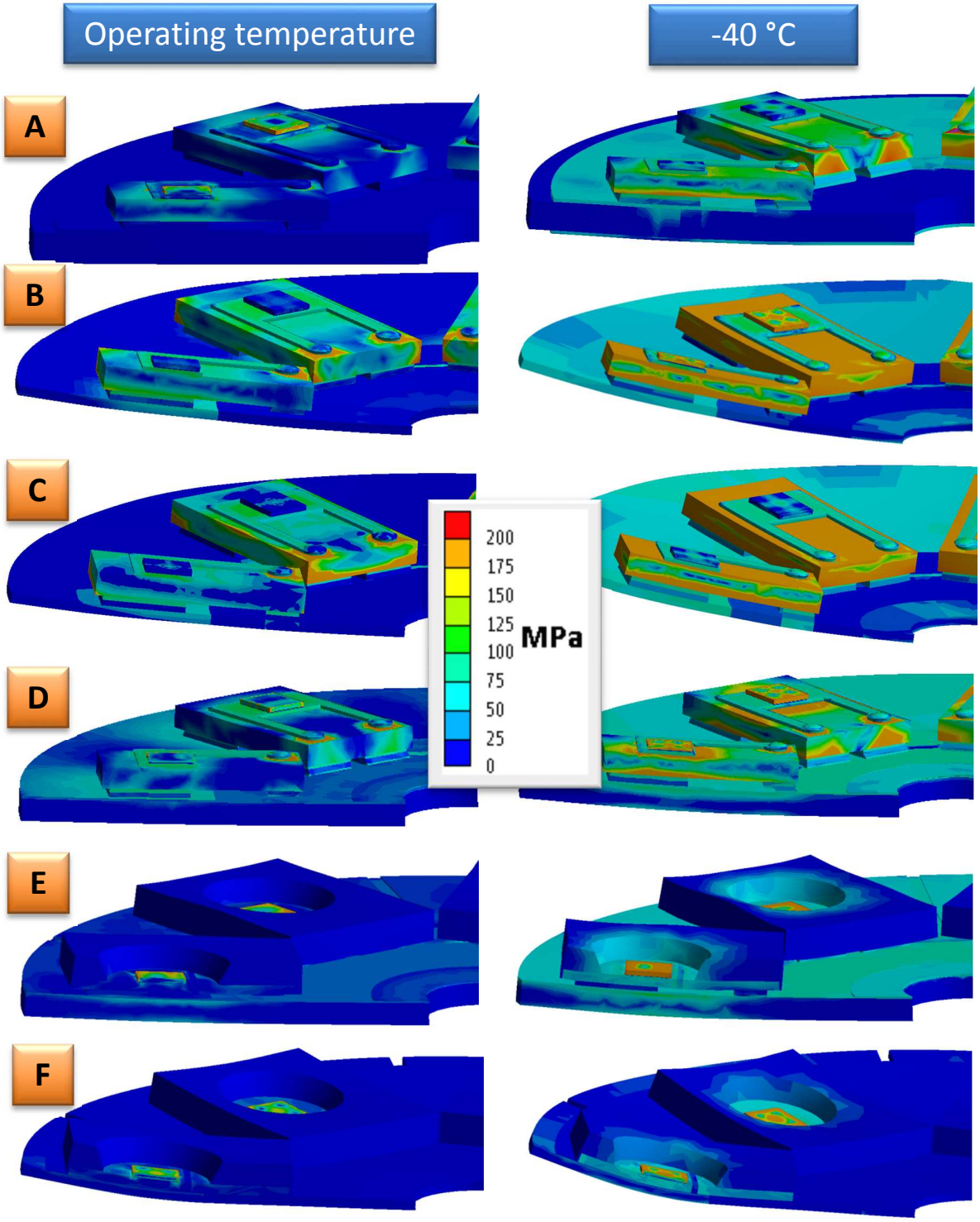

Figure 7.5 - Comparison of thermally induces stress in LED boards structures

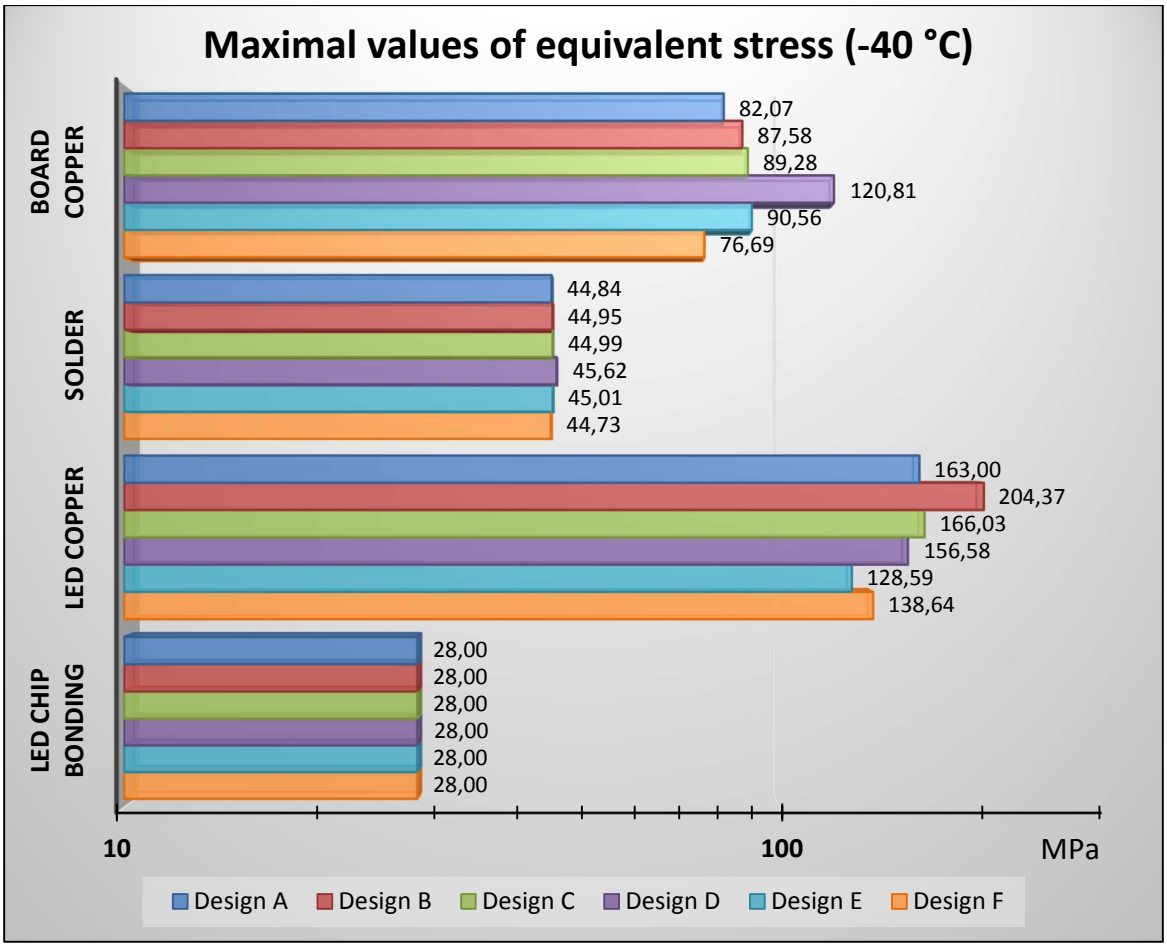

Figure 7.6 - Comparison of maximal values of thermally induces stress in LED boards

Because the initial thermal stress is formed when LED package is soldered on the LED board, it generally reduces when the temperature is increased. Consequently, it is appropriate to compare the boards at the lowest possible temperature of -40 °C. Figure 7.6 shows the comparison of calculated maximal values of equivalent residual stresses in LED board structures. At the first view based only on stress comparison, we can see reduction of thermal stress in LED copper on designs based on IMS board or which is equipped with LFM LEDs. This leads to improve reliability of designs D, E and F. Maximal values of thermal stress in board copper layer is significantly lower than in LED copper layer. Therefore, it can be expected that this layer does not affect the reliability of the whole board. Comparison of solder layer reliability cannot be done by this method due to high ductility of used SAC solder. Let me note, that for highly loaded very ductile material is the plastic component of strain much higher than the elastic component (Figure 7.4). This leads to use the strain based lifetime determining methods shown in the further chapter.

When we look at Figure 7.5 in more detail, we can see the bad stability (high deflection) of designs based on LFM board (design B, C and F). This will probably cause the gap between LED board and thermal cone. Which unfortunately gets worse heat dissipation. If we want to use this types of boards, we have to change the board fixing method. IMS based designs shows the best stability (design D and E).

8. Reliability and Lifetime

The chapter deals with the simulation and evaluation of electronic structure reliability and lifetime. We will focus on gradual degradation of the structure during normal use from mechanical point of view. We will not investigate degradation of electronic components parameters such as reduction of LED luminous flux which is another part of research.

As I pointed out in chapter 4 , the lifetime is reduced by many mechanical, electrical corrosion factors etc. We suppose that designed SSL lamp is being used in conditions defined by manufacturer, for example lamp is not exposed to corrosive or high temperature environment, supply voltage is within the defined limits etc. Than in our case, where structure of SSL lamp is highly loaded by thermally induced stresses which are also frequently cycled, thermo mechanically induced structural changes plays the main role [B25]. The high thermal cycling mainly caused by frequent switching on and off can gradually lead to the component failure. Fatigue failures can occur in many different forms in ductile, brittle, and non-crystalline materials.

Fatigue damage can generally be described in terms of:

- Fatigue hardening/softening and microstructural changes
- Micro-crack nucleation
- Initiation and propagation of the fatal crack.

The fatigue life can be defined as the number of cycles to initiate the fatigue crack and to propagate it to the final size when catastrophic failure occurs. It is not always possible to make the clear distinction between crack initiation and crack propagation. In general approach two possible mechanisms appear by which the defects can occur. High cycle and low cycle fatigue. Both effects blend together and are applied simultaneously.

8.1. High Cycle Fatigue

In the 1860s August Wöhler firstly introduced type of fatigue tests under stress control method which is relevant for applications where low-amplitude stresses induce mainly elastic deformations. This tests are designed for components which has been designed for the long life, more than 10^4 testing cycles is expected. He came with the method of lifetime prediction which appropriately described microstructure fatigue caused by prolonged cyclic thermo-mechanical loading of the structure. This loading caused microstructure damage, micro cracks at the interface of the material grains are formed and prolonged. This behaviour can be observed in almost all materials including fragile ones. Plastic deformation can also occurs in the material mostly in the highly localized way. Stress parameters affecting fatigue life are defined for simple loading by sinusoidal fatigue cycles with non-zero mean stress (Figure 8.1).

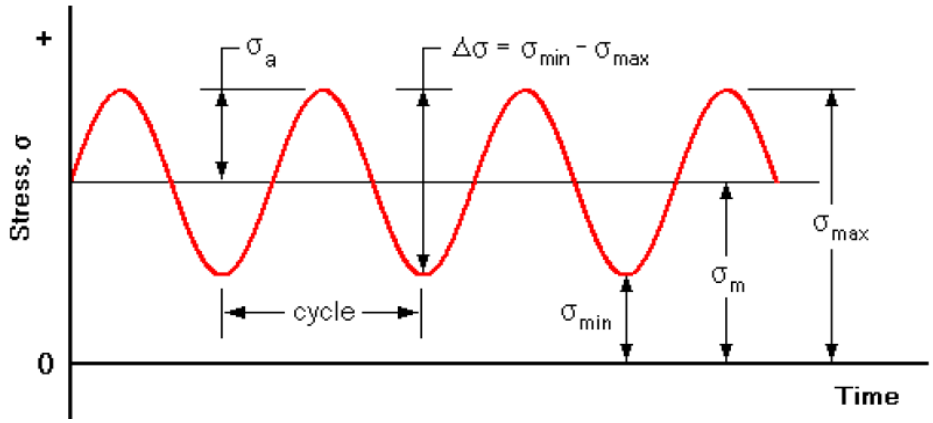

Figure 8.1 - Normalized loading for high cycle fatigue testing

Stress Range $$\Delta\sigma = \sigma_{max} - \sigma_{min} \quad (23)$$

Equivalent alternating stress: $$\sigma_a = \frac{\sigma_{max} - \sigma_{min}}{2} \quad (24)$$

Equivalent mean stress: $$\sigma_m = \frac{\sigma_{max} + \sigma_{min}}{2} \quad (25)$$

Loading ratio: $$R = \frac{\sigma_{min}}{\sigma_{max}} \quad (26)$$

The description of this effect is performed on the basis of Stress-life diagrams (S-N curves or Wöhler curves) which express the proportion between alternating mechanical stress and number of cycles to failure of the material structure. S-N curves describe the fatigue life of nominally defect-free materials with smooth surfaces. S-N curve are schematically shown in Figure 8.2.

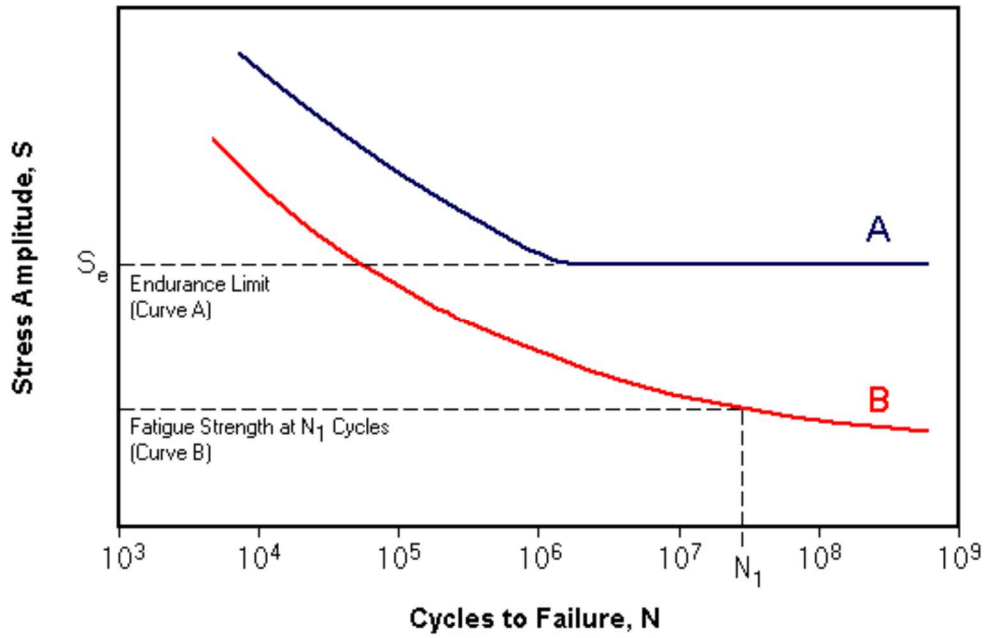

Figure 8.2 - S-N plot showing the material that has the endurance limit (A) and one which does not have the endurance limit (B) [B68]

Some almost metal materials (Curve A) exhibit the endurance limit when applied mechanical stress is less than this limit. It does not violate the structure of materials and the life is close to infinity. Due to the proper design and selection of materials the structure could be kept under mechanical stress endurance limit and can be designed as the structure with the very high durability. The Figure 8.2 shows the simple principle S-N curve of metallic materials.

In the literature most S-N curves are based on zero mean stress. However, it is more often that the time-varying stresses are oscillating near the non-zero mean stress. Multiple S-N curves are determined by the several sets of fatigue experiments. Each curve represents the specific mean stress of that particular material. The non-zero mean stress S-N relation requires huge amount of experiments to obtain the required data and form the mesh over the wide range of mean stresses.

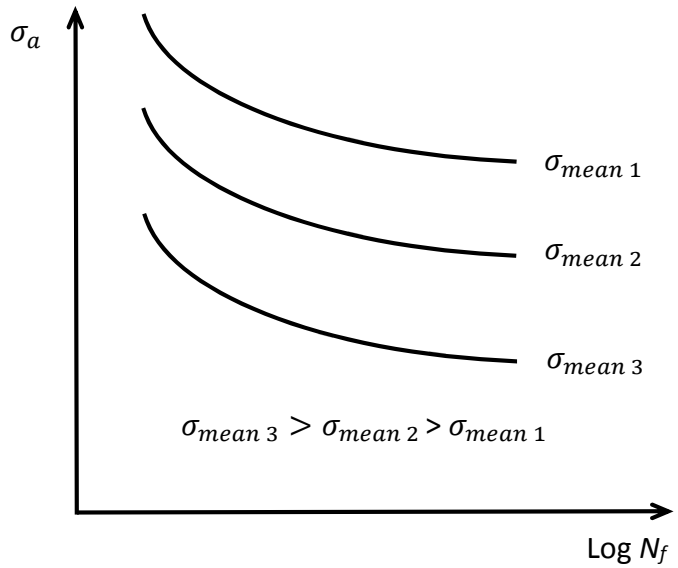

Figure 8.3 - Effect of mean stress on S-N curve [B68]

Therefore, we define the dependence between alternating stress and mean stress by one of approximation theories. All mostly used theories are based on the same zero-mean stress S-N curve which is consequently modified by the following equation [B66]:

$$\sigma_a = \sigma_{f0}\left[1-\left(\frac{\sigma_m}{\sigma_u}\right)^r\right] \tag{27}$$

Where σ_a is the amplitude of alternating stress is, σ_{f0} is the stress at fatigue fracture when the mean stress is zero, σ_m is the mean stress of the actual loading, σ_u is the tensile strength of the material, r is the stress loading factor.

r = 1 is called Goodman line which is close to the results of notched specimens.
r = 2 is the Gerber parabola which better represents ductile metals.

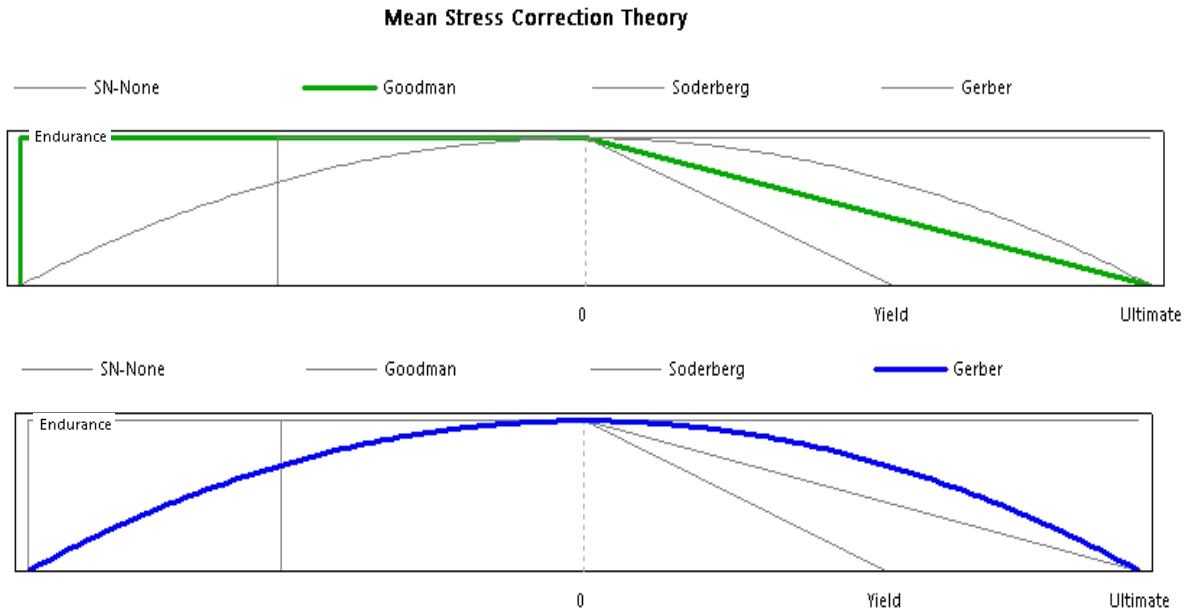

Figure 8.4 - Goodman (top) and Gerber (bottom) approximation for ANSYS [B66]

The Goodman approximation theory can be the good choice for brittle materials, consequently the Gerber theory is usually the good choice for ductile materials. Both approximations might not properly represent the specific behaviour of material and they are only good for uniform mean and alternating stresses. For a better modeling of the real behavior we can define the set of S-N curves which measured separately for different mean stress. Simulation software than fits curves between specified (Figure 8.5).

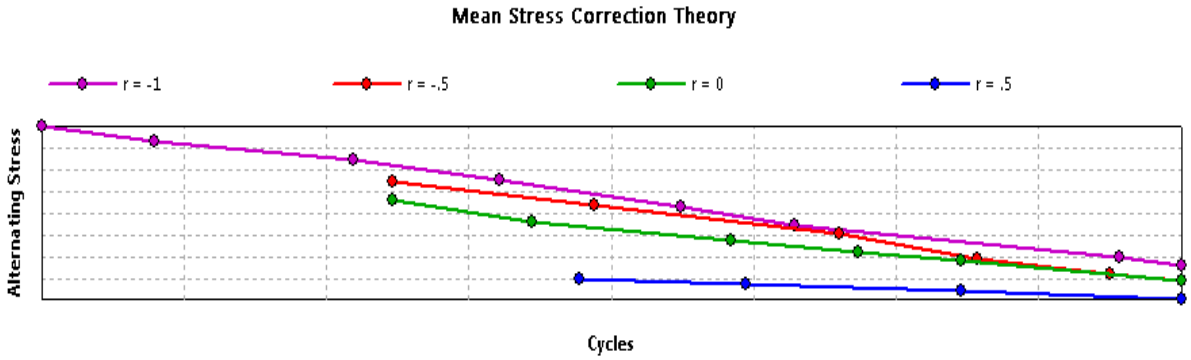

Figure 8.5 - Specified mean stress curves for ANSYS [B66]

From reliability point of view, as most problematic parts of LED board were found LED chip bonding layer, LED metallization, solder and board copper. The high speed thermo-mechanical load cycling life time prediction has been calculated. The initial stress was calculated and Gerber theory was used to approximate influence of mean stress with respect to the fabrication process of all LED boards (soldering, moulding process, etc.).

The thermal cycling range for fatigue analysis was set in the standardized industrial testing range of -40 °C to 120 °C. This type of testing method expects only elastic or plastic contribution of strain therefore the creep strain caused by prolonged high temperature loading had to be eliminated. It can be done by setting the large frequency of performed

testing, in our case frequency of cycling was set to 1 Hz. This value ensures creep strain component less than 1 % of total strain just after third cycle and it came from parametric simulation of creep stress simulation as it is shown on Figure 8.6**.**

Creep strain was calculated by using hyperbolic sine function constitutive model published by Schubert at al [B61], [B69]:

$$\varepsilon_{cr} = A_1[\sinh(\alpha.\sigma)]^n \, exp\left(\frac{-H_1}{k.T}\right) \tag{28}$$

Where ε_{cr} is an equivalent creep strain, σ is equivalent stress, T is temperature (absolute), A_1 = 277 984 s^{-1}, α = 0.02447 MPa^{-1}, n = 6.41 and H_1/k = 6 500 are constants defined by the measurement.

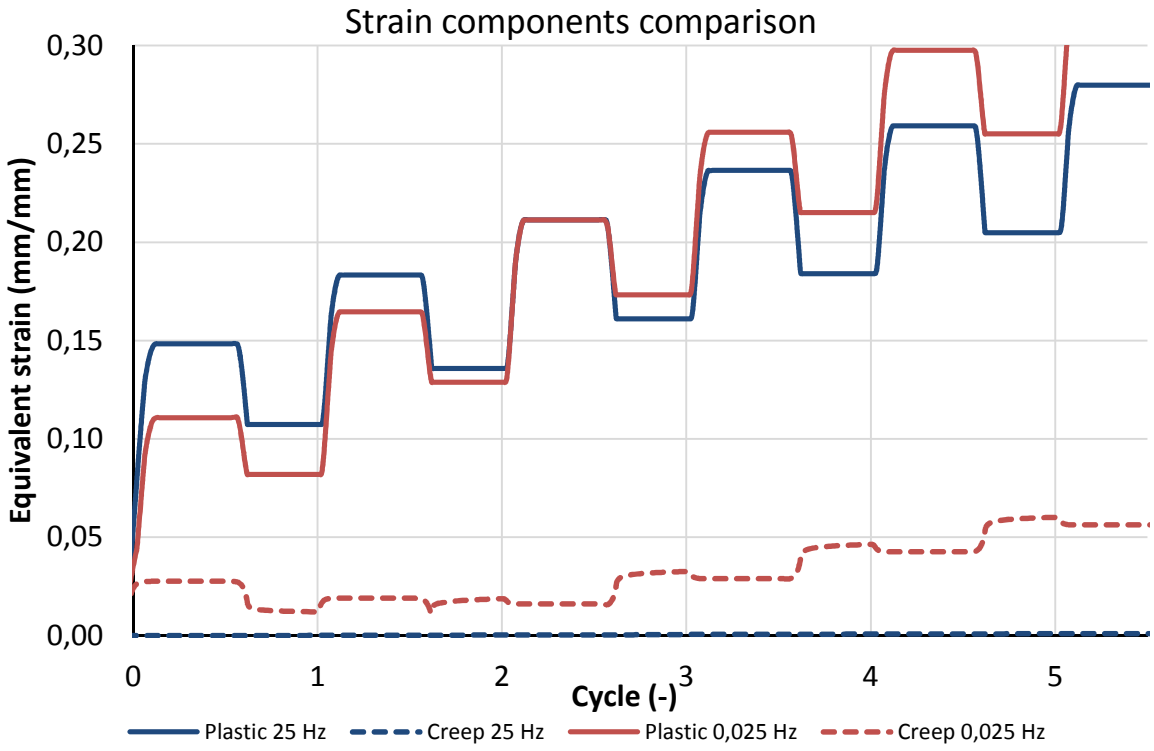

Figure 8.6 - Maximal values of accumulated equivalent creep and plastic strain in structure of LED board at different test loading frequencies.

The method of LED board fixing closely emulates the reality because inner face nodes of the central hole are mechanically fixed as it is fixed in real condition by screw. All other nodes can freely move in all directions.

The results of the simulations cannot show the real value of product lifetime because they does not include all phenomena of real behaviour. Provided analysis shows only the probability of initiation and propagation of cracks in the most mechanically stressed areas in special condition. But it can be used for good comparison between designed LED board prototypes. Results can be also compared with fast vibration tests, which will be mentioned in the next chapter.

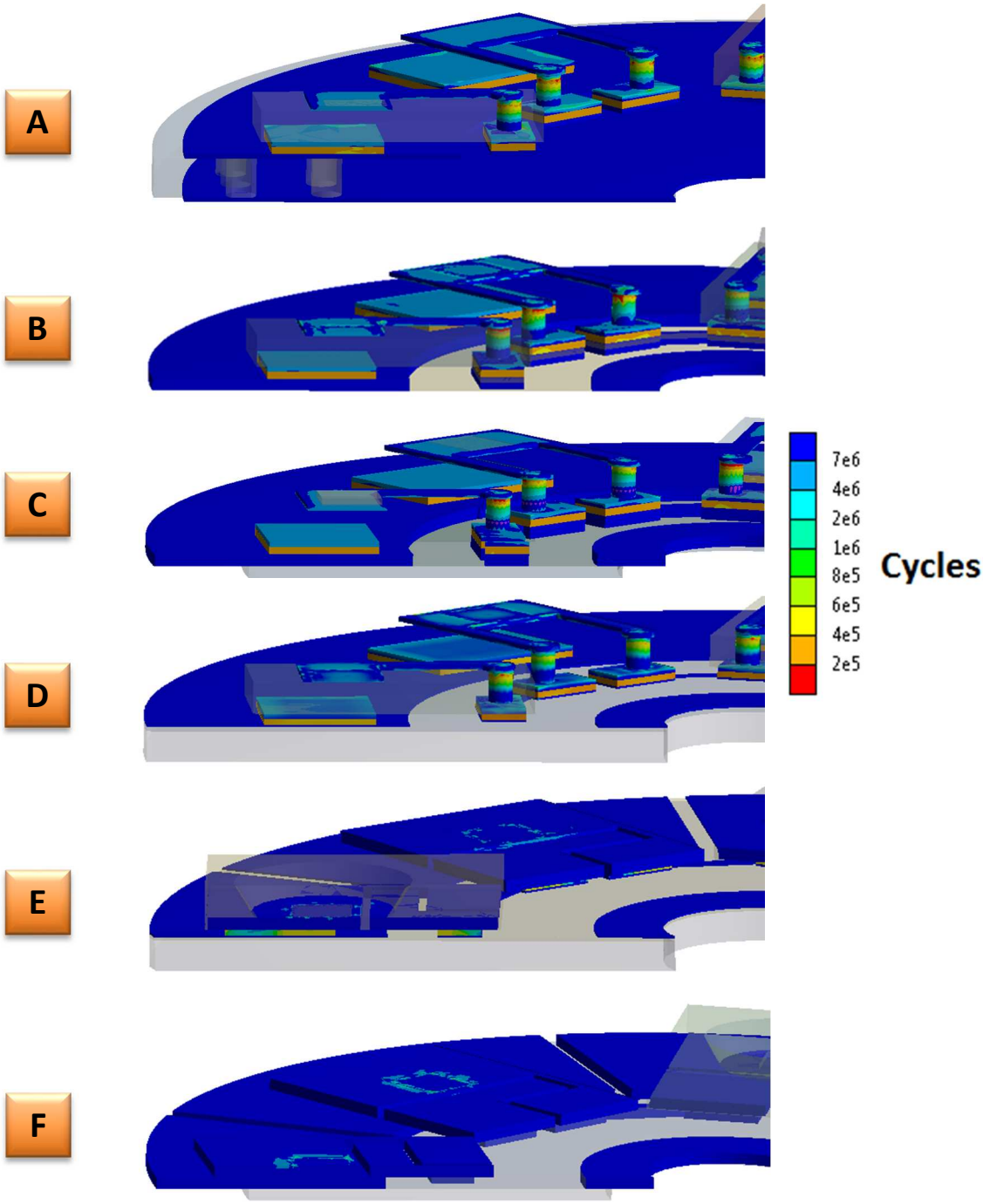

Figure 8.7. - Distribution of calculated life time by the high cycle fatigue method

Figure 8.7 shows the distribution of calculated life time of each LED board design. It represents the number of cycles which lead to mechanical fatigue of critical parts. Failure of LED board can be caused by the failure of any critical parts so we have to compare the designs by minimal value of calculated lifetime[13]. Red colour shows places with lowest number of cycles. The most problematic places can be found in Luxeon LED package metal

[13] The work was published in impacted journal Microelectronics Reliability 2013 [A2] and at international conference ESREF 2012 [A13]

vias that connect the bottom contact of the package and the top LED package metallization. The next problematic part can be found at solder layer between the LED package and the LED board.

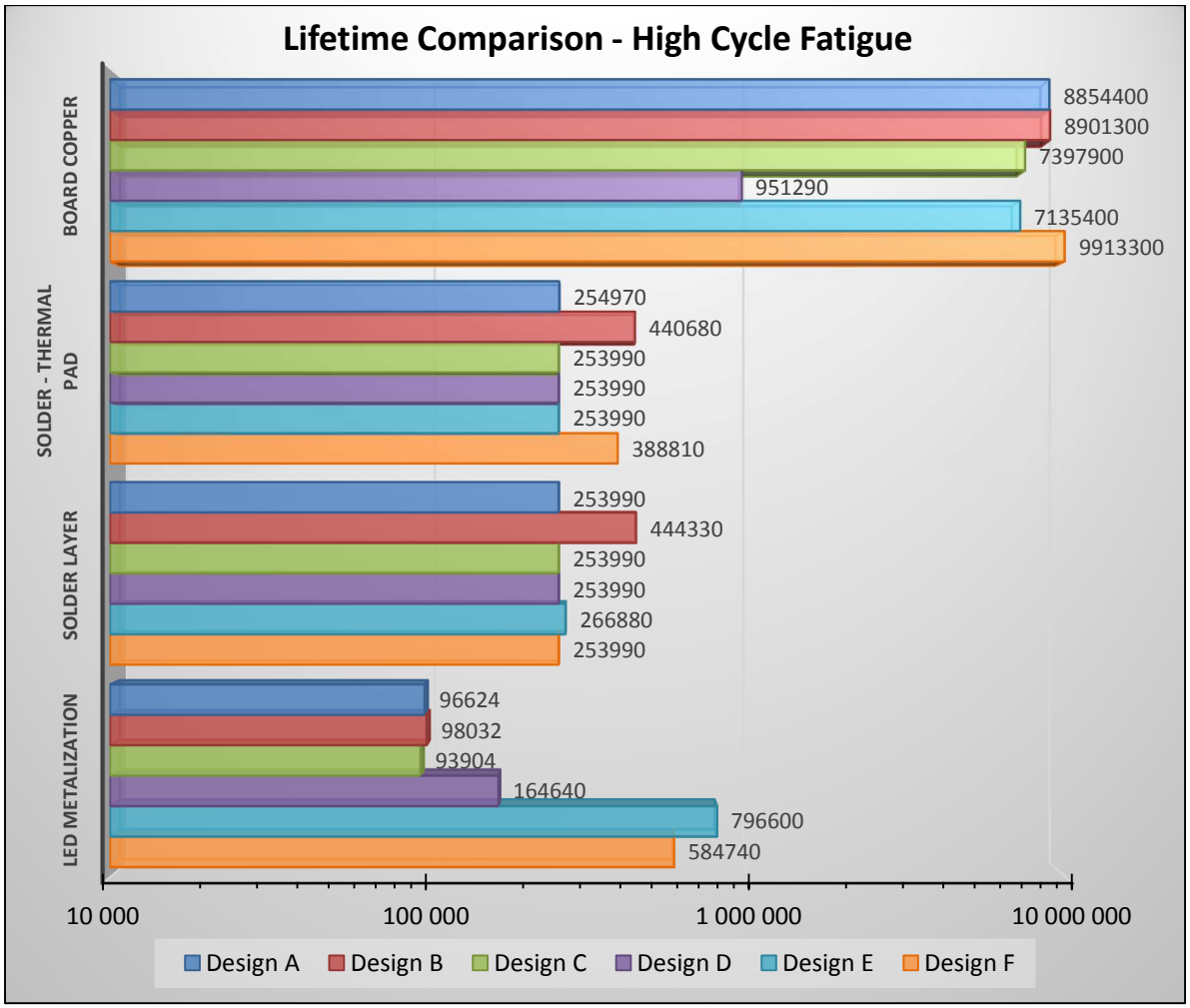

Figure 8.8. - Lifetime comparison evaluated by the high cycle fatigue method

When we compare these parts, we can see the big improvement in LED package design, new LFM package design shows more than four times greater number of cycles to failure than Luxeon LED package design. Design E of IMS board with LFM LEDs shows 796 600 cycles versus Design D with Luxeon LEDs shows 164 640 cycles. We should emphasize behavior of IMS boars as boards which good feature is its displacement stability. LEDs soldered on this boards are not very influenced by deflection of the boards which we can see on great values of the LED metallization cycles (Design D: 146 640 cycles, Design E: 796 600 cycles). During the comparison is not suitable to consider the behavior of the solder layer because in real conditions, lifetime of very ductile solder is mainly influenced by creep behavior. I will discuss it in following chapters.

8.2. Vibration Test Method

In the last chapter I was discussing the simulation method for high cycle fatigue testing and lifetime estimation. Results of provided simulations are not valuable without verification by real measurement. For the purpose, methodology and measuring apparatus for vibration tests is being developed. Since the apparatus for high speed thermal cycling test which enables us to cycle temperature with period of 1 Hz is practically impossible to build, I was forced to change the type of the loading. I have found that for the special purposes of board technologies comparison and for the simulation models improvement high speed thermal cycling can be replaced by the special mechanical cycling. Tested board have to be fixed and mechanically bended by one or more external forces. This must be designed according to the shape and size of the tested board. Mechanical forces applied on LED board can cause very similar stress distribution and mechanical deflection as thermal cycling does. Mechanical parameters of materials are temperature dependent some less, some more. But the most fatigue affecting parameter, the creep strain is eliminated by the high frequency of cycling. By this method we can achieve accuracy of the validation in about few tens to several percent, depending on the complexity of the board.

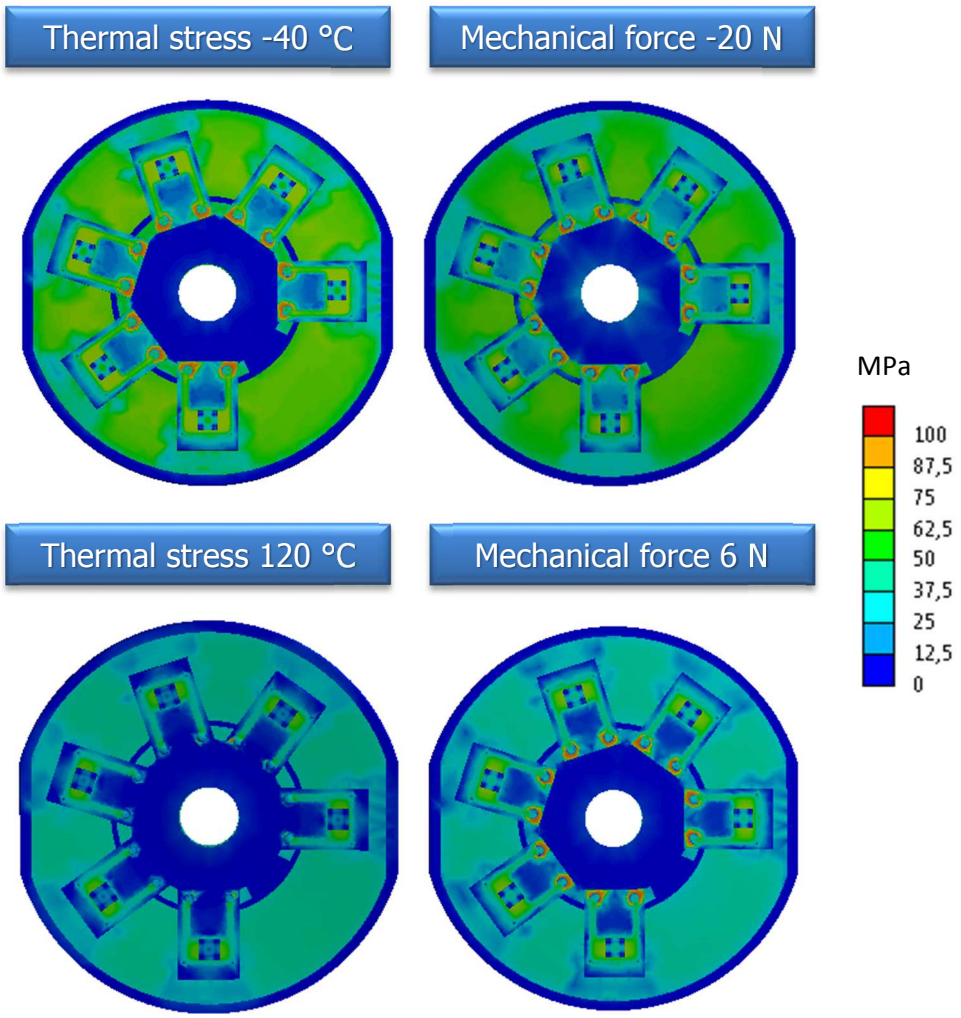

Figure 8.9 - Mechanical and temperature loading of reference FR4 board comparison

The thermally induced stress and strain acting on LED boards can be calculated using thermo-mechanical nonlinear structural analysis. The mechanical force induced stress and strain can be also calculated by FEM analysis. First we obtain stress distribution for extreme temperatures (or our case -40 °C and 120 °C). Than we parameterize the second analysis where only mechanical force is applied on LED board. By using method of optimization we found the forces which causes the similar stress distribution as in case of temperature cycling. We mainly optimize stress values in most problematic parts of design where we expect structural failures. Initial stress (caused by moulding and soldering fabrication process) in structure has to be also taken into the account. The values of this mechanical forces are then applied on measuring apparatus.

In our case of concentric boards only one external force have to be applied on the board. Outside perimeter of the LED board is mechanically fixed at the top and the bottom side, on the surface nodes near to the inner mounting hole is applied external force. Figure 8.9 shows stress distribution for the FR4 master LED board at extreme temperatures (-40 °C and 120 °C) and comparison with stress distribution of applied external mechanical forces (-20 N and 6 N). As we can see stress distributions are almost identical[14].

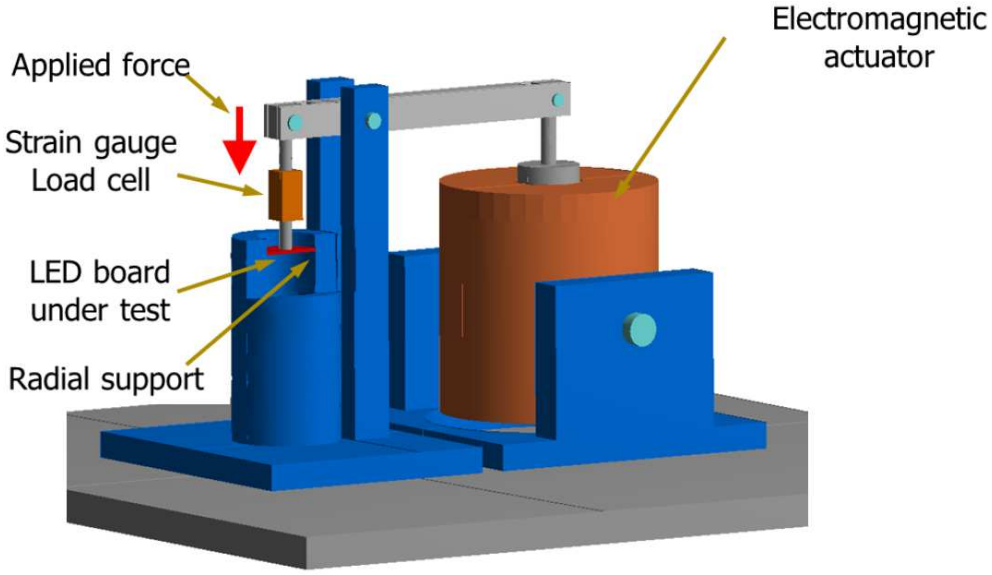

Figure 8.10 - Vibration test apparatus

Developed testing apparatus consists of the few mechanical parts such as electromagnetic actuator (vibrational shaker) the lever to increase the force applied on LED board and the clamping support for LED board (Figure 8.10). The LED board is mechanically fixed on the outside perimeter in specially designed measuring holder. The board is fixed only in the perpendicular direction to main surface, moving in other directions is allowed due to the round shape of holder supports (Figure 8.11). The inner mounting hole of the FR4 board is mechanically coupled to the shaft which imposes the force generated by the shaker. Shaker is powered by AC generator which maintains the constant current with harmonic wave. The constant current ensures the constant force acting on LED board. Mechanical

[14] The work was published in impacted journal Microelectronics Reliability 2012 [A4]

construction is designed as Low loss due to ball bearings, but still it is necessary to measure the acting force.

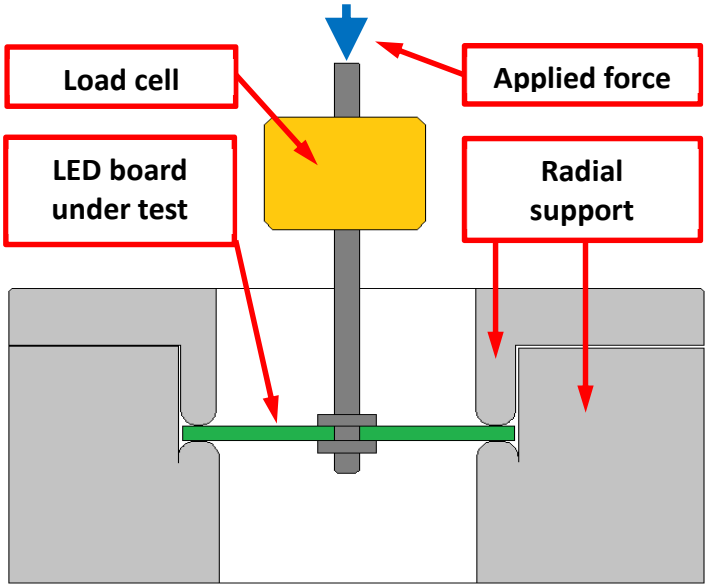

Figure 8.11 - Board fixing in measuring holder

8.2.1. Force Measurement

Force can be measured by loading cell placed on the connecting shaft between LED board and lever. I have designed custom load cell because commercial force sensors are too heavy. Load cell consists of precision measuring beam on which is glued four semiconductor strain gauges by hard cyanoacrylate glue. By using four strain gauges on four sides of the beam, we can sum the contributions of each one and thus we ensures force measurement which is independent on beam bending.

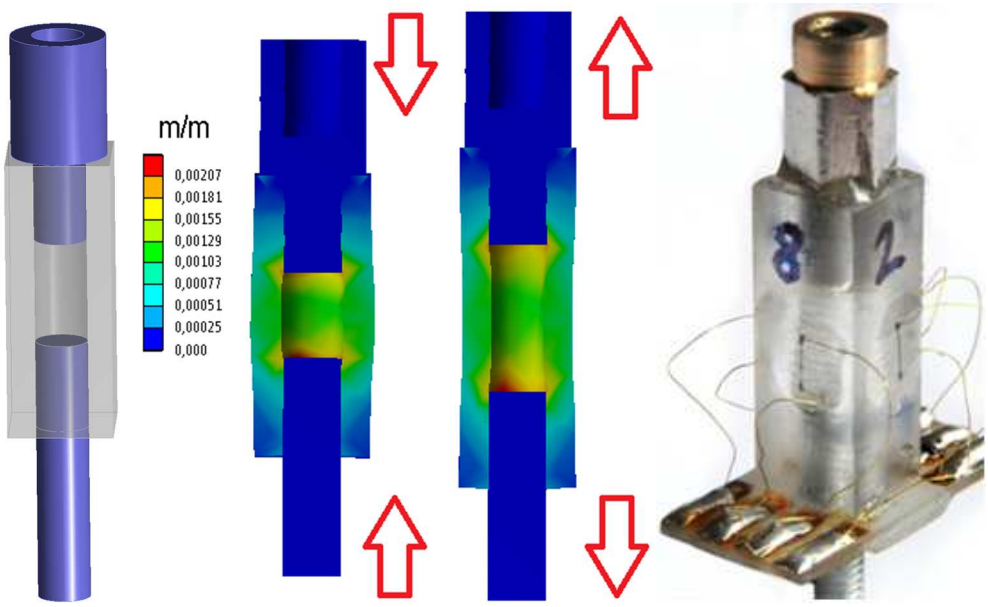

Figure 8.12 - Design of the beam for the force measurement – a) Geometric model; b) Compressive and tensile force acting simulation; c) Real product

As the basic material for beam I chose Poly(methyl methacrylate) which is easily fabricated, it has high value of Yield stress (110 MPa) and it has reasonable Young modulus (1.949 GPa). As we can see at Figure 8.12a, beam has square shape with central hole (S = 28.9 mm^2). Figure 8.12b shows calculations of strain with compressive and tensile force loading of 50 N.

Strain in the middle and at the surface of measuring gauge can be evaluated from simulations or simply computed from equation:

$$\varepsilon = \frac{F}{E.S} \tag{29}$$

Where *F* is the acting force (N), *S* is the area of middle cross-section (m^2) and *E* is Young modulus (Pa).

The main advantages of used semiconductor gauges is the very high sensitivity, small dimensions and simple application. For example the sensitivity is in about 60 times higher which enables precious measuring of the small vibrations and impulses of force. Disadvantage can be seen in nonlinear dependence between resistivity and strain (Figure 8.13) but it can be approximated in standard measuring range by quadratic equation.

$$R_{\varepsilon,25} = R_{0,25}.(1 + C_1.\varepsilon + C_2.\varepsilon^2) \tag{30}$$

Where C_1 is the linear coefficient of deformation rate (-) and C_2 is the quadratic coefficient of deformation rate (-), $R_{0,25}$ is the electrical resistance of the free gauge (without support) at 25 °C (Ω) and $R_{\varepsilon,25}$ is electrical resistance of the deformed strain gauge at 25 °C (Ω).

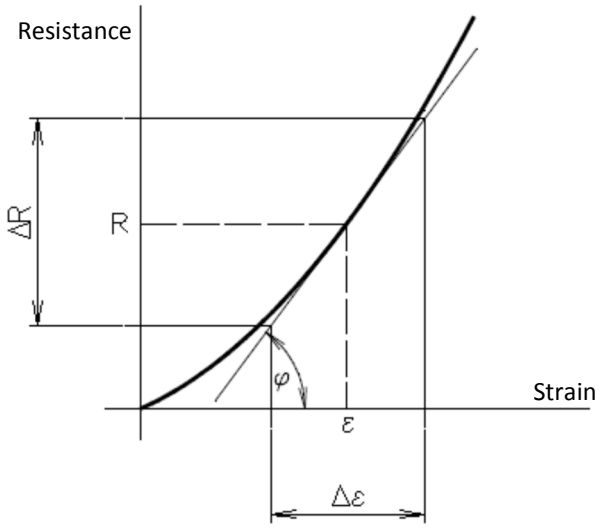

Figure 8.13 - Resistance characteristic of semiconductor strain gauge

The next disadvantage of semiconductor strain gauges is the high value of the resistance temperature dependence. This can be computed from quadratic equation:

$$R_{0,t} = R_{0,25}.(1 + a(t - 25) + .b(t - 25)^2) \tag{31}$$

Where *a* and *b* are the temperature coefficients of the strain gauge resistance (-), *t* is the temperature (°C), $R_{0,25}$ is the electrical resistance of the free gauge at 25 °C (Ω). This dependence can be also eliminated by using temperature compensation by other unloaded gauge with the same temperature. Both strain gauges can be connected to the full-bridge.

In our case, miniature N type semiconductor gauges are used (type AN120-3-35). Gauges are calibrated by the supplied and measured values of C_1, C_2 and $R_{0,25}$ came with them (Table 8.1).

Table 8.1 - Measured values of strain gauges coefficients

AN120-3-35 gauge sensors coefficients			
Number	$R_{0,25}$	C_1	C_2
2	356	-128.9	17 776
4	356	-123.0	16 544
7	373	-127.9	17 575
8	373	-128.0	17 553

For increasing the sensitivity of measurement, each strain gauge is connected in the Winston bridge which is composed of four resistance type elements (Figure 8.14). In our case one of them is measuring gauge and three of them is miniature SMD resistors (type SMD1206 with resistivity 330 Ω ± 5 %). We can make temperature compensation by replacing one of resistors by unloaded gauge but I choose another technique. Only one of the total five strain gauges is unloaded and measured independently by the same data acquisition unit. Compensation is then done by measuring software which also process another measured values and controls the measurement.

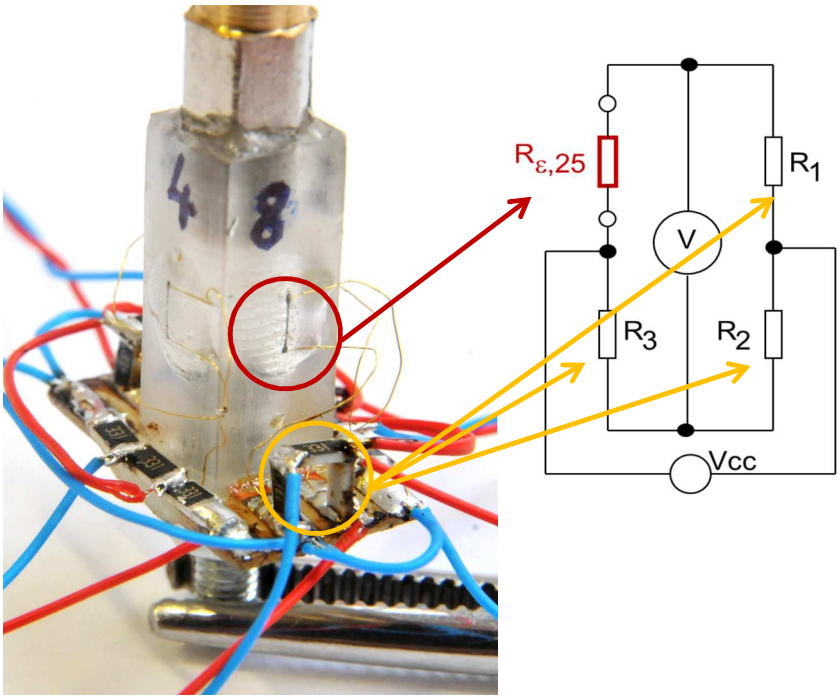

Figure 8.14 - Realization of full-bridge with strain gauge

Measured voltage in the transverse direction of Winston Bridge can be expressed by:

$$V = V_{cc}.\left(\frac{R_3}{R_3 - R_1}\right) - \left(\frac{R_2}{R_{\varepsilon,25} - R_2}\right) \tag{32}$$

Where V is the measured voltage (V), V_{cc} is the supply voltage (V), R_1, R_2, R_3 is the resistivity of used resistors (Ω) and $R_{\varepsilon,25}$ is the electrical resistance of the deformed strain gauge at 25 °C (Ω).

Because of relatively high tolerance of resistivity of resistors used in Winston bridges they have to be calibrated for achieving the high precision of measurement. See the Table 8.2.

Table 8.2 - Measured resistivity of resistors in Winston bridges

Winston bridge resistances (measured)			
Number	R_1	R_2	R_3
T2	325.09	325.69	325.74
T4	325.24	326.08	325.17
T7	326.02	325.17	325.55
T8	325.60	325.38	325.48

Software computes measured force by using equation which combines eq. 29 and 30.

$$F = E.S.\varepsilon = E.S.\frac{-C_1 R_{0.25} \pm \sqrt{(C_1 R_{0.25})^2 - 4.C_2 R_{0.25}.(R_{0.25} - R_{\varepsilon.25})}}{2.C_2 R_{0.25}} \tag{33}$$

Resistance of mechanically stressed strain gauge $R_{\varepsilon,25}$ is the only one unknown variable. It can be expressed from eq. 32:

$$R_{\varepsilon,25} = \frac{R_2}{\frac{R_3}{R_3 + R_1} - \frac{V}{V_{cc}}} - R_2 \tag{34}$$

Than we can write:

$$F = E.S.\frac{-C_1.R_{0.25} \pm \sqrt{(C_1.R_{0.25})^2 - 4.C_2 R_{0.25}.\left(R_{0.25} - \frac{R_2}{\frac{R_3}{R_3 + R_1} - \frac{V}{V_{cc}}} - R_2\right)}}{2.C_2.R_{0.25}} \tag{35}$$

Where F is the acting force (N), S is the area of middle cross-section (m^2) and E is Young modulus (Pa), C_1 is the linear coefficient of deformation rate (-) and C_2 is the quadratic coefficient of deformation rate (-), $R_{0,25}$ is the electrical resistance of the free gauge (without support) at 25 °C (Ω), V is the measured voltage (V), V_{cc} is the supply voltage (V), R_1, R_2 and R_3 is the resistivity of used resistors (Ω).

8.2.2. Structure Failure Detection Method

Another problem which have to be solved is how to determine the number of cycles to failure. As the failure, we can consider the significant degradation of luminous flux or its total loss. In case of force loading, the mechanically induced degradation of current conducting parts is significant. As we can see at Figure 8.8 structure failure can be firstly expected in LED metallization and in solder layer between the board and mounted LEDs. Structure damage occurs mainly in two ways. First the cycling mechanical stress in structure leads to micro crack formation in the volume of body and this changes the active wire of copper or solder joint cross-section which leads to increase of resistance. Secondly the same stress causes the delamination process on interface between solder and copper layers.

During the measurement, it is necessary to evaluate the quality and integrity of the mentioned connections. Considering the fact that through these parts conduct the electric current which is used to power the LEDs, it is possible to determine the integrity of the connection by measuring the impedance of the connection. In most cases, the LEDs are connected in series, therefore the critical connections are in series. By measuring the whole board we can find out the location of the first cracks in the structure. If we leads out the wires from LED joints in top metallization before measurement, we can measure also the occurrence of failure of all these connections independently and thus increase the as the population of solder joints durability.

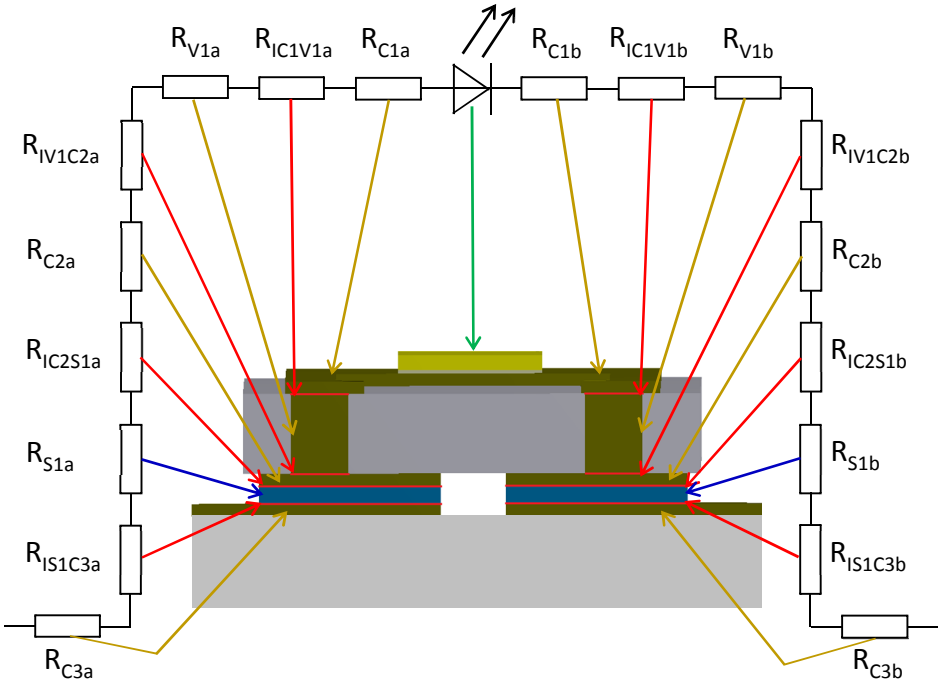

Figure 8.15 - The equivalent electrical circuit of LED structure and connection

R_{C1a}, R_{C1b} – Electrical resistance of top Cu layer of LED package
R_{IC1V1a}, R_{IC1V1b} – Electrical resistance of interface between top Cu layer of LED package and LED package via
R_{V1a}, R_{V1b} – Electrical resistance of via of LED package
R_{IV1C2a}, R_{IV1C2b} – Electrical resistance of interface between bottom Cu layer of LED package and LED pack. via
R_{C2a}, R_{C2b} – Electrical resistance of bottom Cu layer of LED package
R_{IC2S1a}, R_{IC2S1b} – Electrical resistance of interface between bottom Cu layer of LED package and solder layer

R_{S1a}, R_{S1b} – Electrical resistance of solder layer
R_{IS1C3a}, R_{IS1C3b} – Electrical resistance of interface between top Cu layer of LED board and solder layer
R_{C3a}, R_{C3b} – Electrical resistance of top Cu layer of LED board

Resistances in LED housing structure and resistances of LED connection (Figure 8.15) are very low, compared with the static resistance of the LED junction in the operation point are a several orders lower. To ensure evaluation of connection impedance I designed measuring circuit for evaluating of it by using the alternating current.

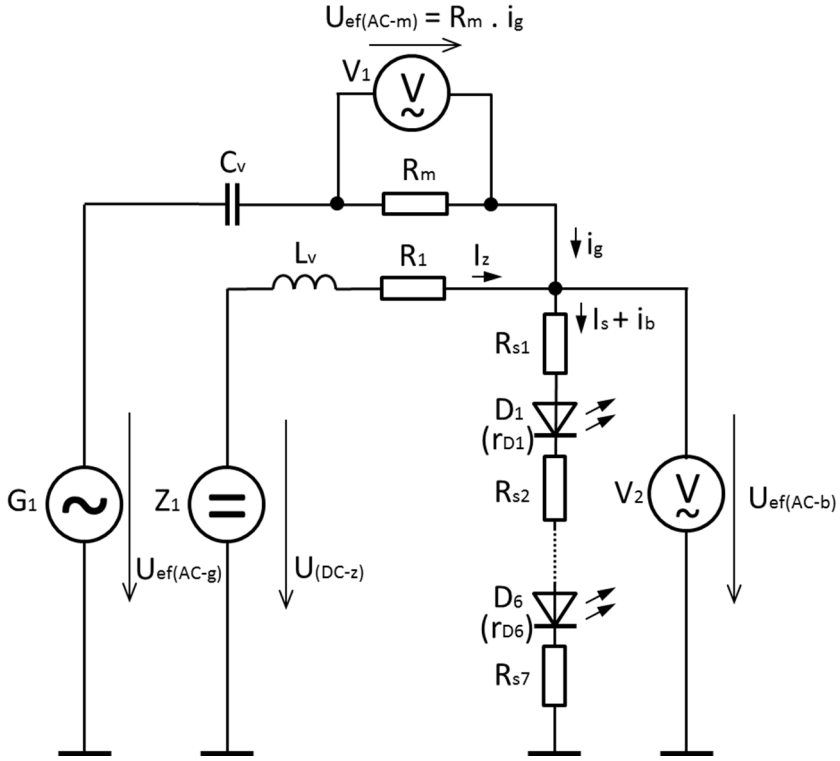

Figure 8.16 - The measuring system for evaluating the dynamic resistance of electrical circuits

Figure 8.16 shows the principal scheme of the measuring system for evaluating the dynamic resistance of electrical circuits on LED boards. The board often contains only one electrical power line that connects a series of all the LED housings D_1 .. D_6 (R_{D6} .. R_{D1} to characterize the dynamic resistance of LED chips and surrounding parts). Quality of connection is limited by the impedance of copper parts and the solder layer (R_{S1} to R_{S7}). DC power supply Z_1 (DC voltage $U_{(DC-z)}$) is used to set the DC working point of LEDs and at the same time determines the thermal power lost in the LEDs and thus the temperature of the whole board. Harmonic generator G_1 (AC voltage $U_{eff\ (AC-g)}$) defines the operating point oscillation around its DC position, which is also measured by a pair of AC voltmeters V_1 (voltage $U_{eff\ (AC-m)}$) and V_2 (voltage $U_{eff\ (AC-b)}$). The resistor R_m is used as the current to voltage converter. The capacitor C_V and the coil L_V is used for frequency separation of circuits in order to DC power supply and the harmonic generator do not affect each other.

8.2.3. High Cycle Fatigue Measurement by Vibration Test Method

Based on previous knowledge system for high cycle vibration measurement was prepared[15]. System consists of mechanical structure which is specifically bending the tested board, circuits for the force measuring and board dynamic resistance measuring and includes also the data acquisition unit which connect control computer with measuring software (Figure 8.17).

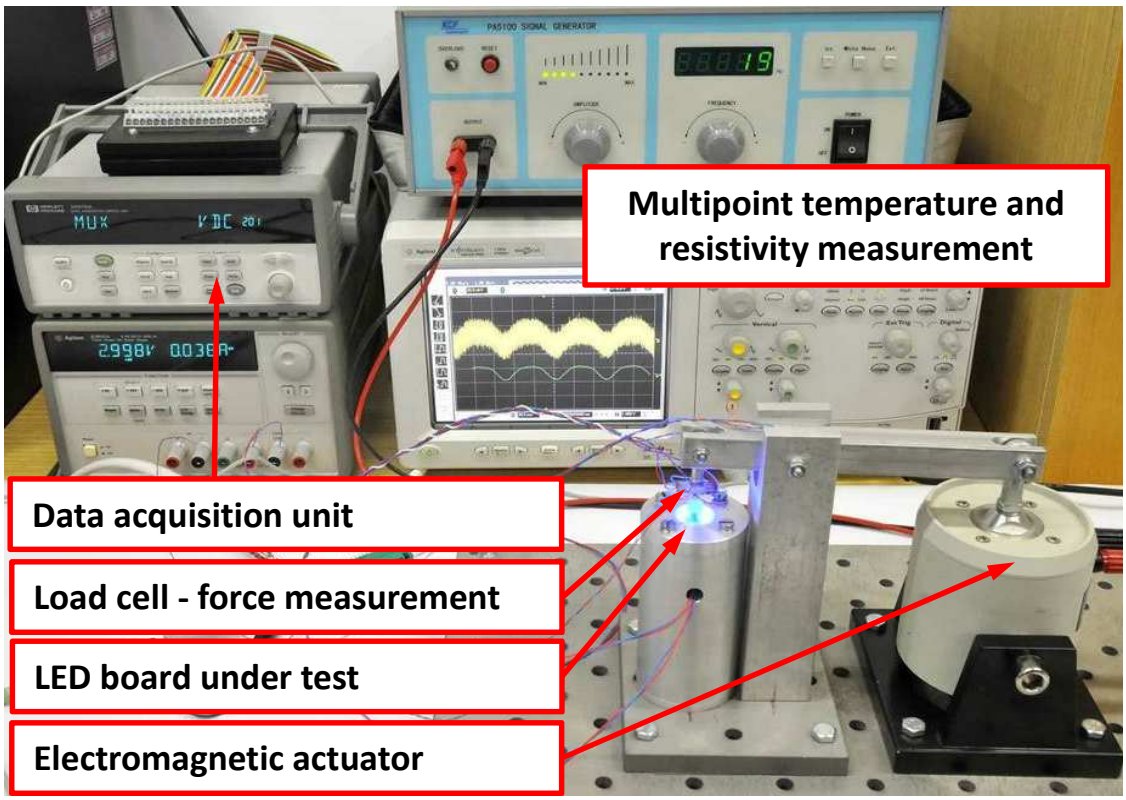

Figure 8.17 - Measuring system for high cycle fatigue evaluating - vibration tests

After fixing of the board into the measuring sink it has to be characterized before cycling process by electrical resistance measurement. Than the software starts measuring procedure and defined mechanical force is applied on the LED board by the shaker. After every 100 cycles, the cycling is interrupted and the resistances are measured. They have to be measured in three different LED board deflections because cracks are opening and closing according to LED board deflection. First value is measured for the maximum of positive force which is equivalent to highest applicable temperature (120 °C in our case), second is for zero force which is also the state of room temperature and the last value is measured for the positive force which is equivalent to the lowest temperature (-40 °C in our case). Values of applied forces have to be evaluated from simulation, see the Figure 8.9 for the reference FR4 board.

[15] The system was registered in 2012 as a functional model [A21]

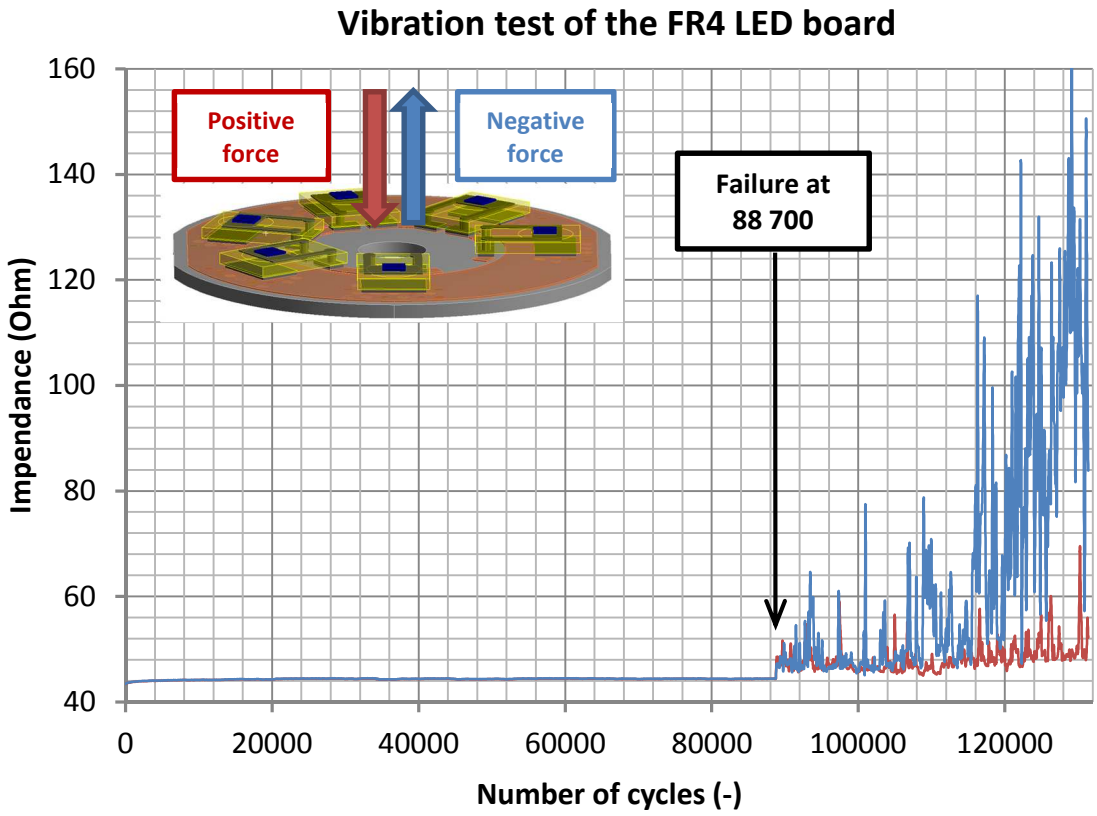

Figure 8.18 - Vibration measurement result – reference FR4 sample 1

The method was verified by measuring two pieces of the reference FR4 LED board (design A) and two pieces of IMS LED board (design D), next boards will be measured in the future after its final fabrication. In case for FR4, failures occurs after 97 800 on the first sample and after 86 500 cycles on the second. In case for IMS, failures occurs after 115 400 on the first sample and after 83 300 cycles on the second. As you can see at Figure 8.18, LED board circuit firstly shows the small impedance increase which was caused by crack formation, than the crack quickly propagates due to the reduced strength of structure. After few hundred cycles, the crack causes total damage of the conductive path which leads to irregular loss of the luminous flux.

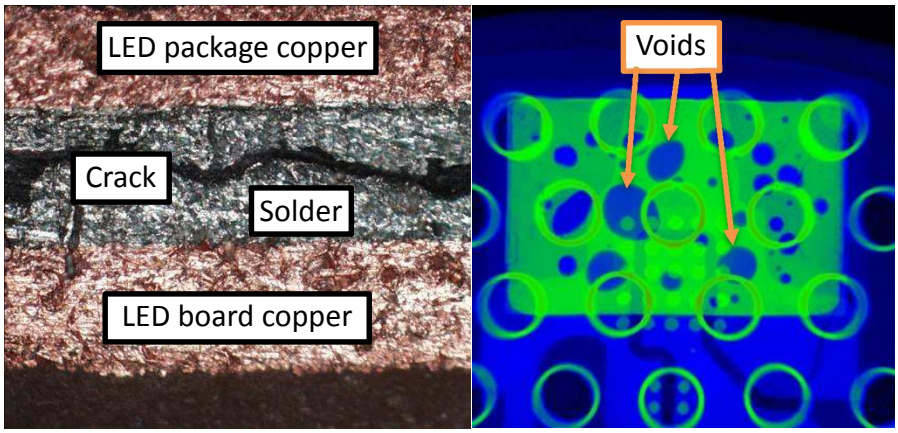

Figure 8.19 - a) Crack in solder layer; b) X-ray image of voids in solder pad

Unlike the simulations of mechanical bending, the results of measurements shows that cracks firstly occurs in the solder layer (Figure 8.19a). Failures in copper layers have not been properly detected because cracks appear mainly in the solder joins. Simulated lifetime value of solder layer is about 50 to 100 percent higher than measured. The shorter measured lifetime is mostly caused by voids in real structure. By using X-ray photography, voids were found in thermal pad solder joints and also in electrical pads joints (Figure 8.19b). The large amount of voids can cause to earlier crack initiation due to the bigger local mechanical stress around the voids. For the next simulations, geometry of simulation models have to be updated according to results of CT detection of real structures.

Table 8.3 - Measurement and simulated life time comparison for FR4 and IMS LED board

	Lifetime (cycles)			
	FR4 sample 1	**FR4 Sample 2**	**IMS sample 1**	**IMS sample 2**
Solder layer simulation	161 500	-	176 070	-
Cu layer simulation	118 550	-	121 410	-
Solder layer measurement	88 700	97 500	115 400	83 300
Cu layer measurement	n/a	n/a	n/a	n/a

Table 8.3 summarises and compares lifetime performance of FR4 and IMS technology. As we can see the better performance according to mechanical vibration tests shows IMS LED board with 121 410 cycles to failure (simulated value) and 115 400 (83 300) cycles to failure (measured value)[16].

[16] The work was published in the impacted journal Radioengineering in April 2013 [A1] and at international conference CIMSim 2013 [A7]

8.3. Low Cycle Fatigue

In the previous chapters, I discussed fatigue behavior of materials which are subjected to high cycle loading. By using of this type of loading, structures composed of brittle materials can be very well tested. But there is one important material which cannot be successfully tested by high cycle loading. The material is the tin solder which is very ductile, its melting point is relatively low. The material high ductility respectively the low value of the yield stress causes the occurrence of the significant values of the plastic strain during the higher values of applied stress. Also the low melting temperature of the tin solder which is near to the room temperature, causes the appearance of creep strain during the prolonged mechanical loading especially at higher temperatures. The solder body energy built-in by the low cycle loading (when plastic or creep strain occurs) causes the microscopic or macroscopic damage of the structure and thus influence the thermo mechanical lifetime. Solder joints especially the lead free types which are subjected to periodical thermo mechanical loading are usually the most problematic parts of electronic systems. Comparatively small number of thermal cycles can lead to solder joints failure. In our case, relatively small solder joints which connects LEDs with the board, are subjected to high mechanical stress caused by different thermal expansion coefficients of the LED housings and the LED board. The stress usually becomes larger than yield stress of the solder and the loading is usually periodical and prolonged at high temperatures, so the high values of plastic and creep strain occurs. Accumulating of the creep strains can initiate cracks in structure that are propagating in each next thermal cycle and latterly causes the total damage of the solder joint. Precious modeling and evaluation of the creep strain is therefore the very important part in determining the lifetime of the electronic systems.

In the last few years, many papers were devoted to modelling of solder pads lifetime. Low cycle fatigue models can be classified by the fatigue driving force parameter used to characterize the fatigue damage process. The models can be divided in five main categories:

- Plastic strain-based
- Creep strain-based
- Energy-based
- Damage-based
- Mechanical stress-based

8.3.1. Plastic Strain Based Models

One of the best known models that are used to calculate reliability of solder joints is **Coffin-Manson** relationship [B70]. This relationship shows the cyclic plastic strain in the joint, caused by differences in the thermal expansion of the material and the expected number of cycles to failure. Experimental data is required to determine the constants. The Coffin–Manson relation assumes that failure is strictly caused by plastic deformation and the elastic strain range has the negligible effect on the low cycle fatigue life.

$$N_f = \frac{1}{2}\left(\frac{2\varepsilon\prime_f}{\gamma_p}\right)^C \quad (36)$$

Where N_f is the number of cycles to failure (-), ε'_f is the empirical constant known as the fatigue ductility coefficient, the failure strain for the single reversal, γ_p is the plastic shear strain amplitude (Pa) and *C* is the empirical constant known as the fatigue ductility exponent. For the simple case the strain amplitude can be calculated from equation 37.

$$\gamma_p = \frac{L.\Delta\alpha.\Delta T}{2h} \quad (37)$$

Where γ_p is the plastic shear strain amplitude (Pa), *L* is the length of SMD housing, $\Delta\alpha$ is the difference of thermal expansion coefficients of SMD housing and PCB, ΔT is the difference between highest and lowest cycling temperatures (K), and *h* is the height of solder joint (m). Better approach is to evaluate the plastic shear strain from a simulation of thermal cycling, value should be determined after stabilizing (about five thermal cycle).

Table 8.4 - Parameters of Coffin-Manson model for different solder types [B70]

Solder type	ε'_f	*C*
Sn-3.5Ag-0.5Cu	3.0685	-0.73
Sn-3.5Ag-1Cu	0.3031	-40.43
SnPb	1.2017	-0.6083

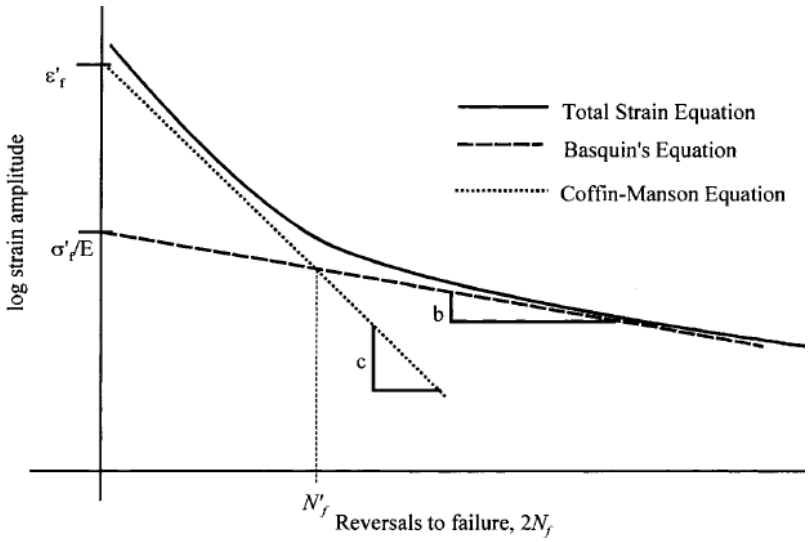

Figure 8.20 - Coffin-Manson-Basquin total strain versus number of cycles to failure [B71]

The Coffin–Manson relationship is universal but not ideal model for solders joints which loading is more prolonged at higher temperatures. The fatigue live is shortened due to the creep effect. Hence, the constants in the Coffin–Manson model are dependent on test temperature and frequency. This model considers only plastic deformations, but we can combine it with Basquin's equation for including the elastic deformations as well. **Coffin-Manson-Basquin** model [B71] improves the approximation of fatigue behaviour in high cycle region.

$$\frac{\Delta\varepsilon}{2} = \frac{\sigma\prime_f}{E}(2N_f)^b + \varepsilon'_f(2N_f)^c \quad (38)$$

Where $\Delta\varepsilon$ is the strain range, σ'_f is the fatigue strength coefficient, E is the elastic modulus, ε'_f is the fatigue ductility, b is the fatigue strength exponent, and c is the fatigue ductility exponent (Basquin's exponent). Coffin-Manson-Basquin model is described by equation called Total equation and connects models for low cycle and high cycle region (Figure 8.20). The low cycle region can be seen on the left side of the curve (left of N'_f) and it is governed by the plastic-strain amplitude (Coffin-Manson equation). The high cycle region is on the right side of curve (right of N'_f) and it is governed by the elastic-strain amplitude (Basquin's equation).

One of modification of the Coffin-Manson model which can be also used for modelling of low cycle fatigue is **Solomon model** [B72]. This model includes temperature dependent parameters for better approximation (Figure 8.21). The model unfortunately does not include the creep behaviour so the estimation of the real lifetime of high power devices is also limited.

$$\Delta\gamma_p {N_f}^{\alpha} = \theta \tag{39}$$

Where $\Delta\gamma_p$ is the plastic shear strain range (-), N_f is the number of cycles to fatigue (-),θ is the inverse of the fatigue ductility coefficient, and α is a material constant.

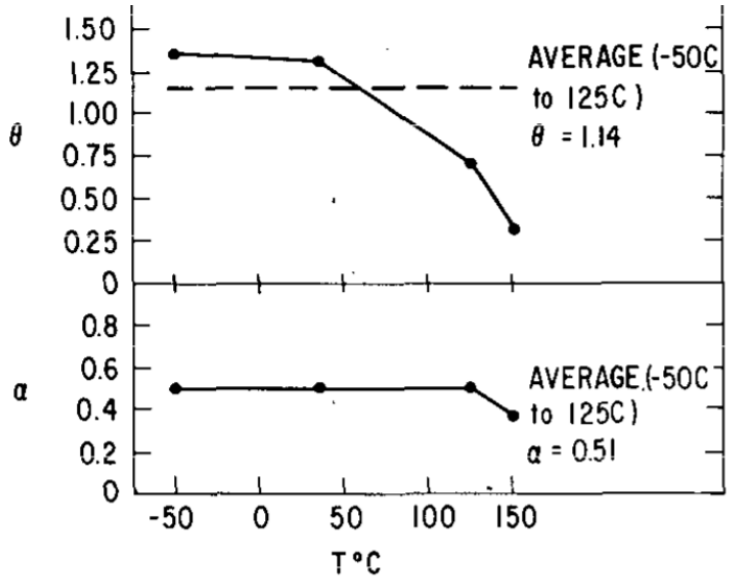

Figure 8.21 - Parameters of Solomon model for SnPb solder [B72]

Next modification of the Coffin-Manson model which also improves Solomon model is **Engelmaier-Wilds model** [B73]. This model also belongs to the category that calculate the low cycle fatigue by using plastic strain. The great advantage of this model is that unlike the Coffin-Manson relationship, also counts with creep strain. Another big advantage is the possibility of counting with the frequency and temperature dependent ductility exponent. Number of cycles to damage can be counted from:

$$N_f = \frac{1}{2}\left(\frac{2\varepsilon'_f}{\Delta D}\right)^C \tag{40}$$

Where N_f is the number of cycles to failure (-), ε'_f is the fatigue ductility coefficient, ΔD is the cyclic fatigue damage and C is the ductility exponent.

$$\Delta D = \left(\frac{F.L_D.\Delta\alpha.\Delta T}{h}\right) \quad (41)$$

Where ΔD is the cyclic fatigue damage, L_D is the maximum distance between SMD housing centre and the most remote housing solder joint, $\Delta\alpha$ is the difference of thermal expansion coefficients of SMD housing and PCB, ΔT is the difference between highest and lowest cycling temperatures (K), and h is the height of solder joint (m).

$$\frac{1}{C} = C_0 + C_1.T_{Sj} + C_2.ln\left(1 + \frac{t_0}{t_D}\right) \quad (42)$$

Where C is the ductility exponent, C_0 determines the relationship between the process of creep and the resulting number of cycles to failure, C_1 is a factor of temperature dependence of the creep rate, C_2 is the factor of time depending on the completion of the process of creep, T_{SJ} is the average cyclic temperature of the solder joint and t_D is the half of cycle time.

$$T_{Sj} = \frac{1}{4}(T_c + T_{c0} + T_c + T_{s0}) \quad (43)$$

Where T_{SJ} is the average cyclic temperature of the solder joint, T_c and T_{C0} is low and high cyclic temperature on the SMD housing, T_s and T_{s0} is low and high cyclic temperature on the PCB.

Table 8.5 - Parameters of Engelmaier-Wilds model for different solder types [B73]

Solder type	ε'_f	C_0	C_1	C_2	T_0
SnPb	0.325	0.442	6.00e-04	-1.74e-02	360
SAC405/305	0.425	0.480	9.30e-04	-1.92e-02	500
SAC205	0.250	0.480	9.30e-04	-1.92e-02	500
SAC305	0.225	0.480	9.30e-04	-1.92e-02	500
SnAg	0.275	0.430	6.30e-04	-1.92e-02	400

8.3.2. Creep Strain Based Models

The creep strain based models focus on the phenomenon of the solder joint deformation caused by the creep. Creep strain is the slow, time-dependent and occurs during long-term exposure to high temperatures[17] under constant load which cases stress lower than the yield stress [B61], [B7]. Creep mechanism has three stages (Figure 8.22) with different speed of deformation. In the primary stage, the strain hardening greater than the softening and the rate of the creep decreases. In the secondary stage the creep is steady and the dependence on time is linear, we can determine the creep rate. In the tertiary stage is forming local consistency failures, such as cavities or cracks. This is followed by integrity damage and fracture. From the constructional point of view is the most important the secondary stage of

[17] In case of metal materials the creep is dominant at homologous temperatures which are higher than 0.3 to 0.5 T_m, where T_m is melting point of the material. The exception is nickel superalloys ≈ 0.75 T_m. SAC305 solder melting point is typically observed at 217 ℃ so the homologous temperature ration at -40 ℃ is about 0.47, deformation will be influence d by creep behavior.

the creep. This is defined between the creep limits, which are the stresses causing the permissible deformation at the given temperature in the given time. Time and permissible deformation are determined by the requirement for the component lifetime. If is crucial only the maintaining of the solder pad integrity (not the specific size of the deformation) then we can define it as the stress strength, which in specified time causes the fracture (t_F).

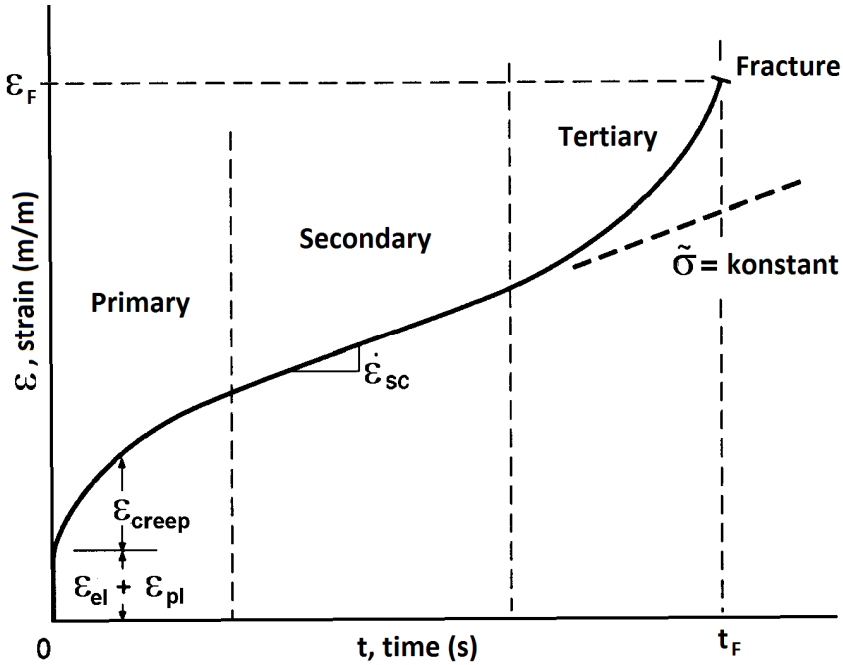

Figure 8.22 - Creep stages

For metallic materials, we can determine two types of creep deformation, i.e., diffusion creep and dislocation creep. The diffusion creep is common in crystal materials and it can occur as the diffusion of atoms in the volume of grains (at lower stress and high temperature) or around grain edges (at lower stress and lower temperature). Diffusion of atoms could induce the release of dislocations and thus facilitate plastic deformation, which is substantially the dislocation creep. The force acting on dislocation in the slip plane is balanced with the reaction force from the precipitate. If the slip plane does not pass through the center of the precipitate, there appears component of force which tries to push the dislocation from the slip plane. Dislocations cannot move in this direction, but its movement can occur when the atoms which form the half-plane edge diffuse. This process is known as the dislocation climbing. Due to it is conditioned by the diffusion, it occurs only at higher temperatures. Dislocation creep is controlled mainly by diffusion processes.

In the case of creep fatigue modelling, we need to evaluate the value of accumulated creep strain during the one thermal cycle. This value can be measured at simple sample of solder joint but on the real board the same loading caused different stresses at the different joints due to the complex geometry. Better understanding can be obtained from the finite element modelling of the LED board model.

Creep strain value can be computed by using one of many creep constitutive equations. These equations approximate creep behaviour in primary, secondary, and/or tertiary creep stages (Figure 8.22). All equations use experimental data which is measured on different solder joints samples. Each solder joint type requires the different equation for correct lifetime estimation.

The steady state creep stain rate for eutectic and near-eutectic solder alloys can be characterized by **Arrhenious rate model (Norton creep law)** [B74]. This model approximates only second (stable) stage of creep and includes the effects of temperature of the solder.

$$\varepsilon_{cr} = A.\sigma^{n}.e^{-(\frac{Q}{R_g T})} \tag{44}$$

Where ε_{cr} is the steady state creep strain rate, σ is the current stress, A and n are experimentally determined material constants, Q is the activation energy for creep, R_g is the universal gas constant, and T is the temperature of the solder (K).

One of the more precious constitutive equation which better reflects reality and which is widely used is **Norton-Power Law (double power law)** [B74]**.**

$$\varepsilon_{cr} = A_1\left(\frac{\sigma}{\sigma_n}\right)^{n1} exp\left(\frac{-H_1}{kT}\right) + A_2\left(\frac{\sigma}{\sigma_n}\right)^{n2} exp\left(\frac{-H_2}{kT}\right) \tag{45}$$

Where ε_{cr} is the equivalent creep strain, σ is equivalent stress, T is temperature (absolute), k is Boltzman constant, A_1 , A_1, H_2 , H_2, n_1, n_2 and σ_n are constants defined by the measurement. Constants were published for example by Wiese at al [6], they used the double power law constitutive model for creep evaluation of SAC405 Flip Chip solder joints.

Table 8.6 - Parameters of Norton-Power Law for SAC405 solder [B74]

Solder type	A_1	H_1/k	n_1	A_2	H_2/k	n_2	σ_n
SAC405	0.4 μs^{-1}	3 223	3.0	1 ps^{-1}	7 348	12	1 MPa

In our case the most important model which is suitable for our type of solder joint published Schubert et al. [B62], [B69]. **Schubert model** uses hyperbolic sine function that due to its shape accurately covers measured creep rate curve of the lead free solder. The model covers two regions of stress-strain rate curve. Material data were collected for different solder alloys such as SAC 305, SAC 307 and SAC 3075 from different sources.

$$\varepsilon_{cr} = A_1\left[\sinh(\alpha.\sigma)\right]^{n} exp\left(\frac{-H_1}{kT}\right) \tag{46}$$

Where ε_{cr} is the equivalent creep strain, σ is equivalent stress, T is the temperature (absolute), k is Boltzman constant, α, n and H_1 are constants defined by the measurement.

Table 8.7 - Parameters of Schubert model for SAC305 solder [B62], [B69]

Solder type	A_1 (s^{-1})	A (MPa^{-1})	n	H_1/k	E (MPa)	CTE (ppm/K)
SAC405	277 984	0.02447	6.41	6 500	61 251–58.5T(K)	20

Evaluation of lifetime of solder joint requires some criterion for the solder joint damage. One of them which is strictly counting with the creep deformation of solder joints is **Knecht-Fox model** [B100]. It proposes the simple matrix creep fatigue model relating the solder microstructure lifetime and the matrix creep strain range.

$$N_f = \frac{C}{\gamma_{mc}} \tag{47}$$

Where N_f is the number of cycles to failure (-), γ_{mc} is the strain range caused by matrix creep and *C* is the constant which depends on failure criteria and solder microstructure.

Deeper investigation can be done by **Syed model** [B61] which is focused on both mechanisms of matrix creep and diffusion process around grain boundaries. In this model, creep strain is partitioned into two parts. Syed published his research of thin small outline packages thermal cycling which indicated that the dominant mechanism changes from grain boundary sliding to matrix creep for faster ramp rates.

$$N_f = (C_1.D_{gbs} + C_2.D_{ms})^{-1} \tag{48}$$

Where N_f is the number of cycles to failure (-), D_{gbs} is the accumulated equivalent creep strain per cycle for the grain boundary sliding, D_{mc} is the accumulated equivalent creep strain per cycle for the matrix creep, C_1 and C_2 are constants evaluated from measurements.

Table 8.8 - Parameters of Syed model for different solder types [B61]

Solder type	C_1	C_2
SAC305	0.106	0.045
SnPb	0.022	0.063

Syed model is one of the most suitable models for our use because it very well reflects the real creep behaviour of lead free solder joints at high temperatures. The big limitation of the Syed model is the absence of the plastic strain, the model is described by Syed as being applicable to solder alloys at high temperatures and slow temperature cycling.

In case of strain based fatigue models plastic strain models can be combined with creep strain models by using **Miner's linear superposition principal**. For example Solomon fatigue model can be combined with the Knecht-Fox model. The Solomon equation ensures fatigue calculation at higher testing temperatures and The Knecht-Fox equation ensures it at low temperatures where creep behaviour is not dominant.

$$N_f = \frac{1}{\frac{1}{N_p}+\frac{1}{N_c}} \tag{49}$$

Where N_f is the number of cycles to fatigue (-), N_p is the number of cycles to failure due to plastic fatigue and N_c is the number of cycles to failure due to creep fatigue.

8.3.3. Energy-based Models

The energy based fatigue models of the soldered joints make the largest group of fatigue models. These models are used to estimate the lifetime of the solder joint calculation of accumulated hysteresis energy. With the increasing number of cycles the cyclic stress-strain curve called hysteresis loop stabilizes and the amplitude of deformation in soft cycle and amplitude of the stress in hard cycling remains constant. The area of the hysteresis loop represents the energy which is absorbed by the unit volume of the material during one cycle. By dividing the energy by the strain energy density of the same cycle is defined the internal damping coefficient, which characterizes the kinetics of accumulation of fatigue damage. Internal damping coefficient is the increasing function of the amplitude of deformation and strongly depends on temperature and frequency of loading. This is due to the application of different micromechanisms of dissipation of the stored energy. Absorbed strain energy reflected in the localized increase in temperature results in early fracture of component. When accumulation of localized plastic deformation during cyclic loading is growing in the most exposed surface layers of material short fatigue cracks are initiated by the dislocation gliding mechanism.

One of the models which is calculating the fatigue energy is the **Pan model**. This model is based on the assumption that stressing energy accumulates in the soldered joints during thermal cycling and eventually reaches the critical value (CASE - Critical accumulated strain energy). The critical value of strain energy density in the SnAgCu solder joints was estimated as C = 4.55 MPa/mm^3. The rest constants of the model can be obtained from the multiple linear regression of the results obtained from finite element analysis (FEA). Constants are highly dependent on solder joint type, size, material etc. This fatigue model assumes that FEA accurately describes both the plastic and creep energies as distinct separable parts for example by using hyperbolic sine creep equations.

$$C = N_f \left(a.E_p + b.E_c\right) \tag{50}$$

Where N_f is the number of cycles to fatigue (-), C is the critical accumulated strain energy, E_p is the plastic strain energy, E_c is the creep strain energy, a and b are the constants.

Akay model is based on the total strain energy which includes both stress and strain information and for that can be a good indicator of solder joint damage.

$$N_f = \left(\frac{\Delta W_{tot}}{W_0}\right)^{1/k} \tag{51}$$

Where N_f is the number of cycles to fatigue (-), ΔW_{tot} is the total strain energy, W_0 and k are fatigue coefficients ($W_0 = 0.1573; k = -0.6342$ for a LCC package with SnPb solder).

Next group of energy based models was firstly published by Liang, Henrichs et al. His methodology accounts for the geometry of the solder joint based on elastic and creep

analyses. **Liang-Henrichs model** calculate the lifetime from the energy-based fatigue failure criterion [B75].

$$N_f = C(W_{ss})^{-m} \tag{52}$$

Where N_f is the number of cycles to fatigue (-), W_{ss} is the stress-strain hysteresis energy density per cycle (psi), *C* and *m* are temperature-dependent material constants evaluated from the low cycle fatigue measurement.

The last model was used by **Darveaux** [B76] who designed the evaluation of crack initiation from the viscoplastic behaviour. The model was applied by many researchers, who defined its constants for other solder joint types. Unlike the Liang and Henrichs, they are counting the number of cycles to initiate the crack so the crack propagation have to be computed by another model.

$$N_0 = C(\Delta W)^{-m} \tag{53}$$

Where N_0 is the number of cycles to failure (-), ΔW is the stress-strain hysteresis energy density per cycle (psi), *C* and *m* are temperature-dependent material constants evaluated from the low cycle fatigue measurement.

Table 8.9 - Parameters of Darveaux model for different solder joint types [B76], [B77]

Model	Solder joint type	*C*	ΔW
Wu et al.	BGA 63Sn37Pb	18 083	1.46
Jung et al.	PBGA 62Sn36Pb2Ag	7 860	1.00

Number of cycles to initiate the crack does not refer the information about the lifetime. Linking the crack initiation with the actual cycles to failure requires the inclusion of crack propagation phenomenon. More precious model, the **Gustafsson model** [B78] expands the knowledge of Darveaux model with computing of crack propagation.

$$N_{\alpha W} = N_{0s} + \frac{a-(N_{0s}+N_{0p})\frac{da_p}{dN}}{\frac{da_s}{dN}+\frac{da_p}{dN}} \tag{54}$$

Where $N_{\alpha W}$ is the number of cycles to failure (-), N_{0s} and N_{0p} are the primary and secondary crack initiation energy, is the total possible crack length.

$$N_{0p};\ N_{0s} = 54.2(\Delta W)^{-1.00} \tag{55}$$

Where N_{0s} and N_{0p} are the primary and secondary crack initiation energy, ΔW is the stress-strain hysteresis energy density per cycle (psi).

8.3.4. Damage Fatigue Models

This wide model group is based on calculating the accumulation of solder joint damage which can be caused by many factors. The models can include damage caused by temperature, humidity, corrosive environment, vibration etc. Contributions of all the types of damage can be counted together.

Palmgren-Miner rule [B79] defines failure by computing the independent damages D_i (i=1,..,n) that the body experiences. It can be also the same type of damage applied at different time.

$$\sum_{i=1}^{n} D_i = D \quad \text{resp.} \quad \sum_{i=1}^{n} \frac{D_i}{D} = 1 \tag{56}$$

Where *D* is the amount of damage, and $\frac{D_i}{D}$ is the fractional damage received from *i*-th source. In case of simple thermo-mechanical loading, we can define the Palmgre-Miner rule as the ration of the numbers of cycles to failure.

$$\sum_{i=1}^{n} \frac{N_i}{N_{fj}} = 1 \tag{57}$$

Where N_i is the number of applied load cycles of type *i*, and N_{fi} is the pertinent fatigue life at the same cyclic load. For the counting of the damage contributions many approximative models were published. This work mainly uses primary approach with using creep strain based models for the lifetime prediction during low cycle measurement. I show only one example which can be appropriate for the various thermal cycling dwell times and ramp rates.

Stolkarts [B80] defined the fatigue damage model which approximates the lifetime from the isothermal cyclic behaviour of SnAg and SnPb solder joints. This model is based on unified creep-plasticity model with including damage parameter. The stress strain hysteresis loop has to be also used to determine the amount of the damage.

$$N_f = \frac{1-(1-d_f)^{k-1}}{(k+1).L} \tag{58}$$

Where N_f is the number of cycles to fatigue (-), d_f is the amount of damage at failure, *k* is the material constant, *L* is counted from time integral of the initial damage rate of remaining undamaged material in the representative volume element.

8.4. Solder Pads Lifetime Modelling

As I have mentioned, the most problematic parts from low cycle reliability point of view should be the LED package solder joints. This chapter focuses on modelling of its low cycle reliability during thermo-mechanical loading and lifetime prediction. This methodology will be shown only on master FR4 board with Luxeon rebel LEDs which makes the reference board. The modelling and testing are performing on all types of boards but just in the case of the reference board all results are now available. But the testing methodology is applied in the same way on all other samples.

The thermal cycling range for the analysis is set to the standardized industrial testing range of -20 °C to 120 °C. Also the influence of the fabrication process of LED boards is included by counting the thermal strain caused by solidification of solder pads during the cooling process after soldering of LEDs on boards. The temperature of solidification (180 °C) is assumed as the solder zero stress temperature, first simulation cycle enables the stress relaxation as will be in real. The temperature profile is set to simulate the profile of the test chamber which was also used for the verification (Figure 8.23). The temperature was cycled with the period of one cycle per hour.

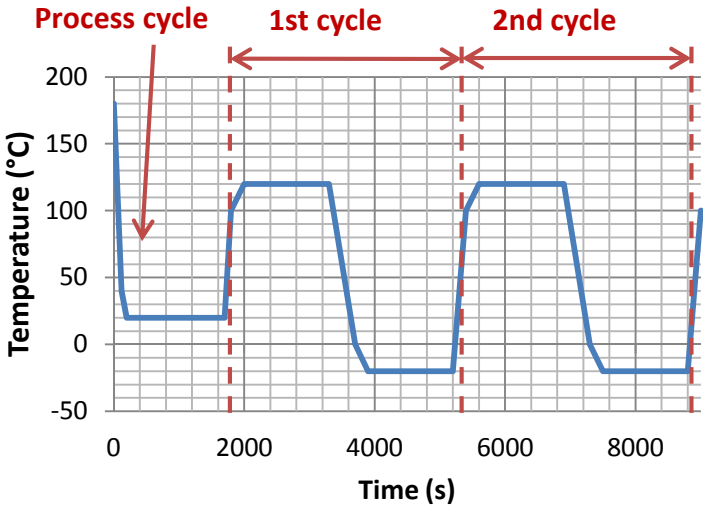

Figure 8.23 - Test chamber temperature profile used in simulations

As I showed in the previous chapters, the temperature profile cases the high and prolonged thermo-mechanical loading of the solder pads. In case of the solder material we expect that elastic and plastic contribution of strain will be in the most time minor in comparison of the creep strain. But this assumption should be proven to decide on the method of the lifetime evaluation. This can be done by computing of all components of the strain and their rates during the simulation of thermal cycling. The methods of the nonlinear simulations of thermal cycling with evaluation of plastic and elastic components of strain were shown in the last chapters. Now we have to extend the simulations by the precious calculation of the creep behaviour of the ductile materials.

In the simple approach it can be seen as the extension of total strain equation by the creep strain formula (Equation 17). The value of the creep strain which depends on the actual value of the loading and prolongation time is proportional to the measured curve for the specific material. The curves of the solder materials referred in the literature is mostly in the shapes of the hyperbolic sine so the Schubert model (Equation 46) very well approximates the creep behaviour of the solder materials. The related papers describe the accuracy of the Schubert approximation (for example [B62], [B69]).

The specified conditions, such as LED board fixing method, thermal profile, external forces etc. closely emulates the real conditions of the composed LED lamp during the thermal oven testing. For the purposes of precious nonlinear simulation of the creep behaviour the model has to be simplified to reduce simulation time. The model of reference board was simplified to the symmetric quarter model and parts which does not significantly influence the solder pads strain were omitted (Figure 8.24). The simplification reduces the simulation time[18] in about twenty times but causes the increase of the simulation error by less than two percent. The inner face nodes of the LED board central hole are mechanically fixed as it is fixed in real condition by the screw. All the other nodes can freely move in all directions.

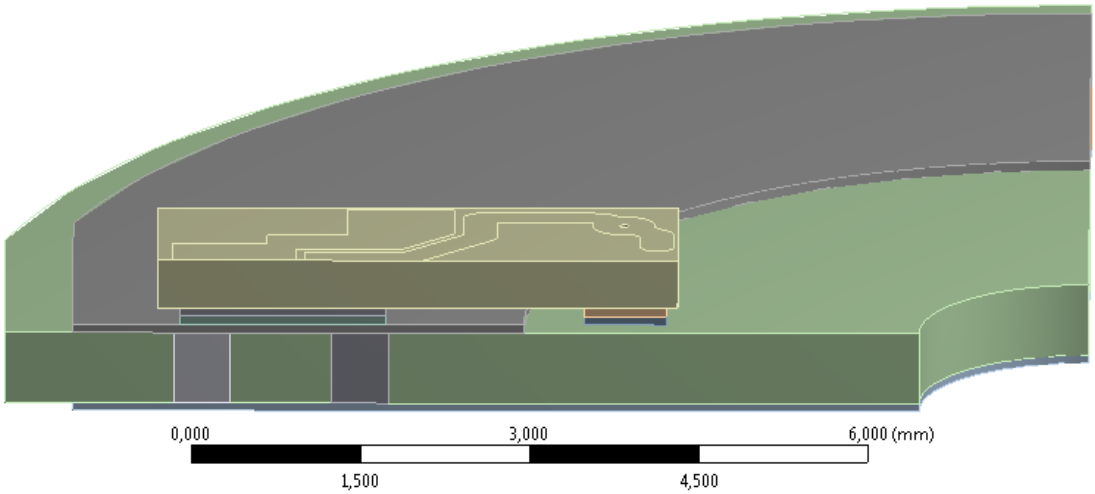

Figure 8.24 - Simplified model of reference LED board

Figure 8.25 shows evaluation of the strain components counted from the simulation of thermal cycling of reference LED board. The rate of the plastic component of strain reaches less than 8 percent of the total strain rate. The elastic strain rate is less than 1 percent of the total strain rate. The rest of the strain rate is caused by the creep behavior of the solder. So we can simplify the lifetime estimation by neglecting the contribution of the plastic and elastic components. After 5 cycles, the creep strain begin the dominant component of the total strain.

[18] The reduced simulation time of the reference LED board is about 12 hour on our simulation computer, prolonged simulation of the non-reduced model eliminates the method benefits. By using the high performance computing techniques the accuracy can be increased.

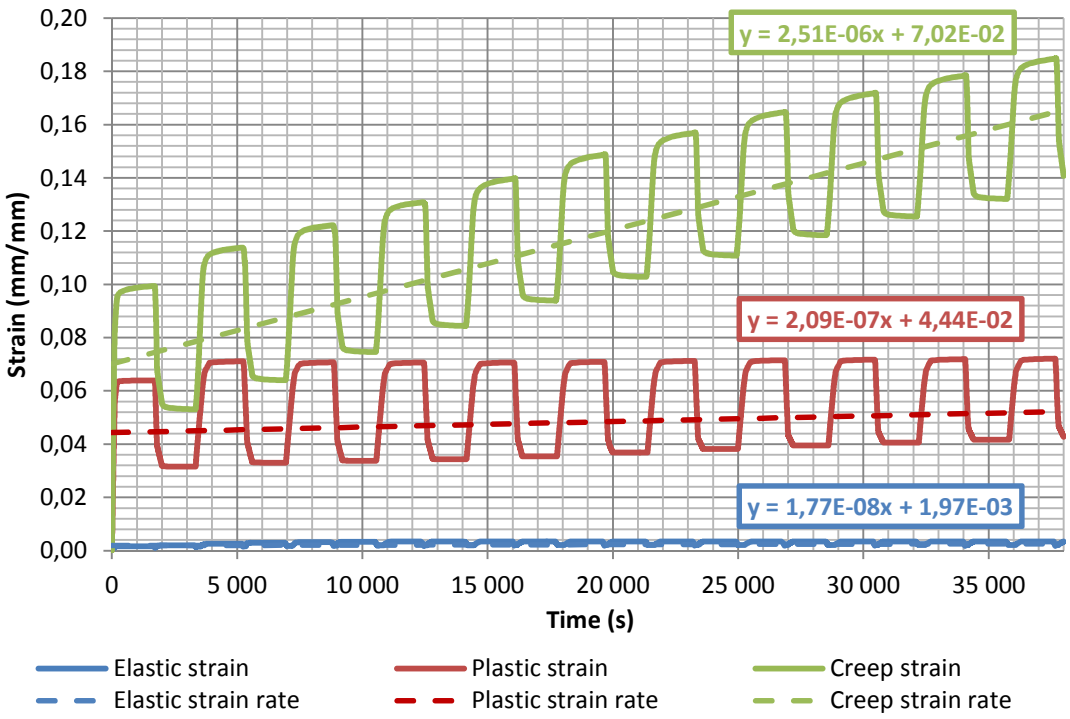

Figure 8.25 - Components of the solder pads strain rate comparison

The creep strain distribution can be evaluated in any loading time so the comparison can be done for example at the ends of sixth and tenth loading cycles (Figure 8.26). This enables the distribution of equivalent strain rate in all computing nodes in the volume of the solder pads. At the end of the loading cycle, the volume temperature reaches the lowest value of the industrial testing temperature (-20 °C in my case) so the thermally induced stress in the structure is the highest.

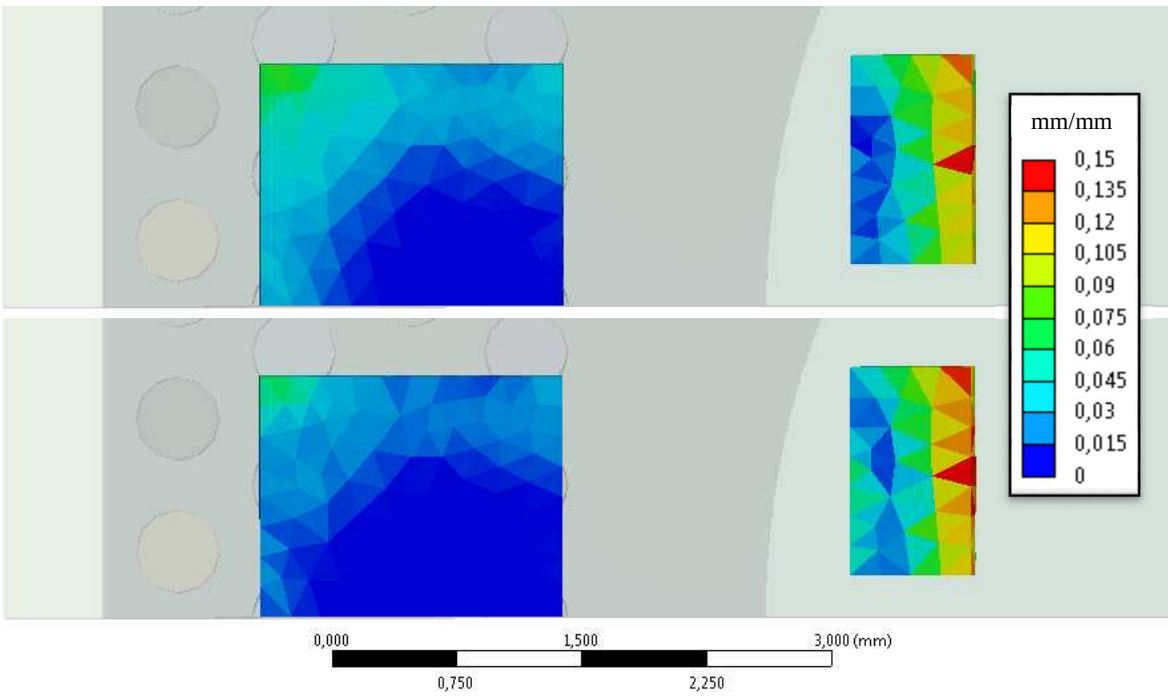

Figure 8.26 - Creep strain component after a) 6th cycle (top); b) 10th cycle (bottom)

The methodology of the lifetime evaluation with using the nonlinear low cycle simulation is based on the set of the creep strain based approximate models such as Knecht-Fox or Syed models. More details can be seen in the chapter 8.3.2. Syed model produces good results of the SAC305 solder lifetime prediction [B61]. In my case where the grain boundary sliding is minor in the comparison of the matrix creep the Syed model can be also simplified. The lifetime calculation can be expressed directly from the accumulated creep. This simplifies the post-processing calculations in FEM simulator. The calculation of the number of cycles to failure with using the total accumulated creep strain is then [B61]:

$$N_f = (0.0468\ \varepsilon_{acc})^{-1} \tag{59}$$

Where N_f is the number of cycles to failure (-),ε_{acc} is the accumulated equivalent creep strain per cycle.

By the post-processing script the distribution of the number of cycles to failure in electrical solder join was obtained. Minimum value of the cycles (2 548) is located in the orange places[19] (Figure 8.27). Possible crack will be probably initiated here. Maximal number of cycles is about one level higher and it is located in the middle of the solder joint[20].

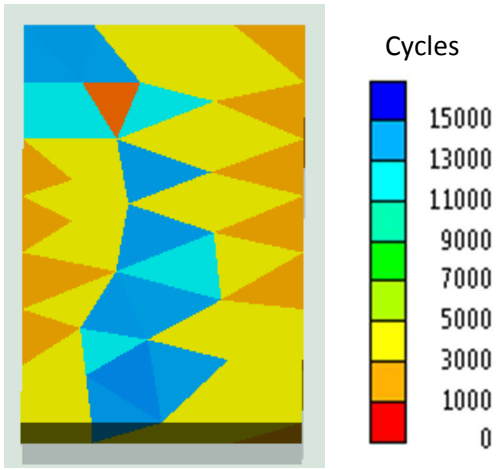

Figure 8.27 - Calculated lifetime in the volume of the solder pad

The results of the simulations cannot show the correct value of the product real lifetime because they do not include all phenomena of the real behaviour. But provided analysis can show the probability of the initiation and propagation of cracks in the most mechanically stressed areas. The lifetime modelling can be used for the good comparison between designed LED board prototypes. The estimated lifetime can be also compared with the results of measurement to improve the accuracy of simulations.

[19] The red triangle represents singular point in the model which is the place where the stress in the mesh does not convergent to the correct value. Simulation result in such place can be neglected.
[20] The work was published at the international conference EDS2013 [A6]

9. Accelerated Thermo-mechanical Lifetime Characterization Method

The chapter describes the methodology of the newly developed unique method for the lifetime testing of the concentric PCB. The method consist of the precious thermo mechanical modelling of the product in conjunction with the specific measurement. The chapter also shows the design of the measurement apparatus, the measurement methodology and the example of its application. As well as the rest of the thesis, the method principles will be shown on the concentric LED boards but it can be also used as the universal testing method. The tested boards are characterized by the circular shape, concentrically mounted components and high operating temperatures. The designed method in combination with the measurement system is designed to be the substitute of slow cyclic testing in the thermal chamber.

The samples of the real product or the product components are usually heated and subsequently cooled in the thermal chamber which usually the specific furnace is allowing the relatively fast cycling of the temperature. Testing samples are cooled or heated mainly by the radiation and the air convection. The heat capacity of the samples and the thermal chamber rapidly slow down the testing process. The temperature range is selected on the basis of the sample real using. The most common temperature ranges are from -20 °C to 100 °C, -40 °C to 120 °C and -55 °C to 125 °C. Depending on the sample size and the type of the chamber, one thermal cycle takes several tens of minutes or units of hours. In our case, where predicted number of the lifetime cycles are more then 2 500, the testing in standard thermal chamber takes more than three months. So the result cannot be flexibly used during the development. The testing is also high energy consuming.

Due to these problems it was necessary to design the new method for the highly accelerated lifetime testing of newly developed boards. The main idea is to replace the slow structure loading caused by the CTE mishmash and the thermal cycling by another equivalent loading. When we look at some specific places in the structure we can find the set of external mechanical forces which causes the same loading in the reliability point of view. In our case we should focus only on the lead-free solder joints for the current conduction because we expect them as the most problematic places of the structure. Its low cycle reliability is mainly influenced by the secondary creep (Figure 8.22) and its increase during one testing cycle (strain rate) [B61]. The setting the same creep strain rate in the solder joints by using the combination of the static temperature and cyclic external forces as by using thermal cycling can produce the same structure damage. So the mechanical forces acting on the measured specimen can replace the lifetime measurement by using the thermal cycling. Directions, sizes and locations of the forces have to be designed to achieve also the equivalent mechanical stress and relative strain, which can occur during the thermal cycling. This ensures the identical direction of the crack propagation.

This method cannot fully replace the thermal cycling because as some of the associated phenomena influencing the sample lifetime is also temperature dependent. But this can significantly improve the accuracy of the reliability simulation model or verify the lifetime estimation of some prototype under development in assumption that another has already been tested by the thermal cycling tests. The major benefit of the system is the possibility of significant shortening of the lifetime testing from the order of months to tens of hours.

Advantages:

- Significant shortening of lifetime testing
- Opportunity to use the test results directly during the prototypes development
- Low cost lifetime testing
- Possibility to set any test profile adequate to any thermal loading profile

Cons:

- During the mechanical loading not all physical phenomena are applied in the same way
- Including the corrosion testing is not effective
- More complex mounting and difficult application of the external forces in the case of the non-concentric PCB

9.1. Methodology for Accelerated Lifetime Testing

The method is based on detailed examination of the simulation models thermo mechanical behaviour of characterized specimens in combination with the specialized measurement. The subsequent measurements by using the newly developed apparatus specify the model parameters and proves the simulation results.

The application procedure is following:

1) Design of detailed 3D model of the sample or model takeover from manufacturing documentation.
2) Thermo mechanical simulations of 3D model using FEM simulation program under the following conditions:
   - Material parameters of individual structure parts are set to correspond with the materials specified in the manufacturing documentation
   - The temperature of zero mechanical stress (simulation parameter) has to be determined corresponding to the solder type and PCB structure
   - PCB is mechanically fixed same way as in real. In case of concentric boards are fixed in the area near their center hole
   - The PCB temperature variation is set in the range of extreme values that can be expected during its use or in the same range of accelerated thermal cycling measurement. According to the technical practice most frequently used range is -20..120 °C.
3) Deriving of the most critical parts of the structure where the level of mechanical equivalent stress exceed the limit of the plastic deformation or is parentally closest to the material ultimate strength.

4) Definition of the set of parameters and equations which describes the phenomena of the creep behaviour in the evaluated critical parts. We can use some of the creep approximations for example the Schubert et.al. hyperbolic sine approximate model (Chapter 8.3.2).
5) Modelling by transient thermo mechanical simulation of the modified model, the result will be the size of periodic increment of strain due to the material creep behaviour in the critical parts of the structure at each of the thermal loading cycles. The testing range of thermal stress (cycling) is the same as in point 2.
6) Estimation of the lifetime based on the evaluated creep strain. We can use some of the lifetime approximation based on the creep strain for example the Syed model [61] (Chapter 8.3.2). This represents the number of cycles we expect during the accelerated thermal cycling test in the thermal chamber.
7) Performing of the transient thermo mechanical simulation of the second model where the loading is changed from the simple thermal loading (same as in the thermal chamber) to the complex equivalent loading of the combination of the static temperature and external mechanical force loading. The mechanical fixing of PCB is the same as in the point 2. The board temperature remains constant during the simulation as well as during the consequent measurement.The board has to be heated to the upper temperature so that the influence of the creep to the total strain is dominant. The temperature can be set in the range of about 30 .. 90 °C, in the case of SAC types of solder I recommend using 70 °C. The cyclic loading is done by the alternating external forces applied on the specific places. In the case of the concentric boards the external force is applied to the area near to board perimeter. The force is acting in the perpendicular direction to its main plane. The lowest and the highest value of the acting force as well as the waveform is evaluated with using methods of the model optimization so that the value of the creep strain in critical parts during the equivalent mechanical loading is almost the same as during the thermal loading (item 5).
8) Characterization of manufactured sample of evaluated board using the specialized measuring apparatus which assembly and usage are described in the following chapter.

The measurement results (the number of cycles to the failure) are equivalent to the values evaluated form the accelerated or non-accelerated (depends on set values) thermal cycling lifetime tests. It can be used for the comparison of the newly developed board prototypes. Because of the low testing time, the results can be directly used for the virtual prototyping.

9.2. Concentric LED Board Testing

The advantage of the printed circuits for the LED lamps can be seen in the circular topology including the concentrically mounted electronic devices, PCBs have mostly circular symmetry. The board has the circular symmetry when we can find the thermal or the mechanical loading which by acting on the centre causes the similar loading on all mounted components on the board. This can be called concentric boards. The typical concentric board (the LED board in this case) is shown on the Figure 9.1.

The simulations show that by applying the mechanical force in the direction perpendicular to the main plane of the circular boards which is applied to the center of the PCB or to the perimeter can be achieved the similar distribution of mechanical stress in critical areas such can be done by the thermal cycling.

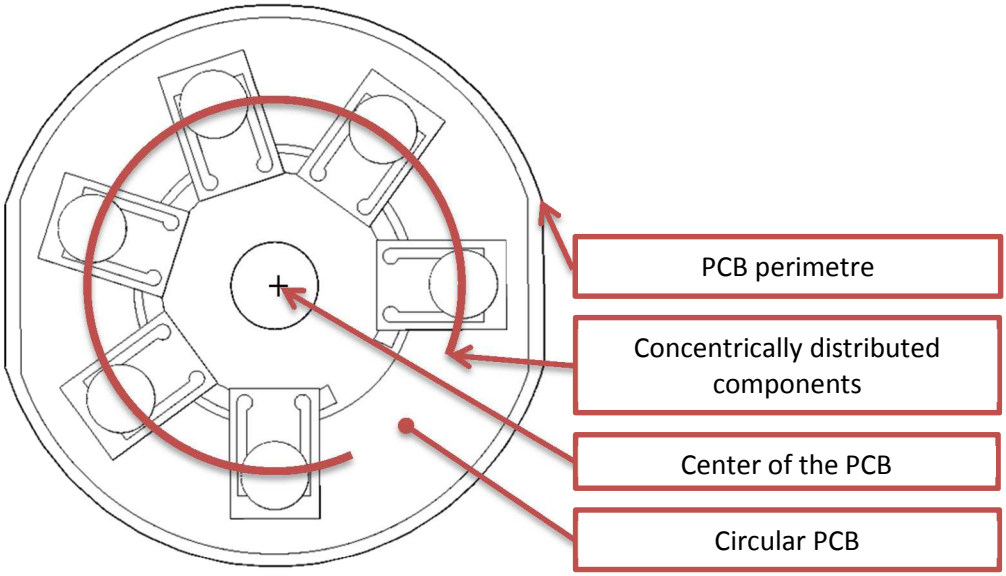

Figure 9.1 - Typical design of the printed circuit board (PCB)

The distribution of the creep strain after fifth cycle of the thermal loading is compared with the distribution of the strain caused by the mechanical loading (Figure 9.2). We can say, that after five cycles, the actual value does not reached to the same values. This is caused by the different initial conditions of both simulations. But this difference quickly vanished because after the few tens of cycles, the preloading creep strain constitute only less than one percent of the totally accumulated creep strain. This preloading creep strain has the minor influence on the total lifetime.

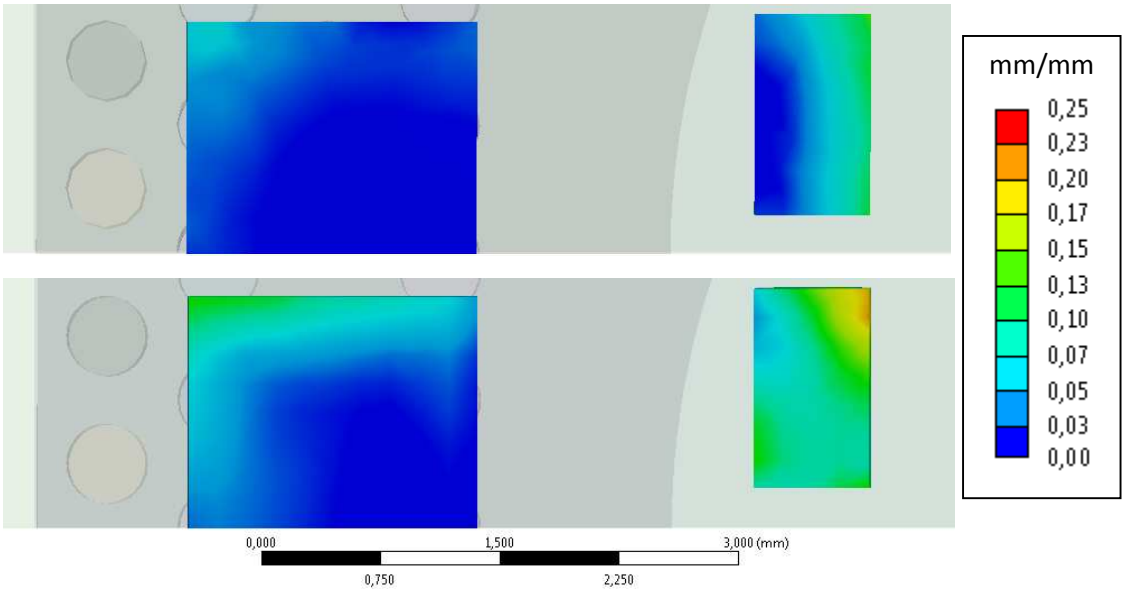

Figure 9.2 - Creep strain after ten cycles a) Thermal loading (top); b) Mechanical loading (bottom)

When we focus on the creep strain distribution, the relative variation between the thermally and the mechanically loaded solder pads volumes shows the values less than twelve percent. This can be considered an acceptable value and will be later compensated by the calibration of the simulation model. More important information can be seen in the maximal value of the creep strain rate. This rate directly affects the speed of the structure damage, as I said previously. The Figure 9.3 shows the comparison of the creep strain rate caused by the thermal loading in the industrial testing range of -20..120 °C and by the equivalent mechanical loading by alternating force of 82 N and constant temperature of 70 °C. These values were obtained by using methods of the model optimization.

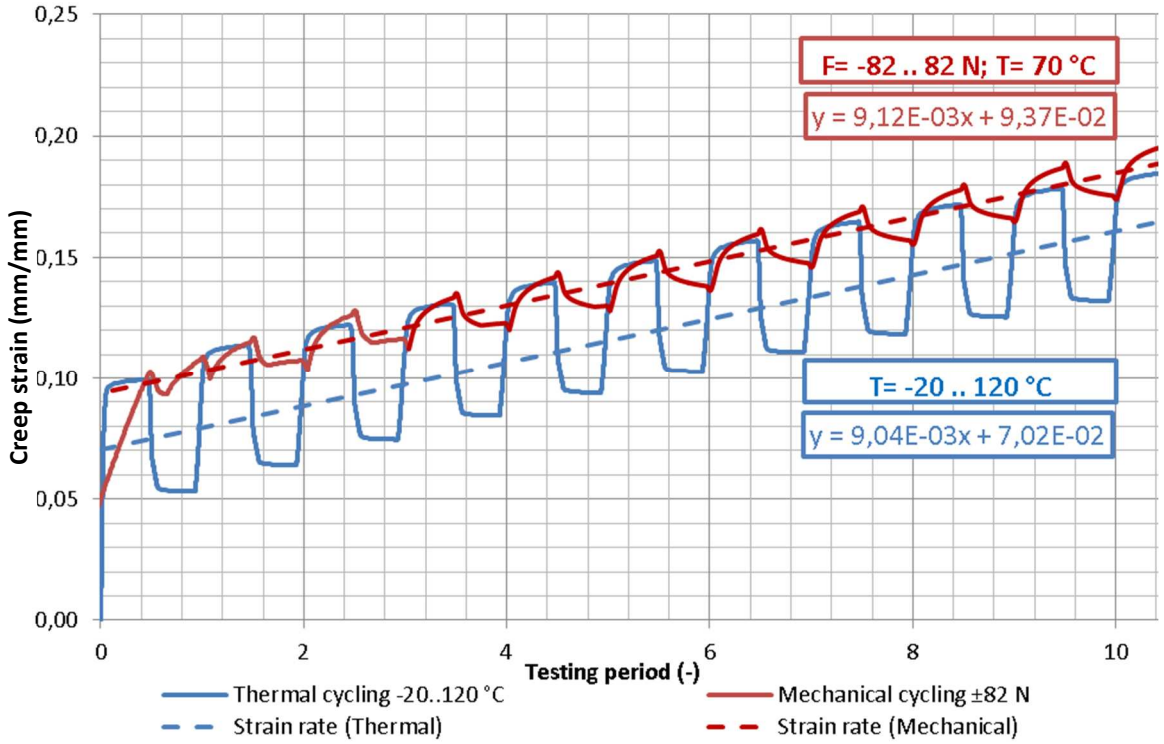

Figure 9.3 - Solder pads creep strain rate comparison

The optimization script can be successfully used for evaluation of the acting force equivalent to another temperature loading ranges. Table 9.1 summarises five optimizations of the equivalent lifetime testing parameters. Parameters are evaluated for thirty times testing acceleration. We can see the influence of the testing range to the expected lifetime.

Table 9.1 - Equivalent testing forces for the Master FR4 LED board lifetime testing

Thermal cycling Period 60 minutes			**Equivalent mechanical cycling** Period 2 minutes, 70 °C		
Temp. range (°C)	Creep str. rate (m/m per cycle)	Cycles to fail. (-)	Force range (N)	Creep str. rate (m/m per cycle)	Cycles to fail. (-)
-20..120	9,04E-03	2 548	±82	9,12E-03	2 529
-40..90	7,35E-03	3 136	±66	7,38E-03	3 124
-20..90	6,86E-03	3 361	±61	6,87E-03	3 358
0..90	6,03E-03	3 827	±54	6,04E-03	3 820
20..90	4,87E-03	4 738	±44	4,89E-03	4 714

9.3. Testing Apparatus Design

The testing apparatus is very complex in terms of the number of technical areas which was used during its development. It contains components from the mechanical engineering (mechanical design and board fixation) from the automation technology (pneumatic control system with pneumatic actuator), from the electronics (support for the measurement system and the PCB power supply) and electrical measurement technology (the automated bus controlled measuring system). Figure 9.6 shows the principal diagram of the measuring apparatus main parts. Because parts are from different technical areas, the diagram also shows the parts interconnection and interactions variables. I will focus on separate parts individually, the design will be shown on the concentric LED boards.

The mechanical structure (Figure 9.4) consists of cushioned support plate 5.1 from the stainless steel sheet with the thickness of 10 mm, which ensures sufficient rigidity of the whole system and prevents further transfer of vibrations from the environment. The plate 5.1 allows mounting of fixing constructions for various samples of various shapes and sizes, as well as the possibility to mount the different types and sizes of mechanical actuators.

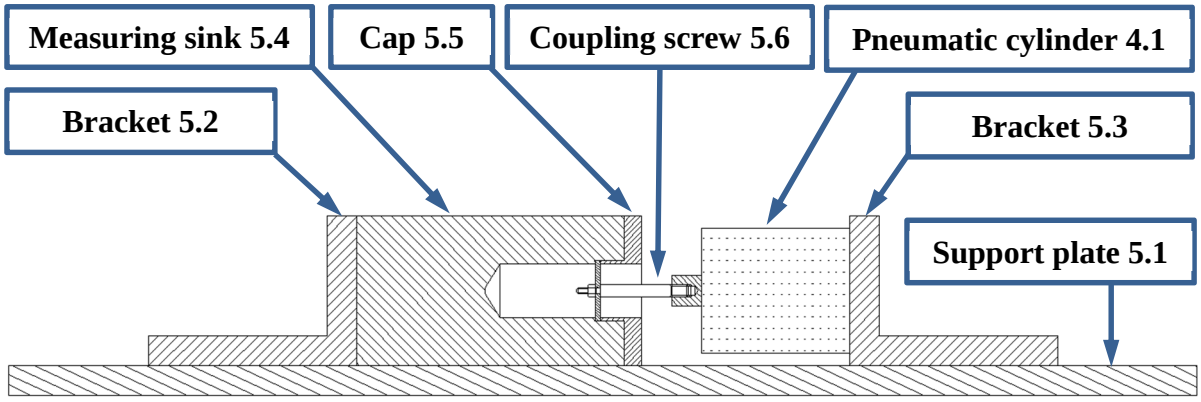

Figure 9.4 - The testing apparatus mechanical design

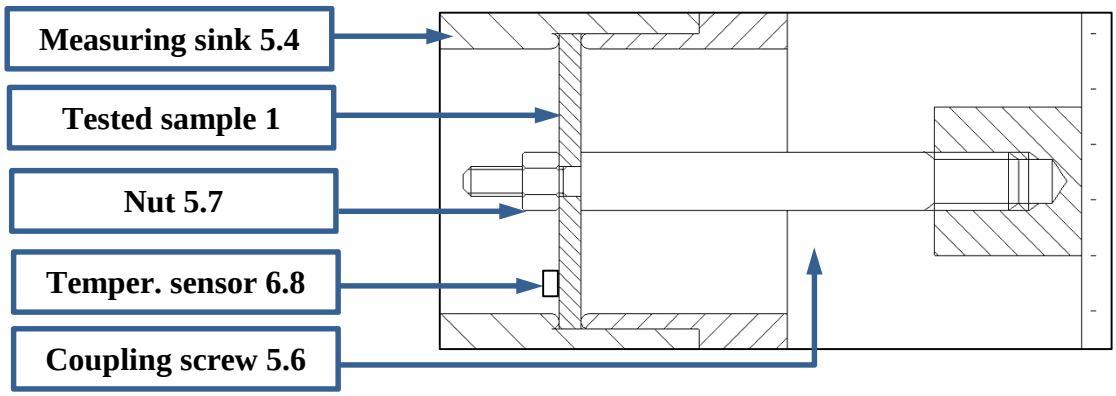

Figure 9.5 - Detail of the tested board fixing and measurement

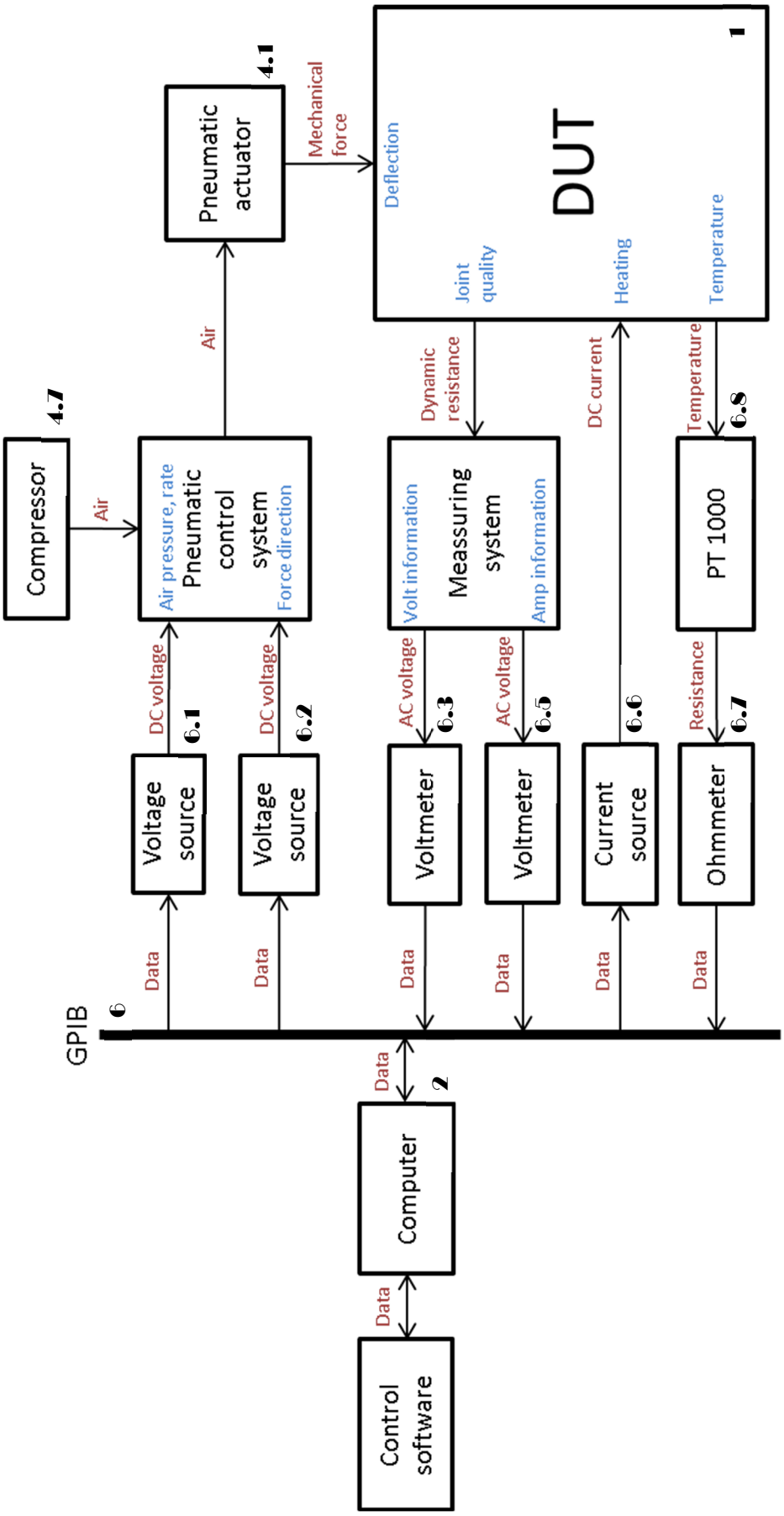

Figure 9.6 - Principal diagram of the measuring apparatus with the parts interaction

To achieve the adequate mechanical loading, it is necessary to choose the proper way of fixing. In the case of concentric circuit boards, the measuring sink 5.4 have to be equipped with the radial support in the direction perpendicular to the printed circuit board. This reduces the friction and allows the almost free movement in the remaining directions. The support formed into the rounded shape reduces the contact surface with the tested board (Figure 9.5, Figure 8.11). The method of fixing reflects the real move freedom during the application of the board in the light source. Coupling screw can be also equipped with the loading cell for the force measurement (same as in the chapter 8.2.1).

Mechanical loading adequate to the thermal is obtained by applying the variable force to the center of the tested board. During each measuring cycle, it is necessary to deliver and maintain the value of the force, including the required rising and falling edges. The referred measuring apparatus uses the compact pneumatic cylinder 4.1 at which we can assume that the applied force is constant over the entire working range of the piston stroke. The force is proportional to the fluid pressure acting on the piston. The fluid pressure, in our case the air pressure is controlled and directed the system of valves (Figure 9.7).

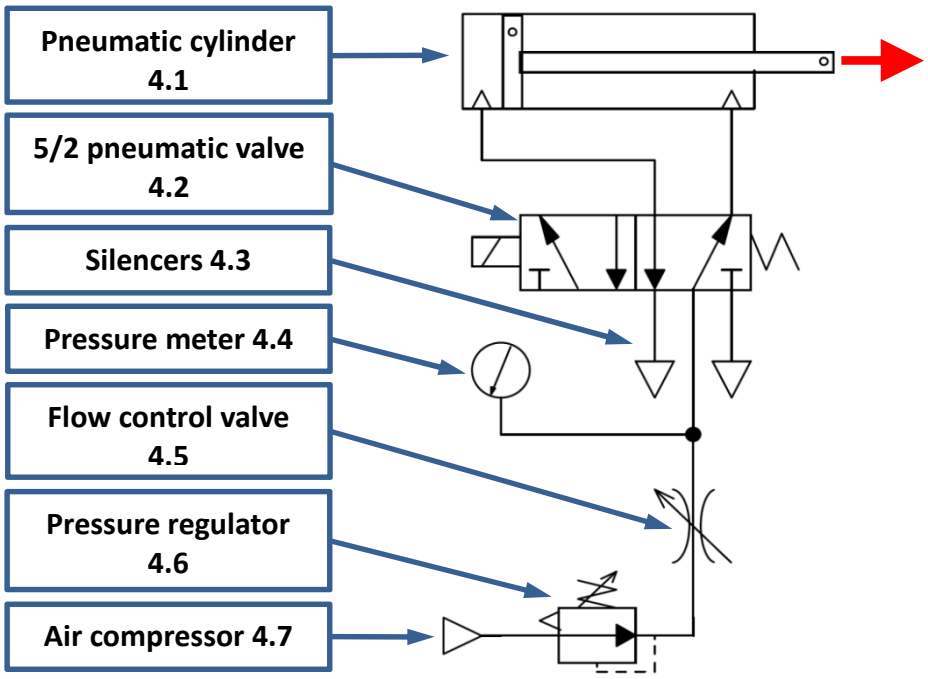

Figure 9.7 - Pneumatic part of apparatus

Pressure regulator 4.6 is electronically controlled by the voltage source 6.1 which ensures accurate setting and keeping the air pressure in the system. 5/2 pneumatic valve 4.2 switches the airflow above and below the piston of the pneumatic cylinder 4.1 and defines the direction of the applied force, the switching is provided by the solenoid which is controlled by the function generator 2.6. Flow control valves 4.5 is used mainly during the high cycle mechanical loading for determining the slopes of the pressure rise and fall, hence the slopes of the acting force. It can be connected not only before the pneumatic valve 4.2, but also

between the pneumatic valve 4.2 and the pneumatic cylinder 4.1. Than it is possible to set the different pressure rise in the both directions of the piston movement. In the case of using the apparatus for the low cycle mechanical loading, when is required the pressure rise in the range of the tents of the bar of per second, the flow control valves 4.5 can be fully opened and the pressure rise can be directly regulated by the pressure regulator 6.4. The pressure profile (applying force profile) can be preciously set by using the control software to fully simulate the real conditions.

All important measurement parameters can be detected and set by using the electric signals measured by universal measurement instruments (6.3, 6.5, 6.7). These are connected to the control computer 2 by communication interfaces for universal bus GPIB 3. The computer controls the measurement, detecting the parameters of measured sample and set the acting variables generated by DC sources (6.1, 6.6) and AC generators (6.2, 6.4) also connected by GPIB. During the measurement, it is necessary to evaluate the quality and integrity of the critical solder joint. Because the directly conduct the supply current it is possible to check the electrical integrity by measuring the impedance of the connection. This can done by the same method I showed in the chapter 8.2.2. Also the acting force calibration can be done with using the loading cell shown in the chapter 8.2.1.

The method requires the temperature increase of the measured sample so that the creep effect during low cyclic mechanical loading becomes significant. One way is to insert the measured sample 1 together with the pneumatic cylinder 4.1 to the thermal chamber with the constant temperature. The testing apparatus offers the alternative way, namely the direct board heating. Due to the high thermal conductivity of the boards for LED lamps and its small contact area with the measuring sink (Figure 8.11), the board can be directly heated by the non-radiative recombination in LEDs and Joule's heat generated in the joints. The board is heated by the current flow through the circuit. This method of heating provides only the limited homogeneity of the temperature distribution, but that is sufficient for such measurement and also more accurately reflects reality. LEDs are supplied by the constant current (current source 6.6), the value is controlled to achieve the specified temperature of PCB, which is also measured using the miniature platinum resistance sensor PT1000 6.8.

The testing apparatus was realized with using of standardized components and available measuring instruments (Figure 9.8), some mechanical parts are custom made[21]. The control software for the automated lifetime measurement was designed in the Agilent VEE software.

[21] The measuring apparatus and its design is protected by national patent application number 304545 [A19] and national utility model application number 26145 [A20]

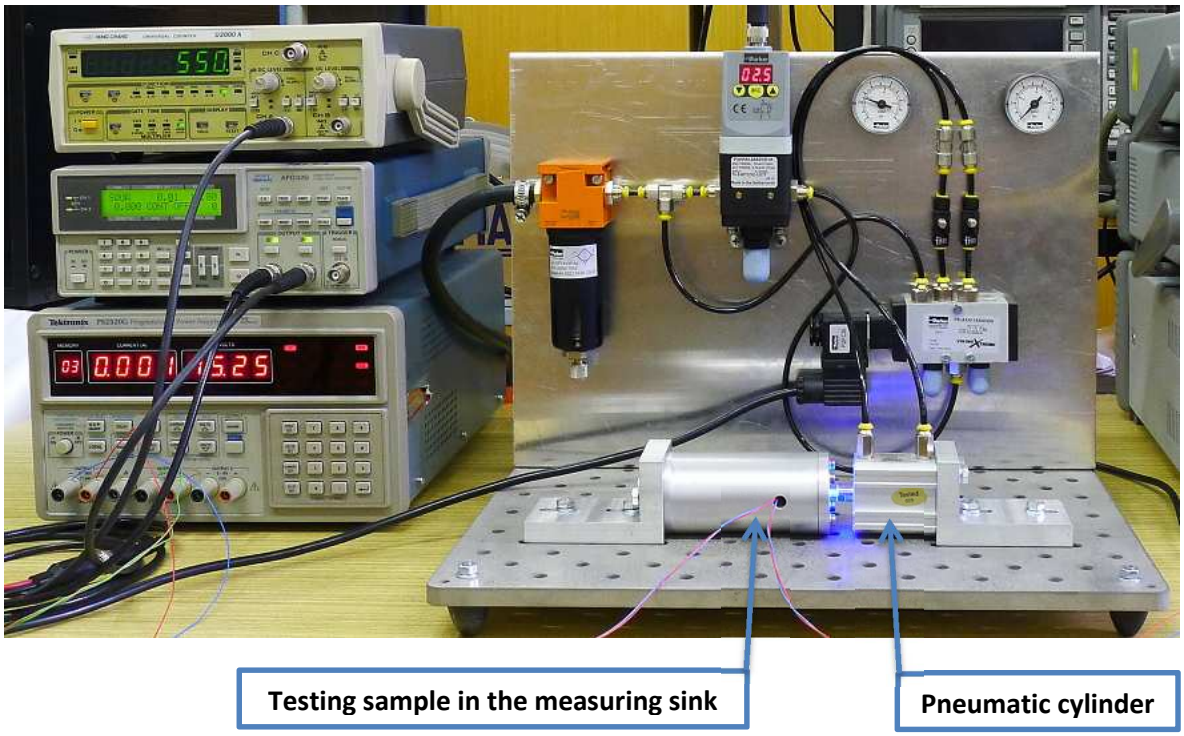

Figure 9.8 - Testing apparatus for the equivalent thermo mechanical lifetime testing

9.4. Lifetime Measurement

The designed testing apparatus was used to prove the lifetime testing methodology and also to calibrate the simulation models. Samples of the reference Master LED board (Figure 6.18a) and samples of the prototype IMS LED board with Luxeon Rebel LEDs (Figure 6.18a) were subjected to the accelerated lifetime testing with using the specified thermo mechanical loading. The loading consists of constant temperature of 70 °C and alternating force with profile near to the temperature profile which is used during the thermal testing in the thermal chamber (Figure 8.23). The minimal and the maximal values of the alternating force were evaluated from the simulations (Table 9.2) and calibrated by using the results of the thermal cycling tests done in the thermal chamber[22].

The board sample is fixed into the measuring sink which is pre-modified according to the sample size and shape. Before cycling process it has to be characterized by the electrical resistance measurement, all connection resistances should be measured independently. Than the measuring software starts with the first step which ensures the reaching the constant sample temperature (70 °C in my case). The second step of measuring flow applies the defined alternating force by controlling the pneumatic system. During each cycle, the dynamic resistances of the LED joints are measured in three different LED board deflections because cracks are opening and closing according to the LED board deflection. First value is

[22] The thermal cycling tests of reference LED board were done by our CSSL project by project partner CNM Barcelona.

measured for the maximum of positive force which is equivalent to the highest applicable temperature (120 °C in my case), second is for zero force and the last value is measured for the positive force which is equivalent to the lowest temperature (-20 °C in my case). We perform the measurement until the obvious increase of dynamic resistance is detected. Than the number of lifetime cycles can be evaluated from the number of testing cycles to the damage formation.

The method was verified by measuring two pieces of the reference FR4 board (design A) and two pieces of IMS board (design D), further boards will be measured in the future after its final fabrication. In case of FR4, failures occurs after 2 432 on the first sample and after 2 685 cycles on the second one. In the case of IMS, failures occurs after 3 820 on the first sample and after 3 352 cycles on the second. Figure 9.9 shows measured values of the master FR4 board (design A) dynamic impedance in all loading cycles, the red line represents the state where the loading force reaches the maximal positive value evaluated from the simulation (82 N) and the blue line represents the minimal negative value (-82 N).

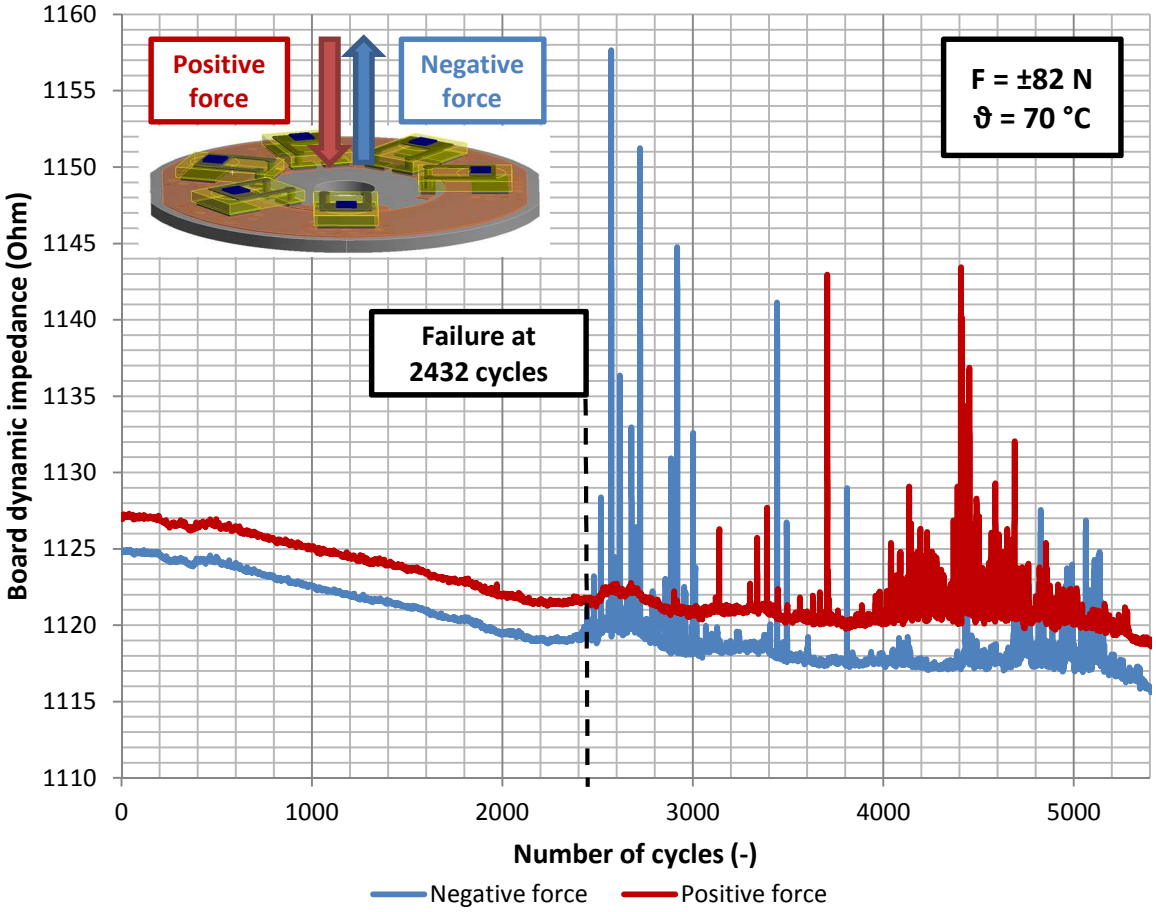

Figure 9.9 - Master FR4 board equivalent thermo mechanical lifetime testing by the force of ±82 N at constant temperature of 70 °C

The Figure 9.10 shows the same results measured on the IMS board with Luxeon Rebel LEDs (design D) but the simulated values of the equivalent loading force reaches the different values (-94 N .. 94 N).

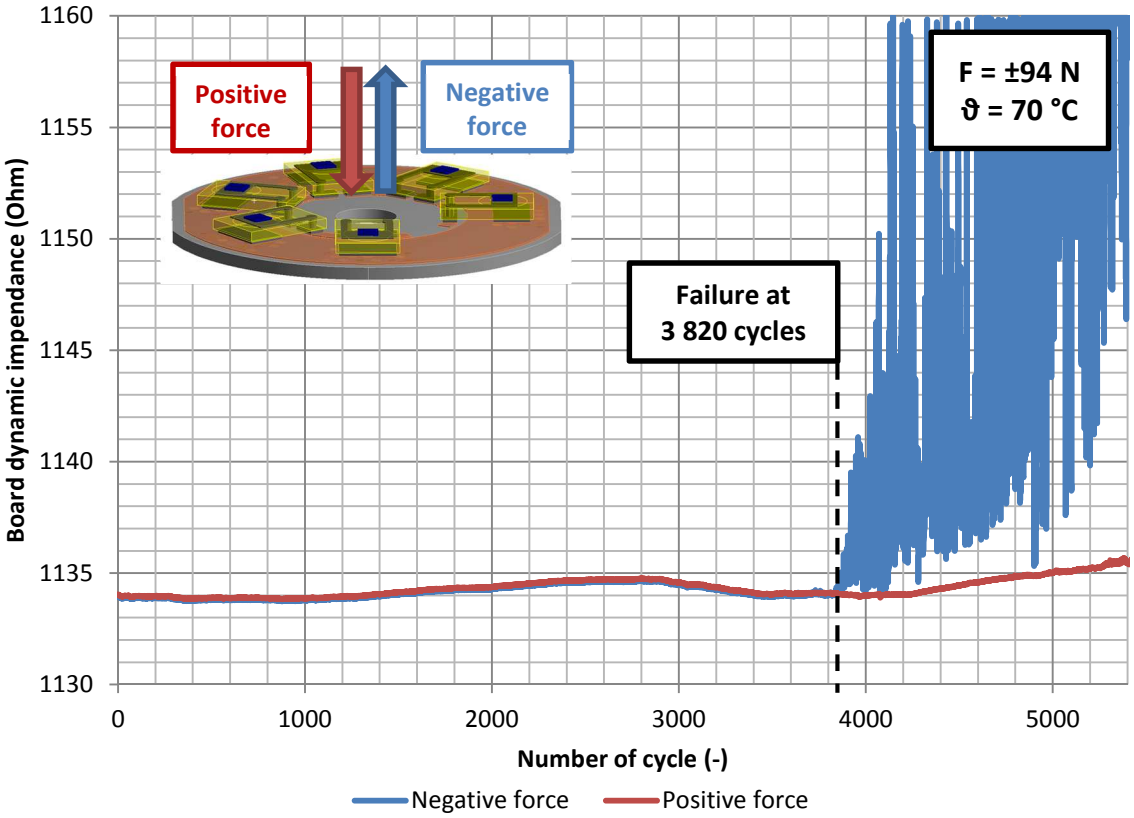

Figure 9.10 - IMS board with Luxeon LEDs equivalent thermo mechanical lifetime testing by the force of ±94 N at constant temperature of 70 °C

As you can see at the Figure 9.9 and the Figure 9.10, during the thermo mechanical loading the measured circuits with serial connections of the solder joints firstly show the small impedance increases which are mainly caused by the cracks formation. The cracks than quickly propagates due to the reduced strength of structures and after few tens of cycles, the cracks causes the total damage of the solder joints which leads to the irregular loss of the luminous fluxes.

The simulated lifetime values of the solder joints differs from the measured by about 15 percent. This is mainly caused by the non-uniform distribution of the problematic voids in the solder layer, fewer than by another inaccuracies of the structures. The voids were found by using the X-ray photography, their influence was statistically evaluated and the simulation models were adjusted. But the statistical variance causes the differences in the lifetime testing results. More information can be seen in the chapter 5.2.

Table 9.2 summarises and compares the lifetime performance of FR4 and IMS technology. The performances were evaluated according to the low cycle thermo mechanical loading which is equivalent to the thermal loading in the range of -20 .. 120 °C. As we can see the better performance shows the IMS LED board with 3786 cycles to failure (simulated value) and 3 820 (3 352) cycles to the failure (measured value)[23].

[23] The work is being prepared for the publication at the international conference ASDAM 2014

Table 9.2 - Measurement and simulated life time comparison for FR4 and IMS LED board

	Lifetime (cycles)			
	FR4 sample 1	FR4 Sample 2	IMS sample 1	IMS sample 2
Solder layer simulation	2 529	-	3 786	-
Solder layer measurement	2 432	2 685	3 820	3 352

I also did the small crack detection study of the master FR4 LED board destructed structure. The Figure 9.11a and Figure 9.11b shows the cross section through one of the electrical solder joint between the LED package and the FR4 board. You can see the cracks formed in the structure. One of the bigger void in solder layer can be seen on the Figure 9.11c. Figure 9.11d shows the top view on the board after LED package removal, in the middle you can see the area where the cracks were formed at the interface of the solder and copper layer (through the intermetallic layer).

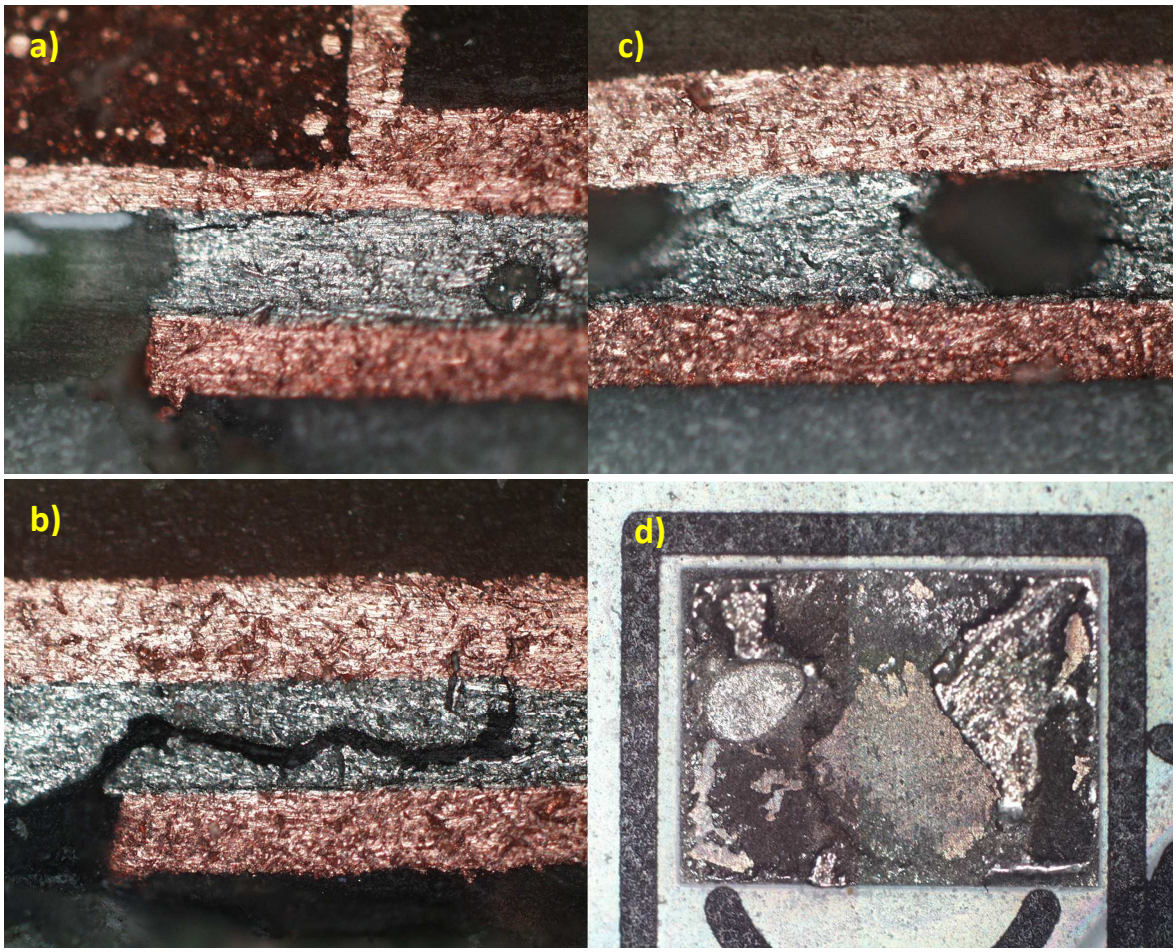

Figure 9.11 – Master FR4 board defectoscopy a); b) Crack in the solder layer; c) Voids in the solder layer; b) Delamination and crack surfaces

10. Comparison

The doctoral thesis presents specific methods for the electronic components reliability modelling and improvement. The methods are mainly based on precious modelling of thermo mechanical behavior and approximative models for the lifetime estimation in conjunction with the verification done by measurements on the newly developed apparatus. This result in possibility of the quick virtual prototyping for reliability improvement of the newly developed electronic product. During the research, the focus was devoted to poorly known issues such as nonlinear mechanical behaviour, temperature dependence, creep effects, effects of deformed geometry, highly accelerated lifetime testing, etc. The performed research brings improvement in the field of development of the new electronic products because it enables quicker lifetime estimation and evaluation. The designer can use the improved methods of virtual prototyping that can offer him the better understanding of his product thermo mechanical behaviour under thermal or mechanical loading. He can also make the lifetime estimation just after a few tens of an hour from the first draft without making the real prototype. With using the results he can quickly optimize the design to reaches better parameters and lower the costs.

Figure 10.1 shows the flowchart of the proposed lifetime prediction methodology which can be used for the decision how deep investigation has to be done. We should decide if the thermal cycling induces only elastic or the combination of elastic and plastic strain or if the creep strain plays the dominant role in some parts (usually solder joints). This enables us using different approaches of the lifetime evaluation which can be made by using the different knowledge shown in specific chapters of presented thesis. The full comparison of presented thesis with other publications cannot be successfully done because the thesis is much more complex. At the slightest approach I can compare the presented nonlinear modeling with some already presented studies. I can include for example the work of E.H. Amalu and N.N. Ekere called the High temperature reliability of the lead-free solder joints in the flip chip assembly [B98]. They present the study of the visco-plastic behaviour of solder joints of two models of the flip chip package mounted on the PCB via SnAgCu solder. The models are using Anand's equations for the solder joints and intermetallic layer behaviour. The special testing board and its model were subjected to the thermal cycling test and its simulation.

Also the work of Ch. Xiangyang, Z. Dejian called Modelling and reliability analysis of lead-free solder joints of bottom leaded plastic (BLP) package [B108] presents the thermo mechanical behaviour of BLP package connected by the lead-free solder joints. They also studied their reliability during the thermal cycling tests by using Anand's model. The shape of the solder body was predicted by the Surface Evolver software tool based on the minimum energy theory. Also, the effects of various solders and solder joint shape on BLP solder joint reliability are provided.

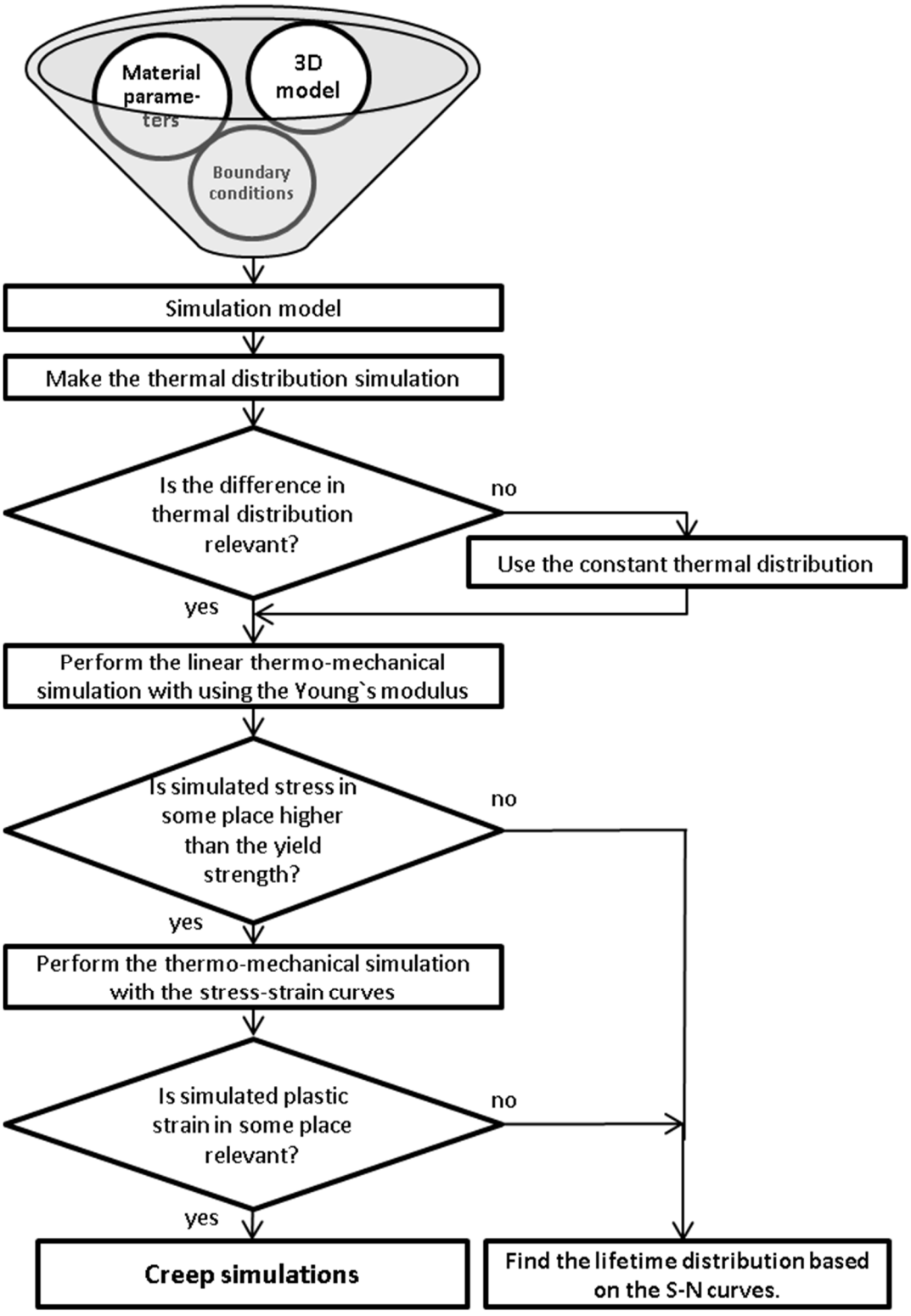

Figure 10.1 - Lifetime prediction methodology

The both presented work and also many others focussing on the PCB reliability usually present only the detailed study of the solder joins behaviour but the authors do not attempt to optimize the lifetime. Therefore I am presenting some new methods how to achieve the better lifetime, performance and lower costs by optimizing the geometry, materials, fixing

etc. The little comparison of the presented competitive work with mine is shown in the Table 10.1.

Table 10.1 - Lifetime prediction methodology comparison

	Lifetime prediction methodology		
Parameter	**E.H. Amalu and N.N. Ekere [B98]**	**Ch. Xiangyang and Z. Dejian [B108]**	**Designed methodology**
Loading type	Thermal cycling	Thermal cycling	Thermal and mechanical cycling
Specimen	Special testing sample	Special testing sample	Real product evaluation and optimization
Body to lifetime prediction	BGA solder joints, IMC layer modelling	Leaded Plastic (BLP) solder joints	All metal parts
Included physical phenomena	Visco-plastic behaviour of the solder, linear approach on another parts	Visco-plastic behaviour of the solder, linear approach on another parts	Visco-plastic behaviour, stress-strain curves, creep behaviour, nonlinear temperature dependence
Effect of the fabrication process	Measured solder bumps diameter	Solder joints shape predicted by Surface Evolver script	X-ray and CT study of the real geometry, effects of the fabrication process

In the field of the product lifetime measurement, I have designed the new method for highly accelerated thermo mechanical testing. It can bring the adequate results as testing in the thermal chamber but in significantly smaller testing time and it also considerably reduces the costs. This method is mainly intended for the concentric printed circuit boards but with the small modification it can be also used for other types and shapes of the PCB. The method and the apparatus are unique and they are protected by national patent application number 304 545 [A19] and the national utility model application number 26 145 [A20]. I have found only the one system which principle is similar. It is called Mechanical Deflection System (MDS) Test and Methodology for PBGA Solder Joint Reliability presented by collective of authors leaded by John H. L. Pang [B19]. The presented system is designed for the BGA solder joints lifetime testing by using the cyclic PCB twisting as the mechanical loading. The special test board with the BGA package is fixed in the grip and connected to the torsion servo motor. The whole apparatus can be inserted to the thermal chamber to achieve a lower testing time. The Board twisting causes solder joint stress which leads to failure.

Versus the Pang's collective work, I present much more complex system which provides more precious mechanical loading. In conjunction with the presented methodology my apparatus is able to achieve the strain distribution similar to the thermally caused. Even on PCB for the real product. My system is able to test the real final PCBs or PCB prototype so it

can be also used for the lifetime evaluation of virtually optimized products. The results of the lifetime testing can be directly used during the product design. Table 10.2 summarises the testing method features; for the comparison I also added features of the thermal chamber testing.

Table 10.2 - Accelerated lifetime testing methods comparison

	Lifetime testing method		
Parameter	**Thermal chamber**	**Pang's system [B19]**	**Designed system**
Loading type	Thermal cycling	Regulated twisting	Regulated force loading
Testing period	Usually 3 600 s	480 s	Usually 120 s
Total testing time	Months	Days	Tens of hours
Specimen type	All PCBs	Special testing boards with one BGA package	Mainly a concentric PCBs
Lifetime prediction	Usually MTTF counting	Darveaux model (viscoplastic)	Syed model and Schubert creep model
Testing cost	High	Low	Low

11. Conclusion and Future Work

Virtual prototyping for the lifetime improvement is still the state of the art in the product development. By using the new approaches and methods the designer is able to prepare a new product in significantly shortened time and with lower cost. The precise and effective design requires also a good understanding of the product structure thermo mechanical behaviour in a wide range of working conditions. This can be done by using modern methods of the adequate computer model simulation which can also include the determination of its short-time and long-time durability. Also the precise and quick verification of determined parameters and behaviour is very important research discipline because the results of simulation have to be proven by the real product measurement.

The development of the new methods for the electronic components reliability evaluation and improvement was the main goal of my research. In this sense the main goal was successfully achieved and also lot of work has been done on related topics.

I can summarize my contribution resulting from my research as:

- **Development of methods for the precious modelling and validation of thermal distribution and the heat transfer optimization for the thermal reliability improve**
  (Chapter 6, the research results were published in impacted journals Microelectronics Reliability 2013 [A2], Radioengineering 2012 [A3] and at international conferences [A10], [A17], [A18])
- **Preparation of the specific measurement setups for thermal evaluation**
  (Chapter 6.2, the research results were published in impacted journals Radioengineering 2013 [A1], Radioengineering 2012 [A3] and at international conference [A18])
- **Development of methods for the complex non-linear modelling of thermo-mechanical issues influencing the reliability of electronic components**
  (Chapter 7, the research results were published in impacted journals Microelectronics Reliability 2013 [A2], Radioengineering 2012 [A5] and at the international conferences [A6], [A9], [A10], [A13])
- **Extend the methods for the product virtual prototyping from thermal, mechanical and reliability point of view**
  (Chapters 6.4, 7.3, 8.1, the research results were published in impacted journal Microelectronics Reliability 2013 [A2] and at the international conferences [A10], [A18])
- **Develop methods for the high cycle and low cycle thermo mechanical lifetime estimation**
  (Chapter 8.1, 8.4, the research results were published in impacted journals Radioengineering 2013 [A1], Microelectronics Reliability 2013 [A2], Microelectronics Reliability 2012 [A4], and at the international conferences [A6], [A7], [A10])

- **Preparation of the specific measurement setups for the high cycle lifetime evaluation**

  (Chapter 8.2, the research results were published in impacted journals Radioengineering in April 2013 [A1], Microelectronics Reliability 2012 [A4] and at international conference [A7])

- **Develop the new highly accelerated characterization method for the lifetime evaluation as the replacement of the thermal cycling tests**

  (Chapter 9, the method and measuring apparatus are protected by national patent application number 304545 [A19] and national utility model application number 26145 [A20])

- **Research the lifetime reduce caused by the structure defects built-in during the fabrication process**

  (Chapter 5.2, 7.2, the research results are being prepared for the publication)

A lot of work still have to be done so the future work will be focussed on the following research topics:

- Study of the air flow and its effects on the heat removal
- Study of the intermetallic compound features and behaviour
- Study of the crack propagation, its formation, rate, direction and its modelling by the mesh division
- Systematic measuring for achieving the better statistics of presented results.

The doctoral thesis presents the knowledge that was obtained during the cooperation in international research projects solved in the Department of Microelectronics FEE CTU. These are mainly following projects: Consumerizing Solid State Lighting Project (CSSL) supported by the ENIAC Joint Undertaking (Grant Agreement no. 120219), MORGaN project under the contract FP7 NMP IP 214610 and CTU SGS grant no. SGS11/156/OHK3/3T/13. The knowledge has been also extended by the independent solving of projects supported by CTU SGS grant no. SGS13/079/OHK3/1T/13 (Methods for lifetime evaluation of electronic structures and systems) and SGS14/074/OHK3/1T/13 (Development of methods for predicting the lifetime evaluation of electronic structures and systems).

List of Figures

List of Tables

Author Publications in the Discussed Topic

Impacted Journals

[A1] J. Formánek, J. Jakovenko: **Thermal Characterization and Lifetime Prediction of LED boards for SSL lamp**, Radioengineering 2013, Vol. 1, No. 22, ISSN 1210-2512, April 2013.

[A2] J. Jakovenko, J. Formánek, X. Perpiñà, X. Jorda, M. Vellvehi, R.J. Werkhoven, M. Husák, J.M.G. Kunen, P. Bancken, P.J. Bolt, A. Gasse: **Design methodologies for reliability of SSL LED boards**, Microelectronics Reliability 2013, vol. 53, no. 8, pp. 1076-1083. ISSN 0026-2714, August 2013.

[A3] J. Jakovenko, J. Formánek, V. Janíček, M. Husák, R. Werkhoven**: High Power Solid State Retrofit Lamp Thermal Characterization and Modelling**, Radioengineering 2012, Vol. 1, No. 21, p. 225-230. ISSN 1210-2512, April 2012.

[A4] X. Perpińà, R. Werkhoven, J. Jakovenko, J. Formánek, M. Vellvehi, X. Jordà, J. Kunen, P. Bancken, P.J. Bolt: **Design for reliability of solid state lighting systems**, Microelectronics Reliability 2012, vol. 9-10, no. 52, p. 2294-2300, ISSN 0026-2714, October 2012.

[A5] V. Janíček, M. Husák, J. Jakovenko, J. Formánek: **Design and Fabrication of 3D Electrostatic Energy Harvester**, Radioengineering 2012, Vol. 21, No. 1, ISSN 1210-2512, April 2012.

International Conferences

[A6] J. Formánek, J. Jakovenko: **Modelling of Creep Behaviour during Thermal Cycling Test of Led Board for SSL Lamp,** EDS IMAPS CS international conference 2013, vol. 1, pp. 5-10. ISBN 978-8-0214-4754-7, June 2013.

[A7] J. Jakovenko, J. Formánek: **Modelling of Reliability by Highly Accelerated Characterization Method for Solid State Lighting LED Boards**, Computational Intelligence, Modelling and Simulation (CIMSim) 2013, Los Alamitos, vol. 1, pp. 384-389, ISBN 978-1-4799-2308-3, September 2013.

[A8] V. Janíček, M. Husák, J. Formánek, J. Jakovenko: **Evaluating the 3D Energy Harvester,** EDS IMAPS CS international conference 2013, vol. 1, pp. 125-132. ISBN 978-8-0214-4754-7, June 2013.

[A9] J. Formánek, K. Brinkfeldt, A. Laposa, J. Jakovenko: **Pressure Sensor Package Simulation in a Large Temperature Range**, EDS IMAPS CS international conference 2012. Brno: VUT in Brno, FEKT, vol. 1, pp. 132-137. ISBN 978-80-214-4539-0, June 2012.

[A10] J. Jakovenko, J. Formánek, B. Pardo, X. Perpiñà, R.J. Werkhoven, J.M.G. Kunen, P. Bancken, P.J. Bolt: **Thermo-Mechanical Evaluation and Life Time Simulation of a High Power LED Lamp Boards**, IEEE Eurosime 2012, ISBN: 978-1-4673-1511-1, April 2012.

[A11] K. Brinkfeldt, J. Formánek, A. Laposa, J. Jakovenko, E. Adolfsson, P. Johander: **Simulation of High Temperature Pressure Sensor Packaging and Interconnection**, IEEE Eurosime 2012, ISBN: 978-1-4673-1511-1, April 2012.

[A12] J. Jakovenko, J. Formánek, R.J. Werkhoven, J. Kunen, P. Bolt, P. Bancken, V. Molata, V. Kotě, T. Nápravník, M. Husák: **Design and life time evaluation of various LED boards for SSL lamp,** EDS IMAPS CS international conference 2012, ISBN 978-80-214-4539-0, June 2012.

[A13] X. Perpiñà, R. Werkhoven, J. Jakovenko, J. Formánek, M. Vellvehi, X. Jordà, J. Kunen, P. Bancken, P.J. Bolt: **Design for Reliability of Solid State Lighting Systems**, 23rd European Symposium on Reliability of Electron Devices, Failure Physics and Analysis, ESREF 2012, October 2012.

[A14] P. Kulha, J. Jakovenko, J. Formánek: **FEM Thermomechanical Simulation of Low Power LED Lamp for Energy Efficient Light Sources,** Renewable Energies & Power Quality Journal (RE&PQJ) [online], no. 10, pp. 1-4, ISSN 2172-038X, April 2012.

[A15] V. Janíček, M. Husák, J. Formánek , J. Jakovenko : **3D Electrostatic Energy Harvester**, Technical Proceedings of the 2012 NSTI Nanotechnology Conference and Expo, NSTI-Nanotech 2012 , pp. 118-121, ISBN 978-1-4665-6275-2, June 2012.

[A16] P. Kulha, J. Jakovenko, J. Formánek: **FEM Thermomechanical Simulation of Low Power LED Lamp for Energy Efficient Light Sources**, ICREPQ12 International Conference on Renewable Energies and Power Quality, Universidad de Vigo, vol. 1, ISBN 978-84-615-6648-8, March 2012.

[A17] J. Jakovenko, R. Werkhovent, J. Formánek, J. Kunhen, P. Bolt, P. Kulha, P. Bancken: **Thermo-mechanical Modelling and Characterization of High Power Solid State LED Lamp**, EDS IMAPS CS international conference 2011, pp. 178-201, ISBN 978-80-214-4303-7, June 2011.

[A18] J. Jakovenko, R. Werkhoven, J. Formánek, J. Kunhen, P. Bolt, P. Kulha: **Thermal Simulation and Validation of 8W LED Lamp**, IEEE Eurosime 2011, ISBN 978-1-4577-0105-4, April 2011.

Patents, utility models and functional models

[A19] J. Formánek, J. Jakovenko: **Measuring system for accelerated characterization of service life of concentric printed circuits**, National patent application number 304 545, Czech Industrial Property Office, 14. 5. 2014.

[A20] J. Formánek, J. Jakovenko: **Measuring system for accelerated characterization process of concentric printed circuit service lives,** National utility model application number 26 145, Czech Industrial Property Office, 25. 11. 2013.

[A21] J. Formánek, J. Jakovenko: **Measuring system for high cyclic mechanical loading of electronic components,** functional model 2012.

[A22] J. Formánek: **Reflectionless characterization chamber for thermal imaging**, functional model 2011.

[A23] J. Formánek, J. Novák: **Control Unit for Time-based Scanning**, functional model 2010.

[A24] J. Formánek: **Variable measure system with an adjustable comparison**, functional model 2010.

References

[B1] M.-Y. Tsai, C. H. Jeter Hsu, C. T. Otto Wang: **Investigation of Thermomechanical Behaviors of Flip Chip BGA Packages During Manufacturing Process and Thermal Cycling**, IEEE transactions on components and packaging technologies, vol. 27, no. 3, Sept. 2004.

[B2] F.E. Stam, E. Davitt: **Effects of thermomechanical cycling on lead and lead-free (SnPb and SnAgCu) surface mount solder joints**, Microelectronics Reliability, pp. 1815-1822, 2001.

[B3] J.H.L. Pang, T. Tan, S.K. Sitaraman**: Thermo-mechanical analysis of solder joint fatigue and creep in a flip chip on board package subjected to temperature cycling loading**, Electronic Components and Technology Conference, pp. 878-83, 1998.

[B4] J. Liang, N. Gollhardt, P.S. Lee, S. Heinrich, S. Schroeder: **An integrated fatigue life prediction methodology for optimum design and reliability assessment of solder inter- connections**, Advances in Electronic Packaging, proceedings of the Pacific Rim/ASME International Intersociety Electronic and Photonic Packaging Conference INTERpack'97, vol. 2, 1997, pp. 1583-92.

[B5] T. Pan: **Critical accumulated strain energy (case) failure criterion for thermal cycling fatigue of solder joints**, Journal of Electronic Packaging, Transactions of the ASME 1994, pp. 163-70.

[B6] H. Chunyue: **Thermal Fatigue Life Analysis and Forecast of PBGA Solder Joints On the Flexible PCB Based on Finite Element Analysis,** 2008, International Conference on Electronic Packaging Technology & High Density Packaging (ICEPT-HDP 2008).

[B7] A. Syed, W. Lin, E.-S. Sohn, and S.-W. Cha: **Plastic Deformation and Life Prediction of Solder Joints for Mechanical Shock and Drop/Impact Loading Conditions**, Electronic Components and Technology Conference, 2007.

[B8] T. Chokshi, D. Peroulis: **Stress-induced failure modes in high-tuning range RF MEMS varactors**, Microwave Conference, vol.3, no., pp.4 pp.,, 4-6 Oct. 2005.

[B9] Y. N. Zaiazmin, I. Azid: **Comparison between ANSYS and CATIA Simulation Capability in Simulating Round Shape Diaphragm of MEMS Piezoresistive Pressure Sensor**, Electronics Manufacturing and Technology, 31st International Conference, pp. 191-195, Nov. 2007.

[B10] AF. Malik, M. Shoaib, S. Naseem, S. Riaz: **Modeling and designing of RF MEMS switch using ANSYS**, Emerging Technologies, 2008. ICET 2008. 4th International Conference, pp.44-49, Oct. 2008.

[B11] A. Tambat, Hung-Yun Lin, G. Subbarayan, Dae Young Jung, B. Sammakia: **Simulations of Damage, Crack Initiation, and Propagation in Interlayer Dielectric Structures: Understanding Assembly-Induced Fracture in Dies**, Device and Materials Reliability, IEEE Transactions on , vol.12, no.2, pp. 241-254, June 2012.

[B12] D. Calvez, F. Roqueta, S. Jacques, L. Bechou, Y. Ousten, S. Ducret: **Crack Propagation Modeling in Silicon: A Comprehensive Thermomechanical Finite-Element Model Approach for Power Devices**, Components, Packaging and Manufacturing Technology, IEEE Transactions on , vol.4, no.2, pp. 360-366, Feb. 2014.

[B13] Hongtao Ma, M. Ahmad, Kuo-Chuan Liu: **Reliability of Lead-Free Solder Joints Under a Wide Range of Thermal Cycling Conditions**, Components, Packaging and Manufacturing Technology, IEEE Transactions, vol.1, no.12, pp.1965-1974, Dec. 2011.

[B14] Y.S. Chen; C. L. Hong, T. J. Huang: **Accurately simulate the thermal cycling test with improved mechanical reliability test for electronic components**, Microsystems Packaging Assembly and Circuits Technology Conference (IMPACT), 2010 5th International conference, pp. 1-4, Oct. 2010.

[B15] M. Bevan, M. Wuttig: **Complex fatigue of soldered joints comparison of fatigue models**, Electronic Components and Technology Conference, pp. 127-33, 1997.

[B16] Q. Xueli, Bin Zhou, L. Guoyuan, Z. Pengfei, E. Yunfei: **Effect of fixation method on solder joint vibration fatigue reliability of high density PCB assembly**, Electronic Packaging Technology and High Density Packaging (ICEPT-HDP), 2011 12th International Conference, pp. 1-4, Aug. 2011.

[B17] S. K. W. Seah, E. H. Wong, C. S. Selvanayagam, J. F J M. Caers, W. D. Driel, N. Owens, Y.-S. Lai: **A Comprehensive Test Method for Bridging the Gap between Product and Board Level Drop Tests**, Electronics Packaging Technology Conference, 2008. EPTC 2008. 10th, pp .1102-1107, Dec. 2008.

[B18] L. Yang, S. Fenglian, Z. Hongwu, Z. Zhang, Y. Zhou, Qin: **Harmonic vibration test for accelerated reliability assessment of board level packaging**, Strategic Technology (IFOST), 2012 7th International Forum, pp.1-5, Sept. 2012.

[B19] J.H.L. Pang, Kar Hwee Ang, X.Q. Shi, Z.P. Wang: **Mechanical deflection system (MDS) test and methodology for PBGA solder joint reliability**, Advanced Packaging, IEEE Transactions, vol.24, no.4, pp. 507-514, Nov 2001.

[B20] Y. Narukawa, M. Ichikawa, D. Sanga, M. Sano, T. Mukai: **White light emitting diodes with super-high luminous efficacy**, Journal of Physics D: Applied Physics 43, 2010.

[B21] K.V.S.S.S.S. Sairam: **Optical Communications**, Laxmi Publications (P) LTD, New Delphi 2007.

[B22] OMS LED academy materials, online at: http://www.omslighting.com/led-academy-en, [cited on 14. 11. 2011].

[B23] N. Holonyak, S. F. Bevaqcua: **Coherent (visible) light emission from Ga(As1-xPx) junctions**, Applied Physics Letter, No. 4, pp. 82-83, 1962.

[B24] J. Biard, E. Bonin, W. Carr, G. Pittman: **GaAs infrared source for optoeletronic applications,** Solid-State Circuits Conference, Digest of Technical Papers, IEEE International, 1963.

[B25] Z. Liu, S. Liu, K. Wang, X. Luo: **Status and prospects for phosphor based white LED packaging**, Frontiers of Optoelectronics in China 2, No. 2, pp. 119–140, 2009.

[B26] Huei-Huang Lee: **Finite Element Simulations with ANSYS Workbench 13**, SDC Publications, ISBN 1585036536, 608 pages, March 2011.

[B27] **LED Driver Lifetime and Reliability**, Philips Electronics N.V. promotion material, Oct. 2011.

[B28] D.J. Wilkins: **The Bathtub Curve and Product Failure Behavior**, Reliability HotWire, Issue 21, Nov. 2002.

[B29] J. DeVale: **Traditional Reliability**, Carnegie Mellon University, Dependable Embedded Systems, 1998.

[B30] J. Pecht, M. Pecht: **Long-term non-operating reliability of electronic products**, Boca Raton, CRC Press, 1995.

[B31] S.-H. Choi, S.-H. Shin, Y.-K. Lee, S.-M. Choi, S. Yi, H.-H. Kim: **Thermal Transient Characteristics of Die Attach in High Power LED Packages**, Microelectronics Reliability, sv. 48, p. 445–454, 2008.

[B32] **LED packaging,** Dow Corning datasheet 1679a.

[B33] **LED Thermal Management**, Dow Corning datasheet 1683, 2010.
[B34] **Atlas of Stress-Strain Curves 2nd edition**, ASM International 2011, ISBN 0-87170-739X.
[B35] J.W. Yoon, H.S. Chun, S.B. Jung: **Reliability Analysis of Au–Sn Flip-Chip Solder Bump Fabricated by Co-Electroplating**, Journal of Materials Research 22, No. 5,pp. 1219-1229, 2007.
[B36] M.R. Krames, O.B. Shchekin, R. Mueller-Mach, G.O. Mueller, L. Zhou, G. Harbers, M.G. Craford: **Status and Future of High-Power Light-Emitting Diodes for Solid-State Lighting**, Journal Of Display Technology 3 (2007), pp. 160-175.
[B37] Robert Lingard: **Thermal Management of White LEDs**, Pacific Northwest National Laboratory, 2009.
[B38] **COMSOL material database**, COMSOL, 2011.
[B39] J.P. Clech: **An obstacle-controlled creep model for Sn-Pb based lead-free solders,** SMTA International Conference (SMTAI 2004, Chicago), Sept. 2004.
[B40] R. Sandström, J. Hallgren: **Stress strain flow curves for Cu-OFP, Materials Science and Engineering**, Royal Institute of Technology (KTH) Gunnar Burman, Bodycote Materials Testing AB, 2009.
[B41] W.S. Lee, I.Y. Hanb, Jin Yu, S.J. Kim, K.Y. Byuna: **Thermal characterization of thermally conductive underfill for a flip-chip package using novel temperature sensing technique**, Thermochimica Acta 455, pp. 148-155, 2007.
[B42] G. Li, B. G. Thomas, J. F. Stubbins: **Modeling creep and fatigue of copper alloys,** Metallurgical and Materials Transactions A, 2000, Vol. 31A, No. 10, pp. 2491-2502.
[B43] www.valleydesign.com/sappprop.htm, [cited on 14. 11. 2011].
[B44] www.philipslumileds.com/pdfs/AB32.pdf, Philips, [cited on 14. 11. 2011].
[B45] http://www.witcombv.nl/en/products/witcom-thermally-conductive-polymer-compounds, Witcom Engineering Plastic, [cited on 14. 11. 2011].
[B46] http://www.coolpolymers.com/dseries.asp, Cool Polmers, [cited on 14. 11. 2011].
[B47] http://www.coolpolymers.com/eseries.asp, Cool Polmers, [cited on 14. 11. 2011].
[B48] www.engineeringtoolbox.com/emissivity-coefficients, [cited on 14. 11. 2011].
[B49] T. Nishikawa, Y. Umehara, S. Honda, H. Awajil: **Mechanical Properties of Porous Alumina at High Temperature**, Journal of the Ceramic Society of Japan, Volume 112, Issue 20-I, pp. 1405 - 1407, Sept. 2004.
[B50] J. Wachtman, W. Tefft, D. Lam, C. Apstein: **Exponential Temperature Dependence of Young's Modulus for Several Oxides**, Phys. Rev., Vol. 122, Issue 6, pp. 1754-1759, June 1961.
[B51] B. Fiedler, T. Hobbiebrunken, M. Hojo, K. Schulte, **Influence of stress state and temperature on the strength of epoxy resins**, ICF2011, 2011.
[B52] A. Gladkov, A. Bar-Cohen: **Parametric dependence of fatigue of electronic adhesives**, Adhesive Joining and Coating Technology in Electronics Manufacturing, 1998. Proceedings of 3rd International Conference, pp. 116-124, Sept. 1998.
[B53] B. Fischer, A. Behrends, D. Freund, D. Lupton, J. Merker: **High Temperature Mechanical Properties of the Platinum Group Metals, Platinum Metals**, Phys. Rev., Volume 43, Issue 1, pp. 18-28, Jan. 1999.
[B54] R. Taylor: **Thermal expansion of solids**, ASM International, ISBN0871706237, 300 pages, Jan. 1998.
[B55] www.ioffe.ru/SVA/NSM/semicond, [cited on 22. 7. 2012].
[B56] www.matweb.com, [cited on 22. 7. 2012].

[B57] www.matbase.com, [cited on 22. 7. 2012].
[B58] www.ramaer.nl, [cited on 22. 7. 2012].
[B59] www.injectorall.com/techsheetFR4.htm, [cited on 22. 7. 2012].
[B60] Lianqiao Yang, Sunho Jang, Woongjoon Hwang, Moowhan Shin: **Thermal analysis of high power GaN-based LEDs with ceramic package**, Thermochimica Acta, Volume 455, Issues 1–2, pp. 95-99, ISSN 0040-6031, April 2007.
[B61] A. Syed: **Accumulated Creep Strain and Energy Density Based Thermal Fatigue Prediction Models for SnAgCu Solder Joints**, Proceedings of ECTC, 2004.
[B62] A. Schubert, R. Dudek, E. Auerswald, A. Gollbardt, B. Michel, & H. Reichl: **Fatigue life models for SnAgCu and SnPb solder joints evaluated by experiments and simulation**, Proceedings of 53rd Electronic Components and Technology Conference, pp. 603-610, 2003.
[B63] A. Poppe, C.J.M. Lasance: **On the standardization of thermal characterization of LEDs,** Semiconductor Thermal Measurement and Management Symposium, SEMI-THERM 2009, 25th Annual IEEE, pp.151-158, March 2009.
[B64] http://www.yegopto.co.uk/, [cited on 17. 9. 2012].
[B65] M. V., X. J., Xavier Perpiñà, **Thermal simulation and validation activities**, CNM, Barcelona, Spain, 2010.
[B66] ANSYS 13.0 reference manual and promotional materials, ANSYS 2012.
[B67] X. Wang, X. Sun: **Three-dimensional simulations of air–water bubbly flows**, International Journal of Multiphase Flow, Volume 36, Issues 11–12, pp. 882-890, ISSN 0301-9322, Dec. 2010.
[B68] W.D. Callister: **Fundamentals of materials science and engineering: an integrated approach**, Hoboken, Waveland Press Inc, 2008.
[B69] Schubert, R. Dudek, J. Auersperg, D. Vogel, B. Michel, H. Reichl: **Thermo-mechanical reliability analysis of flip chip assemblies by combined microDAC and the finite element method**, Advances in Electronic Packaging, Proceedings of the Pacific Rim/ASME International Intersociety Electronic and Photonic Packaging Conference INTERpack'97, vol. 2, pp. 1647-54, 1997.
[B70] K.N. Subramanian: **Lead-free Electronic Solders**, A Special Issue of Journal of Material Science, Materials in Electronics, Springer, 2007.
[B71] L.T. Nguyen, G.S. Selvaduray, W.W. Lee: **Solder joint fatigue models: review and applicability to chip scale packages**, Microelectronics Reliability, sv. 40, pp. 231-244, 2000.
[B72] H.D. Solomon: **Fatigue of 60/40 Solder**, Components, Hybrids, and Manufacturing Technology, IEEE Transactions, vol.9, no.4, pp.423-432, Dec. 1986.
[B73] W. Engelmaier: **Pb-free solder creep-fatigue reliability models updated and extended**, Global SMT & Packaging, pp. 36-38s, Sept. 2009.
[B74] S. Wiese, E. Meusel, K.-J. Wolter: **Electronic Components and Technology Conference**, 2003.
[B75] J. Liang, N. Gollhardt, P.S. Lee, S. Heinrich, S. Schroeder: **An integrated fatigue life prediction methodology for optimum design and reliability assessment of solder interconnections,** Advances in Electronic Packaging, Proceedings of the Pacific Rim/ASME International Intersociety Electronic and Photonic Packaging Conference INTERpack'97, vol. 2., pp.1583-92, 1997.
[B76] S.X. Wu, J. Chin, T. Grigorich, G. Mui, C. Yeh: **Reliability analysis for fine pitch BGA package,** Electronic Components and Technology Conference, pp. 737-41, June 1998.

[B77] W. Jung, J.H. Lau, Y.H. Pao: **Nonlinear analysis of full matrix and perimeter plastic ball grid array solder joints**, Nepcon West'97, pp. 1076-95, 1997.
[B78] G. Gustafsson: **Solder joint reliability of a lead-less RF-transistor**, Electronic Components and Technology Conference, pp. 87-91, June 1998.
[B79] M. A. Miner: **Cumulative Damage in Fatigue**, ASME Journal of Applied Mechanics, Vol. 12, 1945.
[B80] V. Stolkarts, B. Moran, L.M. Keer: **Constitutive and damage model for solders**, Electronic Components and Technology Conference, pp. 379-85, June 1998.
[B81] C.J. Humphreys: **Solid-state lighting**, Mrs Bulletin 33, April 2008, pp. 459-470.
[B82] N. Narendran, N. Maliyagoda, A. Bierman, R. Pysar, M. Overington: **Characterizing white LEDs for general illumination applications**, Lighting research center, 2000 http://lightingresearch.org/programs/solidstate/pdf/SPIE3938-39_Narendran.pdf.
[B83] Fan, Bingfeng, Hao Wu, Yu Zhao, Yulun Xian, Gang Wang: **Study of Phosphor Thermal-Isolated Packaging Technologies for High-Power White Light-Emitting Diodes,** IEEE Photonics Technology Letters, pp. 1121-1123, 2007.
[B84] S. Haque, D. Steigerwald, S. Rudaz,B. Steward, J. Bhat, D. Collins, F. Wall, S. Subramanya, C. Elpedes, P. Elizondo, P.S. Martin: **Packaging challenges of high-power LEDs for solid state lighting,** IMAPS - International Symposium on Microelectronics, 2000.
[B85] X. Luo, B. Wu, S. Liu: **Effects of moist environments on LED module reliability**, IEEE Transactions on Device and Materials Reliability 10, pp. 182-186, 2010.
[B86] **Updated Lumiled's chart with data from product catalogues and press releases**, Navigant Consulting, Inc. 2009.
[B87] Chun-Jen Weng: **Advanced thermal enhancement and management of LED packages**, International Communications in Heat and Mass Transfer, Volume 36, Issue 3, pp. 245-248, ISSN 0735-1933, March 2009.
[B88] M. Dyble: **Solid State Lighting Introduction**, Osram training material, Oct. 2009.
[B89] M. J. Marongiu: **Thermal Management of High-Power LED Systems**, LED Professional review, no. 13, pp. 47-50, 2009.
[B90] A. Uddin, A.C. Wei, T.G. Andersson: **Study of Degradation Mechanism of Blue Light Emitting Diode**, Thin Solid Films, vol. 483, pp. 378-381, 2005.
[B91] D. Steigerwald, J. Bhat, D. Collins, R. Fletcher, M. Holcomb, M. Ludowise, P. Martin, S. Rudaz: **Illumination with solid state lighting technology**, IEEE Journal of Selected Topics in Quantum Electronics, vol. 8, No. 2, pp. 310-320, 2002.
[B92] R. Lingard: **Thermal Management of White LEDs**, Pacific Northwest National Laboratory, 2009.
[B93] M.H. Chang, D. Das, P.V. Varde, M. Pecht: **Light emitting diodes reliability review**, Microelectronics Reliability, vol. 52, Issue 5, pp. 762-782, ISSN 0026-2714, May 2012.
[B94] S. Pimputkar, J.S. Speck, S.P. DenBaars, S. Nakamura: **Prospects for LED lighting**, Nature Photonics, vol. 3, pp. 179-181, 2009.
[B95] Lighting research center: **Characterizing white LEDs for general lightining**, http://lightingresearch.org/programs/solidstate/pdf/SPIE3938-39_Narendran.pdf, 2009.
[B96] E.F. Schubert, J.K. Kim, H. Luo: **Solid-state lighting-a benevolent technology**, Reports on Progress in Physics, vol. 69, pp. 3069-99, 2006.
[B97] T.H. Courtney: **Mechanical behavior of materials**, Long Grove, Waveland Press Inc, 2005.

[B98] E.H. Amalu, N.N. Ekere**: High temperature reliability of lead-free solder joints in a flip chip assembly**, Journal of Materials Processing Technology, vol. 212, issue 2, pp. 471-483, ISSN 0924-0136, Febr. 2012.

[B99] W.W. Leea, L.T. Nguyena, G.S. Selvaduray: **Solder joint fatigue models: review and applicability to chip scale packages**, Microelectronics Reliability 2000, pp. 231-244.

[B100] S. Knecht, L. Fox: **Integrated matrix creep: application to accelerated testing and lifetime prediction**, Solder joint reliability theory and applications (Chapter 16), Van Nostrand Reinhold, New York 1991.

[B101] N. Narendran, Y. Gu, J.P. Freyssinier, H. Yu, L. Deng: **Solid-state lighting: failure analysis of white LEDs**, Journal of Crystal Growth, vol. 268, issues 3–4, pp. 449-456, ISSN 0022-0248, Aug. 2004.

[B102] S.F. Wen, W.Z. Yan, X.S. Wang, J. Liu, Z.F. Yue: **Prediction of strength using bending test method**, Materials and Design 31, pp. 1828–1832, 2010.

[B103] D. Alfred Hancq: **Fatigue Analysis in the Ansys Workbench Environment**, Ansys Inc., May 2003.

[B104] Y. Liu, S. Mahadevan: **Multiaxial high-cycle fatigue criterion and life prediction for metals**, International Journal of Fatigue 27, pp. 790–800, 2005.

[B105] Wei-hui Zhong, and Ji-ping Hao: **Finite Element Analysis Model of High Cycle Fatigue Damage for Metal Structure**, Earth & Space 2006, April 2006.

[B106] **Guidelines for Accelerated Reliability Testing of Surface Mount Solder Attachment**, IPC-SM-785, Institute for Interconnecting and Packaging Electronic Circuits, Nov. 1992.

[B107] W.D. van Driel, X.J.Fan (editors): **Solid State Lighting Reliability, Components to Systems**, Springer, ISBN 978-1-4614-3066-7, 2013.

[B108] Ch. Xiangyang, Z. Dejian: **Modeling and reliability analysis of lead-free solder joints of bottom leaded plastic (BLP) package**, High Density Microsystem Design and Packaging and Component Failure Analysis, Conference HDP'06, pp.247-253, June 2006.

[B109] R.E. Sonntag, C. Borgnakke, G.J. Van Wylen: **Fundamentals of Thermodynamics**, John Willey and Sons Inc., 6th Edition, ISBN 978-0471152323.